Defense Nuclear Agency
Alexandria, VA 22310-3398

DNA-TR-88-109

Design Concepts for Hardened Communications Structures

W. J. Flathau
W. G. Smith
JAYCOR
P.O. Box 1607
Vicksburg, MS 39180

April 1990

Technical Report

CONTRACT No. DNA 001-85-C-0412

Approved for public release;
distribution is unlimited.

Destroy this report when it is no longer needed. Do not return to sender.

PLEASE NOTIFY THE DEFENSE NUCLEAR AGENCY, ATTN: CSTI, 6801 TELEGRAPH ROAD, ALEXANDRIA, VA 22310-3398, IF YOUR ADDRESS IS INCORRECT, IF YOU WISH IT DELETED FROM THE DISTRIBUTION LIST, OR IF THE ADDRESSEE IS NO LONGER EMPLOYED BY YOUR ORGANIZATION.

DISTRIBUTION LIST UPDATE

This mailer is provided to enable DNA to maintain current distribution lists for reports. We would appreciate your providing the requested information.

- ☐ Add the individual listed to your distribution list.
- ☐ Delete the cited organization/individual.
- ☐ Change of address.

NAME: _____

ORGANIZATION: _____

OLD ADDRESS	CURRENT ADDRESS
_____	_____
_____	_____
_____	_____

TELEPHONE NUMBER: ( ) _____

SUBJECT AREA(s) OF INTEREST:

_____	_____
_____	_____
_____	_____

DNA OR OTHER GOVERNMENT CONTRACT NUMBER: _____

CERTIFICATION OF NEED-TO-KNOW BY GOVERNMENT SPONSOR (if other than DNA):

SPONSORING ORGANIZATION: _____

CONTRACTING OFFICER OR REPRESENTATIVE: _____

SIGNATURE: _____

CUT HERE AND RETURN

Director
Defense Nuclear Agency
ATTN: TITL
Washington, DC 20305-1000

Director
Defense Nuclear Agency
ATTN: TITL
Washington, DC 20305-1000

REPORT DOCUMENTATION PAGE

Form Approved OMB No. 0704-0188

1. AGENCY USE ONLY *(Leave blank)*	2. REPORT DATE	3. REPORT TYPE AND DATES COVERED
	900301	Technical 860130 to 871231

4. TITLE AND SUBTITLE

Design Concepts for Hardened Communications Structures

5. FUNDING NUMBERS

C - DNA 001-85-C-0412
PE - 62715H
PR - S
TA - C
WU - DH009194

6. AUTHOR(S)

William J. Flathau and William G. Smith

7. PERFORMING ORGANIZATION NAME(S) AND ADDRESS(ES)

JAYCOR
P.O. Box 1607
Vicksburg, MS 39180

8. PERFORMING ORGANIZATION REPORT NUMBER

J650-87-002/2461

9. SPONSORING/MONITORING AGENCY NAME(S) AND ADDRESS(ES)

Defense Nuclear Agency
6801 Telegraph Road
Alexandria, VA 22310-3398
SPSD/McDugald

10. SPONSORING/MONITORING AGENCY REPORT NUMBER

DNA-TR-88-109

11. SUPPLEMENTARY NOTES

This work was sponsored by the Defense Nuclear Agency under RDT&E RMC Code B344085466 S C 00102 25904D.

12a. DISTRIBUTION/AVAILABILITY STATEMENT

Approved for public release; distribution is unlimited.

12b. DISTRIBUTION CODE

13. ABSTRACT *(Maximum 200 words)*

An important component of any hardened command and control structure is the antenna system that provides communication with the outside world. Two types of antennae were considered; i.e., the whip type and the directional. The whip type for short-range communication and the directional for use primarily with satellites. In the super high-frequency range, the use of directional antennae having parabolic dishes greater than 8 feet in diameter are common. In the very extra high-frequency range, dishes that are 2 to 3 feet in diameter are used. The whip-type antenna should extend up to, say, 60 feet in the air. Based on this background, a family of structures was designed that can protect whip and directional antennae from the blast and shock effects from a 1-MT device for ground surface overpressure ranging from 15,000 to 500 psi.

As the antennae, transmitters, receivers, power supplies, and lifting mechanisms will be located within such structures, appropriate shock spectra plots were developed to determine if the fragility level of pertinent equipment will be exceeded and for use in designing shock isolation systems. Button up periods of 1 week and 4 weeks were considered.

14. SUBJECT TERMS

Hardened Antenna Structures; Cost and Hardness Tradeoffs
Buried Structures; Blast and Shock
Design Methods

15. NUMBER OF PAGES

174

16. PRICE CODE

17. SECURITY CLASSIFICATION OF REPORT	18. SECURITY CLASSIFICATION OF THIS PAGE	19. SECURITY CLASSIFICATION OF ABSTRACT	20. LIMITATION OF ABSTRACT
UNCLASSIFIED	UNCLASSIFIED	UNCLASSIFIED	SAR

CLASSIFIED BY N/A since Unclassified.

DECLASSIFY ON. N/A since Unclassified.

PREFACE

This research effort was sponsored by the Defense Nuclear Agency under RDT&E RMSS Code B 3440 85466 SC 00102 25904D, Contract No. DNA001-85-C-0412, and monitored by Mr. James D. Cooper. The constructive comments and direction furnished by Mr. Cooper are appreciated by the authors.

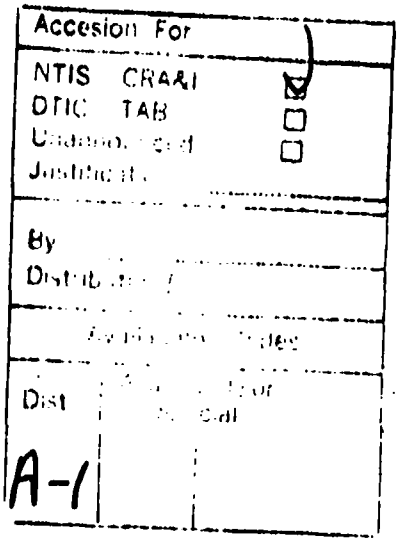

CONVERSION TABLE

CONVERSION FACTORS, NON-SI TO SI (METRIC) UNITS OF MEASUREMENT

Non-SI units of measurement used in this report can be converted to SI (metric) units as follows:

Multiply	By	To Obtain
degree (angle)	0.01745	radians
feet	0.3048	metres
feet per second	0.3048	metres per second
inches	2.540	centimetres
inches^3 (volume; section modulus)	16.38706	cubic micrometres
inches per second	2.540	centimetres per second
inches^4 (second moment of area)	0.4162314	micrometres to the fourth power
kilotons	4.184	megajoules
kips (1,000 pounds force)	4448.22	newtons
kips per square inch	6.894757	megapascals
microinches	0.0254	megametres
pounds (force) per square inch	6.894757	kilopascals
pounds (mass)	0.45359237	kilograms
pounds (mass)-seconds squared per inch	17.858	kilogram-seconds squared per metre
square feet	0.09290304	square metres
square inches	6.4516	square centimetres
tons (nuclear equivalent of TNT)	4184.0	megajoules

TABLE OF CONTENTS

LIST OF ILLUSTRATIONS

LIST OF ILLUSTRATIONS (CONTINUED)

LIST OF ILLUSTRATIONS (CONTINUED)

LIST OF TABLES

SECTION 1

INTRODUCTION AND BACKGROUND

A most important component of any hardened command and control structure is the antenna system that provides the communication link with the outside world. Consequently, either the antenna system or the structures housing such antennae need to be hardened to resist specified threats. It is probably not practical to harden either exposed whip or directional antennae for overpressures greater than, say, 25 psi. Consequently, blast and EMP hardening is achieved by housing antennae in structures designed to resist specified overpressure levels.

Whip-type or telescoping antennae extend up to about 60 feet in the air and have an operating range of about 100 miles, depending on terrain features. Directional antennae have parabolic dishes and can be beamed to satellites for world-wide communications. The diameter of the dish is dependent upon the frequency range of the communication system. For example, in the super high-frequency (SHF) range, parabolic dished having diameters 8 feet and greater are common. In the extra high-frequency (EHF) range, dishes having diameters 2 to 3 feet in diameter are realistic.

Based on the size and function of these antennae, it reasonable that a family of flush-buried, silo-type structures having internal diameters of 48, 96, and 144 inches up to 20 feet in length should conceivably house any of the antenna types including necessary components, i.e. transmitters, receivers, power supplies, etc. It is anticipated that an overpressure range from 1 kilobar (approximately 15,000 psi) to 500 psi from a 1-MT device should meet the requirements for most design considerations and consequently has been used as the basis of design for this report.

For the whip antenna, a concept is shown in Figure 1 using a silo-type structure with a removable closure that will house an antenna that can be telescoped into the air. Two generalized schemes are shown in Figure 2 for a pop-up and fold-out and a pop-up directional antenna. The use of a fold-up antenna minimizes the size of the hardened structure and hence its cost.

1.1 OBJECTIVE.

The objective is to provide design guidance for a family of structures that can protect whip and directional antennae from the blast and shock effects from a 1-MT device for ground surface overpressures ranging from 15,000 to 500 psi.

1.2 SCOPE.

The pertinent weapons effects criteria for a 1-MT device detonated on and over a dry, sandy, silty soil terrain were first defined. These effects necessary for design included the crater size, the ejecta field, airblast, and ground shock for ground surface air overpressure levels ranging from 15,000 to 500 psi. As the antennae, transmitters, receivers, power supplies, and lifting mechanisms will be located within such structures, appropriate shock spectra plots were developed to determine if the fragility level of pertinent equipment will be exceeded and for designing shock isolation systems. The static resistances of a family of silo-type structures having internal diameters of 4, 8, and 12 feet and lengths up to 20 feet were determined for the pressure ranges of interest. Both slab and dome-type closures were considered. The influence of strain rate and the triaxial state of stress of concrete were examined to show the significance of these parameters in determining the resistance of the silo system to overpressure. Power requirements were determined to push the closures through an ejecta field. Lifting and/or handling mechanisms for slab and dome closures as well as lifting mechanisms for the various types of antennae were also examined. The relative cost of the various elements of a hardened silo structure to include the lifting systems is presented in terms of overpressure level. From this information, cost trade-offs versus distance can be studied. Finally, an assessment was made describing where improvements are needed for design procedures, what supporting data are pertinent, and what field tests are needed to support the role of hardened structures to house antennae.

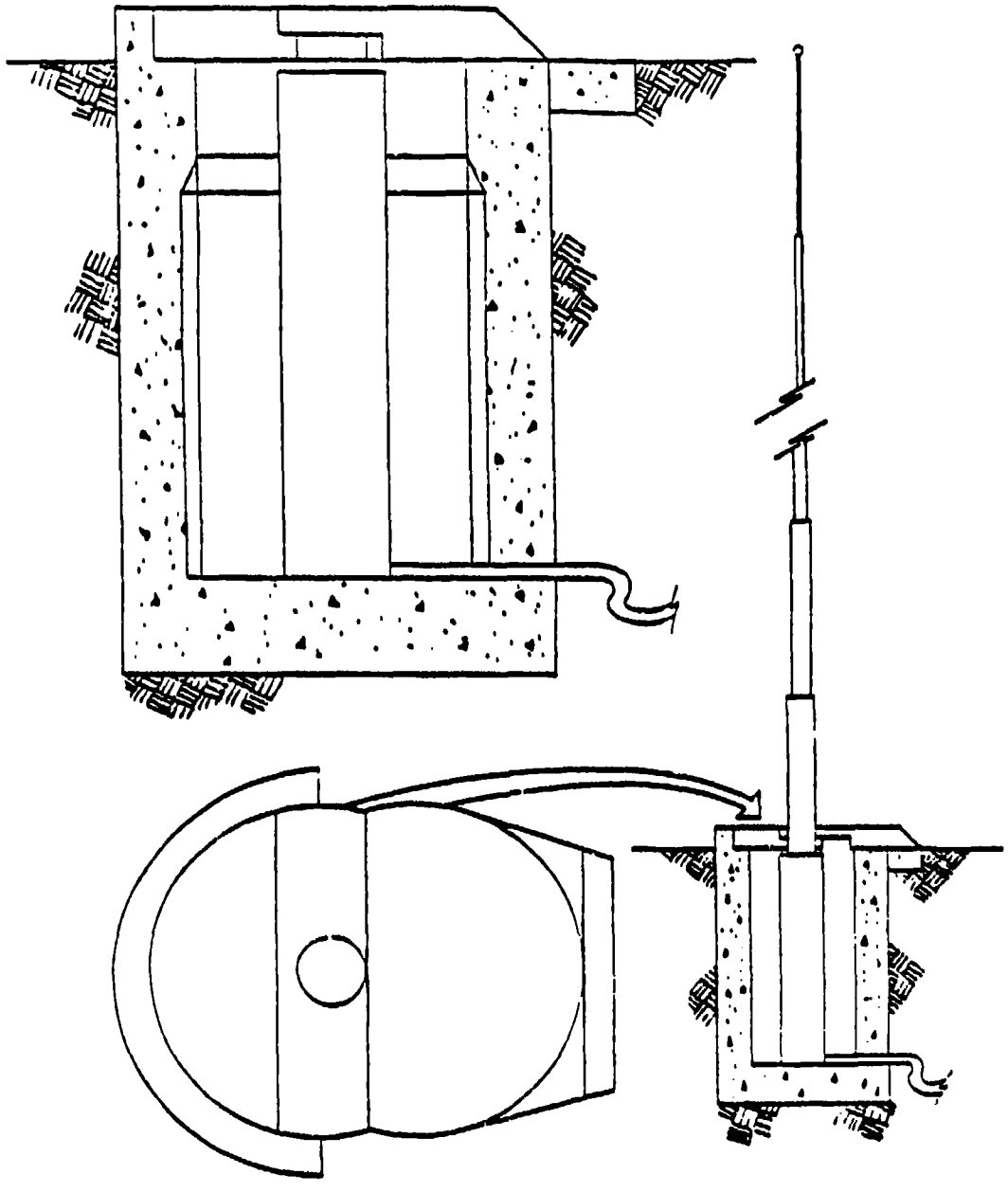

Figure 1. Design concept for structure housing a whip antenna.

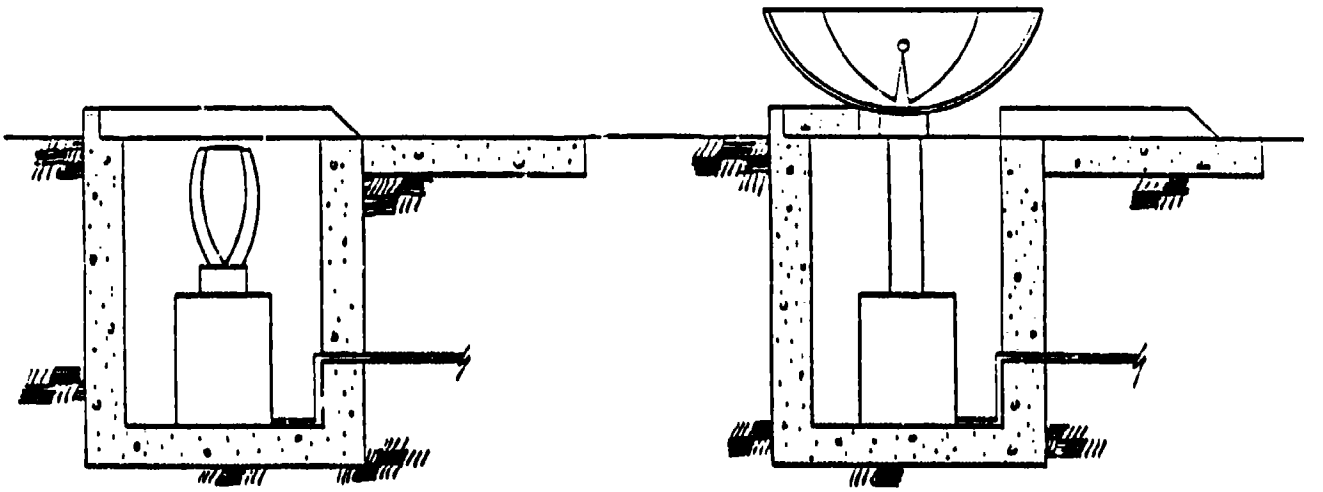

a. Pop-up and fold-out directional antenna scheme.

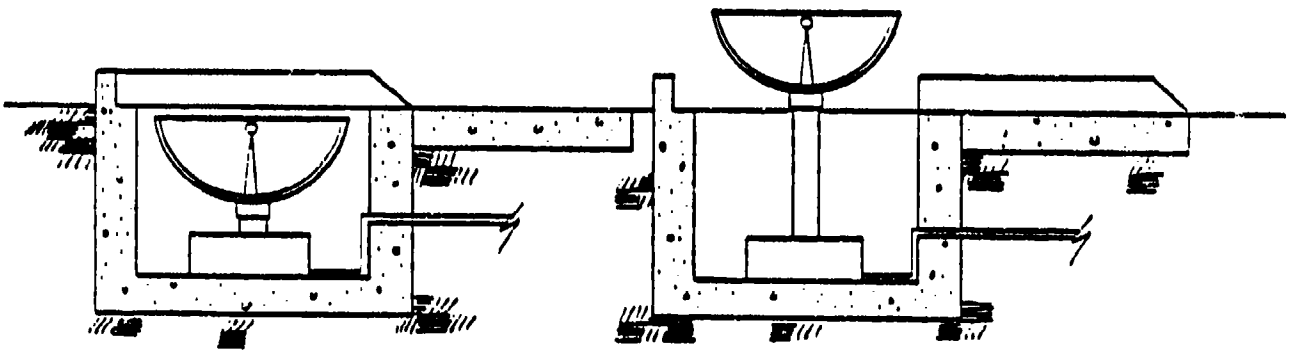

b. Pop-up, small diameter, directional antenna scheme.

Figure 2. Design concepts for structures housing directional antennae.

SECTION 2

WEAPONS EFFECTS LOADING PARAMETERS

In the design of any system, it is first important to establish the input loading conditions. The loading conditions generated by the detonation of an explosion that need to be considered in the design of a structure include airblast, ground shock (airblast, direct, and crater induced) and ejecta. We shall assume for demonstration and design purposes a 1-MT weapon detonated in a dry soil environment. The weapon can be detonated above, on, or below the ground surface; each of these detonation geometries produces a different set of maximum loading conditions. For example, it is possible for an airburst to maximize ground surface air overpressure values but minimize cratering effects. We shall examine the different possible detonation geometries and determine a consistent set of loading conditions.

In establishing the loading condition produced by the detonation of a nuclear device, we used the Air Force Design Manual (Reference 8), computer codes (Reference 14) developed by the Defense Nuclear Agency (DNA), and the American Society of Civil Engineers Manual 42 (Reference 2).

2.1 DETONATION GEOMETRIES.

Three burst conditions for a 1-MT weapon were assumed, as shown in Figure 3, for a dry soil site, say, a dry sandy silt. Height-of-burst (HOB) and surface burst geometries were considered for airblast loading conditions. The near-surface (charge below ground surface) condition was selected to produce maximum horizontal direct-induced ground motion, crater size, and maximum ejecta.

2.2 AIRBLAST.

The optimum HOB for a 1-MT weapon to produce 10,000 psi out to a range of 900 feet is about 600 feet. The optimum HOB is about 800 feet to produce a ground surface air overpressure of 5,000 psi at a ground range of about 1,000 feet. As we are interested in overpressures up to 1 kilobar (15,000 psi), an HOB of 500 feet was selected as being a reasonable

condition for the aboveground burst of interest. Shown in Figure 4 are the peak ground surface air overpressure distance relationships (Reference 14) for a HOB of 0 and 500 feet. At a range of 650 feet, the peak pressures based on the DNA code (Reference 14) are about 6 percent lower than the Brode-Speicher predictions (Reference 2) and about 4 percent lower at a range of 900 feet. The positive phase duration and impulse for a 1-MT surface burst for an HOB of 0 and 500 feet are shown in Figure 5. Shown in Figure 6 is the airblast shock front velocity (U) with range for an HOB of 0 and 500 feet for a 1-MT weapon. However, based on conversations with Mr. James D. Cooper, of the DNA, and recent information, it will be assumed that a burst at a 500-foot HOB will produce about the same airblast conditions as an HOB of zero. Hence, the conditions for an HOB of zero will be used for the calculations for airblast in this report.

2.3 CRATER EFFECTS.

The crater volume, radius, depth, and both the median and maximum thicknesses of ejecta for a 1-MT detonation for a zero HOB are shown in Figure 7. For comparison purposes, the median ejecta thickness with range for an HOB of 0 and depth of bursts (DOB) of 5 and 10 feet are shown in Figure 8. The crater dimension for the two DOB conditions are also shown. The ejecta with distance has been shown on an expanded vertical scale so that the magnitude of this soil cover can be better appreciated, especially when considering the problem of pushing a closure system protecting an antenna through such an earth cover. Also, the volume of a crater is an important factor when estimating near-surface late-time ground motions. It should also be noted that for HOB's greater than about 100 feet, there will be no craters.

2.4 GROUND SHOCK.

Ground shock propagation in a real geologic situation, i.e. layers of soil, water tables, and rock interfaces, is a very complex phenomena. For design purposes we have selected a simple geologic condition, a dry homogeneous soil. Even though such a geometry is simple, the range of loading conditions developed are realistic when considering the design of

near-surface hardened structures. There are basic, accepted categories of ground shock, namely: airblast induced, direct induced, and crater induced that will be described in the following sections.

2.4.1 Airblast-Induced Ground Shock.

An expanding airblast wave loads the ground surface imparting an air-induced ground shock. The character of the induced ground shock is strongly influenced by the relative values of the airblast shock velocity and the wave velocity of the ground media. The induced ground shock propagates as compression waves (dilatational waves), shear waves, and surface waves. There are three regions of interest for the ground surface, air overpressure wave, i.e. superseismic, transseismic, and subseismic.

The superseismic region is defined as that where the shock front velocity of the airblast exceeds that of the dilatational and shear wave velocities of the ground medium:

$$U > C_p > C_v \qquad (2.1)$$

where:

U = Airblast shock front velocity.

C_p = Dilatational wave velocity in ground medium.

C_v = Shear wave velocity in ground medium.

Since the airblast velocity in the superseismic region is greater than the dilatational or shear wave velocities, no disturbances are propagated in front of the airblast wave.

The transseismic region is defined when the airblast shock front velocity becomes less than the dilatational wave velocity but greater than the shear wave velocity:

$$C_p > U > C_v \qquad (2.2)$$

The subseismic region is defined by the condition when the airblast shock front velocity is less than both the dilatational and shear wave velocities:

$$C_p > C_v > U \qquad (2.3)$$

In the so-called outrunning region for both the transseismic and subseismic regions, the ground disturbances can become quite complex and the motions are primarily horizontal.

In an elastic medium, it has been shown (Reference 19) that for materials with a Poisson's ratio (μ) ranging between 0.3 and 0.4, the dilatational wave velocity is about twice that of the shear wave. The shear wave velocities (Reference 19) for low stress levels (seismic energy) for a fine silty sand for shallow depths, say, up to 20 feet, are approximately 500 to 600 ft/s. Associated dilatational wave velocities of 1,200 ft/s are reasonable. For our design case, we shall assume that:

$$C_p = 1,200 \text{ ft/s}$$

$$C_v = 500 \text{ ft/s}$$

Based on airblast, the ground ranges of interest extend from about 600 to 2,000 feet from ground zero (GZ). By examining Figure 6, it is obvious that our domain of interest is in the superseismic region as the airblast shock front velocity is about 6,000 ft/s at a range of 2,000 feet, which is much greater than the dilatational wave speed at that range. Hence, it is reasonable to assume that a one-dimensional procedure for ground shock predictions is adequate. The flat entry angle that air-induced ground shock wave makes with the ground surface supports this assumption and is shown in Figure 9 for ground ranges of 700 and 2,000 feet from GZ.

A one-dimensional approximation of the air-induced ground shock is discussed in the following sections.

2.1.1.1 Vertical Stress, Particle Velocity, and Displacement. The stress, particle velocity, and displacement as functions of time and depth for the one-dimensional elastic case (r = 1) are as follows (Reference 8):

$$\sigma_z(z,t) = p\left(t - \frac{z}{C_L}\right) \tag{2.4}$$

$$v_z(z,t) = \frac{p\left(t - \frac{z}{C_L}\right)}{\rho\, C_L} \tag{2.5}$$

$$d_z(z,t) = \int_{z/C_L}^{t} v_z(z,t)\,dt \tag{2.6}$$

$$\text{for} \quad t > \frac{z}{C_L}$$

where:

z = Depth.

t = Time.

σ_z = Vertical stress.

$p(t)$ = Overpressure time history.

C_L = Loading wave propagation velocity.

v_z = Vertical particle velocity

ρ = Mass density of soil.

d_z = Vertical displacement.

Solutions for the case of no strain recovery ($r = 0$) have been determined for nuclear overpressure functions and are as follows (Reference 8):

$$\sigma_z(z,t) = P_{so}\left\{\left(1 - \frac{t}{t_o}\right)^n + \frac{z\,t_o}{C_L(n+1)t^2}\left[1 - \left(1 - \frac{t}{t_o}\right)^{n+1} - (n+1)\left(1 - \frac{t}{t_o}\right)^n\left(\frac{t}{t_o}\right)\right]\right\} \tag{2.7}$$

$$v_z(z,t) = \frac{P_{so}\,t_o}{\rho\, C_L\, t(n+1)}\left[1 - \left(1 - \frac{t}{t_o}\right)^{n+1}\right] \tag{2.8}$$

$$\text{for} \quad \frac{z}{C_L} < t < t_o \quad \text{and} \quad p(t) = P_{so}\left(1 - \frac{t}{t_o}\right)^n$$

The parameters t_o and n should be selected so that the approximation contains the same impulse as the actual airblast overpressure up to the maximum time of interest. Measured field data show that rise time increases as the stress wave propagates into the ground. In order for the stress wave to be more realistic, the initial arrival is assumed to occur at a time as follows (Reference 8):

$$t_i = \frac{z}{C_i} \qquad (2.3)$$

where:

t_i = Wave front arrival.

z = Depth.

C_i = Velocity of wave front.

The velocity (C_i) of the wave front should be assumed as the insitu seismic velocity. The peak stress is assumed to occur at a time equal to z/C_L .

The assumption of one-dimensional wave propagation in a homogeneous half space is not exactly a true representation of the real world, especially when assuming elastic conditions. However, the prediction procedures are reliable estimates of response for relatively homogeneous sites and estimates of the incident wave propagating into the upper layer of layered sites at early times after airblast arrival.

Shown in Figures 10 through 14 are the normalized, vertical stress and particle velocity profiles for peak overpressure values of 15,000, 10,000, 5,000, 1,000, and 500 psi, respectively, for depths (z) of 5, 10, and 20 feet.

The loading wave propagation velocity (C_L) for a dry sandy-silt soil was estimated to vary from about 800 to 600 ft/s (Reference 20) for ground surface overpressures ranging from 15,000 to 500 psi. Therefore, for calculation purposes, values of C_L of 800, 750, 700, 600, and 600 ft/s

were used at overpressure ranges of 15,000, 10,000, 5,000, 1,000, and 500 psi, respectively. Equations 2.7 and 2.8 were used to generate values of stress and particle velocity for the case where no strain recovery (r = 0) occurs. These values also compared favorably to the results from a one-dimensional computer code (Reference 20). The code was also used to predict values for the case of complete strain recovery (r = 1), i.e. elastic case. An estimate of rise time for the case of no strain recovery (r = 0) is also shown. The rise time for the elastic case (r = 1) is zero. The actual rise time is most likely some value between the limits described for the r = 0 and 1 cases, respectively.

2.4.1.2 Peak Vertical Displacement. An approximate expression can be used to estimate peak vertical displacement as follows (Reference 8):

$$d_{max} = \frac{I_m}{\rho C_L} \qquad (2.10)$$

where I_m is the total airblast impulse. Peak displacements versus range are shown in Figure 15.

2.4.1.3 Maximum Vertical Acceleration. The maximum vertical downward acceleration is related to the shape of the rise to maximum velocity. If a linear rise of particle velocity is assumed, then the maximum acceleration is as follows (Reference 8):

$$a_{max} = \frac{v_{max}}{t_r} \qquad (2.11)$$

where:

a_{max} = Maximum acceleration.

v_{max} = Maximum particle velocity.

t_r = Rise time to maximum velocity.

At the ground surface, the rise time (t_r) is about equal to the rise time of the airblast. The rise time values of interest that results in acceleration values comparable to measured field values is on the order of 0.001 sec. Using a value of $t_r = 0.001$ in Equation 2.11, an expression for peak vertical acceleration at the ground surface is as follows (Reference 8):

$$a_{max} = 150\ g \left[\frac{P_{so}}{100\ psi}\right] \left[\frac{1000\ fps}{C_L}\right] \left[\frac{115\ pcf}{\gamma}\right] \quad (2.12)$$

where C_L corresponds to surface soil conditions. Values of C_L associated with the overpressure (P_{so}) level were described in Section 2.4.1.1. Values of peak vertical surface acceleration versus range are shown in Figure 16.

2.4.1.4 Horizontal Stress and Motions. One-dimensional methods present little information on horizontal stresses and motions. Procedures however have been developed from empirical approaches and two-dimensional calculations. In general, the procedure assumes some factor (K) times the vertical stress or motion to produce a consistent horizontal value.

Horizontal stress is determined by multiplying the vertical stress by the coefficient of earth pressure at rest (K_o), see Table 1. The relationship is as follows:

$$\sigma_h = K_o\ \sigma_v \quad (2.13)$$

In general, K_o is really not a constant, but varies with stress level, strain rate and whether the soil is being loaded or unloaded. For highly saturated soils, K_o approaches unity. The recommended horizontal-to-vertical ratios for homogeneous and layered sites is shown in Table 2.

Using the information in Table 2, the ratios of peak horizontal to peak vertical ground shock components for the superseismic region are shown in Table 3. The values of K_o shown in Table 1 are based on soil stresses up to 1,000 psi. As we are interested in much higher stresses, values of K_o for stresses shown in Table 3 are based upon Reference 20 and conversations with Dr. Behzad Rohani of the U.S. Army Engineer Waterways Experiment Station. To determine horizonnal waveforms, the ground shock component values of the vertical waveform are multiplied by appropriate K values.

2.4.2 Direct-Induced Ground Shock.

Direct ground shock results from the initial stress wave caused by the direct coupling of energy into the ground at the detonation point. For

fully contained bursts, it is the only form of ground shock that exists. For high-altitude bursts it is nonexistent. For bursts at or near the surface of the ground, direct-induced ground shock is an important effect in the close-in region. For the design case discussed in this report, we are particularly interested in the surface and near-surface burst conditions.

Most of the empirical data however is for fully contained bursts. Using scaling relationships, assumptions regarding coupling, material properties, and free surface effects, near-surface predictions can be related to those for contained bursts. Based on experiments in soil, it has been observed that the attenuation rate for motion is greater in the region below the charge than the region closer to the ground surface.

For a contact burst on dry soil, the estimates of motion on the axis directly beneath the burst are as follows (Reference 8):

$$d = 0.5 \text{ in.} \left[\frac{W}{1 \text{ Mt}}\right]^{5/6} \left[\frac{R}{1 \text{ kft}}\right]^{-3/2} \tag{2.14}$$

$$v = 2.5 \text{ ft/sec} \left[\frac{W}{1 \text{ Mt}}\right]^{2/3} \left[\frac{R}{1 \text{ kft}}\right]^{-2} \tag{2.15}$$

$$a = 5 \text{ g} \left[\frac{W}{1 \text{ Mt}}\right] \left[\frac{R}{1 \text{ kft}}\right]^{-4} \tag{2.16}$$

The peak stress associated with direct-induced ground shock can be estimated as follows:

$$\sigma = \rho \, C_L \, v \tag{2.17}$$

where:

σ = Peak stress.

ρ = Mass density.

C_L = Loading wave velocity.

v = Peak particle velocity.

The value C_i can be estimated from laboratory and insitu stress-strain data or taken as approximately one-half the seismic velocity in soil and soft rock. Typical measured waveforms have been used to estimate waveforms associated with predicted peak radial motion. The rise time (t_r) to peak velocity (or stress) can be assumed as follows (Reference 8):

$$t_r = \frac{1}{12}\frac{R}{C_i} \text{ to } \frac{1}{6}\frac{R}{C_i} \tag{2.18}$$

where:

t_r = Rise time.

R = Range.

C_i = Seismic velocity.

The positive or outward phase duration (t_d) of the velocity pulse can be estimated as follows (Reference 8):

$$t_d = \frac{1}{2}\frac{R}{C_i} \text{ to } \frac{R}{C_i} \tag{2.19}$$

The compressive phase duration of the stress pulse may also be approximated from Equation 2.19. The direct-induced estimates described are confined to the axis directly beneath the burst. The motions off the vertical axis, especially near the ground surface, are strongly influenced by surface effects. The refinement to include surface effects are inconsistent with observed data. However, even though conservative, it is recommended that the equations shown be used for all other radials through the charge.

Shown in Figure 17 are estimated plots of peak horizontal displacement, velocity and acceleration with range. The horizontal stress with range is shown in Figure 18. It can be observed that the horizontal stresses and motions for direct-induced ground shock in the 600- to 2,000-foot range are relatively small compared to the values for the air-induced ground shock case.

2.4.3 Crater-Induced Ground Shock.

From studies of ground motion resulting from high-explosive and nuclear cratering bursts, correlations have been identified between late-time crater formations and late-time near-surface ground motion.

2.4.3.1 Horizontal Displacement. The following equations are good representations of peak horizontal displacements (d_h) for above and below surface charges (Reference 8):

$$d_h = \frac{0.45\ V_a^{4/3}}{R^3} \quad \text{(above surface)} \tag{2.20}$$

$$d_h = \frac{0.1\ V_a^{4/3}}{R^3} \quad \text{(half buried and below surface)} \tag{2.21}$$

where:

d_h = Peak horizontal displacement.

V_a = Apparent crater volume.

R = Range.

An expression was developed to describe the permanent horizontal displacement (d_{hp}) for aboveground, surface tangent spheres that is representative for near-surface nuclear bursts:

$$d_{hp} = \frac{0.2\ V_a^{4/3}}{R^3} \tag{2.22}$$

It has been observed that about 50 percent of the peak displacement is recovered for a near-surface nuclear burst independent of ground material.

2.4.3.2 Horizontal Velocity. An expression that relates peak crater-induced horizontal particle velocity (v_h) as a function of crater volume within a factor ± 4 is as follows (Reference 8):

$$\frac{v_h}{c_e} = 0.01 \left[\frac{R}{V_a^{1/3}}\right]^{-2} \tag{2.23}$$

where:

v_h = Peak horizontal particle velocity.

C_e = Effective wave velocity.

R = Range.

t_i = Arrival time of first signal from burst.

V_a = Apparent crater volume.

The effective velocity (C_e) is approximately equal to the seismic velocity for unlayered sites. For our case, we shall assume C_e equal to the seismic velocity.

A relationship that correlates rise time to peak horizontal displacement and crater volume within a factor ± 5 is as follows:

$$t_p = \frac{50}{C_e}\left[\frac{V_a^{2/3}}{R}\right] \qquad (2.24)$$

Vertical crater-induced ground motion analyses indicates that vertical displacements, peak velocities, and rise time to peak displacement are approximately the same as the corresponding horizontal values at the same range.

Plots of peak horizontal displacement, permanent displacement, and particle velocity for ranges of interest for this study are shown in Figure 19.

2.5 SHOCK SPECTRUM.

The elastic shock spectra for the three ground motions, i.e. air, direct and crater induced have been examined. These spectra define the bounding, maximum values of displacement, velocity and acceleration as a function of the natural frequency of a single-degree-of-freedom (SDOF) system subjected to a prescribed transient motion at the attachment point within a structure. The response of the SDOF system to support motions is, of course, strongly dependent upon both the physical characteristics of the system and the nature of the support motion. The input support motion at the attachment point is assumed to be the same as that defined by the free-field expressions for displacement, velocity and acceleration which, of course, varies with distance from GZ.

Empirical methods have been developed where the internal shock spectrum of a structure can be determined by amplifying the free-field motion values of displacement, velocity and acceleration. To develop the internal shock spectrum, amplification factors (Reference 13) for 5 percent critical damping of 1.4, 1.7, and 2.1 for displacement, velocity and acceleration, respectively, were used. These spectra are very useful as preliminary design tools and are often applicable for final design purposes. For more precise values, a complex analysis is required, i.e. finite-element analysis of the structure located in, say, a soil island.

2.5.1 Air-Induced Ground Shock.

The response spectra associated with the airblast-induced ground shock are shown in Figures 20 and 21 for vertical and horizontal motions, respectively. The maximum free-field motions used to construct the spectrum were determined by using Equations 2.10, 2.11, and 2.12. The spectrum is shown for three overpressure levels: 15 ksi, 10 ksi, and 500 psi, corresponding to ground ranges of 600, 700, and 1,975 feet from GZ, respectively. The angle the airblast-induced dilatational wave makes with the ground surface increases with range from GZ, see Figure 9. Hence, the horizontal component of motion with respect to the vertical component also increases with range. The "K" factors shown in Table 3 are based on range (overpressure level) and were used to determine the free-field horizontal components of motion used in developing the horizontal shock spectra shown in Figure 21. This helps to explain the increase in horizontal displacement with range, as shown in Figure 21.

2.5.2 Direct-Induced Ground Shock.

The type support motion in the structure resulting from direct-induced ground motion is essentially horizontal. Therefore, using the expressions for horizontal displacement, velocity and acceleration given by Equations 2.14, 2.15, and 2.16, respectively, for direct-induced shock, the maximum values were calculated and the spectral amplification factor applied. The response spectra is shown in Figure 22 for overpressures of 15 ksi, 10 ksi, and 500 psi, respectively. Note that the horizontal spectra for the airblast-induced ground motion (Figure 21) is greater than the value for direct-induced motion (Figure 22).

2.5.3 Crater-Induced Ground Shock.

The free-field motions associated with late-time, crater-induced ground shock are calculated using Equations 2.20 and 2.23 and are shown in Table 4 for five overpressure values. Crater-induced motions produce large horizontal displacements; however, little acceleration is associated with such motions. Under these conditions, the frequency content of the motion is very low and in all probability less than that of any of the internal components of a structure. The isolation of the internal components would therefore be easily achieved since masses on relatively stiff springs undergoing small accelerations would generate very little displacement or force in the spring, i.e. the components would simply "ride along" with the ground motion. Because of the insignificant acceleration values, response spectra for crater-induced motions for our cases of interest are essentially academic.

2.5.4 Equipment Fragility Level.

The fragility levels (References 6 and 3) of certain items of equipment associated with communication systems are shown in Figure 23 for both vertical and horizontal motions. As can be observed for the class of components shown (pipes, radio receivers, electrical panel boards, batteries, air-conditioning units, and monitoring and control devices) and for frequencies greater than 5 Hz, the "sure safe" acceleration levels range from about 7 to 20 g's.

It is quite obvious by studying the vertical and horizontal response of shock spectra shown in Figures 20 and 21, that the equipment described in Figure 23 would require shock isolation in order to survive. For example, assume we are interested in a radio receiver that has a natural frequency of 50 Hz. From Figure 23, it is observed that the "sure safe" acceleration level at 50 Hz is about 14 g's. If this equipment was in a structure located at the 500-psi ground surface overpressure range, the maximum acceleration would be about 700 g's (well in excess of the "sure safe" value of 14 g's for the equipment) and the peak displacement about 0.3 foot. Because of the relatively small displacement (approximately 4 inches), the design of the required shock isolation system is relatively uncomplicated.

If the equipment was located in a structure at the 5,000-psi ground surface overpressure level, the spectral displacement would be about 3 feet. The shock isolation system would now have to consider motions up to 36 inches which presents more complications than the case when the equipment was in the structure at the 500-psi range. For large motions it will probably be desirable to consider a shock isolated platform on which equipment is placed.

Table 1. Ratio of horizontal to vertical soil pressures (Reference 1).

Soil Description	K_o, for Stresses Up to 1,000 psi (690 N/cm^2) Dynamic Undrained	Static Undrained	Static Drained
Cohesionless soils, damp or dry	1/4	1/3 dense 1/2 loose	1/3 dense 1/2 loose
Unsaturated cohesive soils of very stiff to hard consistency*	1/3	1/2	1/2
Unsaturated cohesive soils of medium to stiff consistency*	1/2	1/2	1/2
Unsaturated cohesive soils of soft consistency*	3/4	1/2 to 3/4	1/2 to 3/4
Saturated soils of very soft to hard consistency* and cohesionless soils	1	1	1/2 stiff 3/4 soft
Saturated soils of hard consistency*	3/4 to 1	1	1/2
Saturated soils of very hard consistency*	3/4	1	1/2
Rock	Obtain from tests on rock cores and correlate with seismic data		

*Consistency Definitions:

Consistency	Unconfined Compression Strength - q_u - tsf (N/cm^2)		Standard Penetration Test - N - blows per ft (m)	
Very soft	< 0.25	(< 2.4)	< 2	(< 0.6)
Soft	0.25-0.50	(2.4-4.8)	2-4	(0.6-1.2)
Medium	0.50-1.00	(4.8-9.6)	4-8	(1.2-2.4)
Stiff	1.00-2.00	(9.6-19.1)	8-15	(2.4-4.6)
Very stiff	2.00-4.00	(19.1-38.3)	15-30	(4.6-9.1)
Hard	4.00-20.00	(38.3-191)	> 30	(> 9.1)
Very hard	> 20	(> 191)		

Table 2. Recommended ratios of peak horizontal to peak vertical ground shock components in the superseismic region (Reference 1).

	Homogeneous Sites	Layered Sites	
		Wave Front	Late Time
Stress	K_o	K_o	--
Acceleration	$\tan\left(\arcsin \frac{C_L}{U}\right)^*$	$\tan\left(\arcsin \frac{C_L}{U}\right)$	--
Velocity	$\tan\left(\arcsin \frac{C_L}{U}\right)^*$	$\tan\left(\arcsin \frac{C_L}{U}\right)$	2/3
Displacement	$\tan\left(\arcsin \frac{C_L}{U}\right)^*$	--	1

*If $\tan(\arcsin \frac{C}{U}) > 1$, let peak horizontal component equal the peak vertical component.

Table 3. Ratios (%) of peak horizontal to peak vertical ground shock components, superseismic region for a dry, silty sand.

Ground Shock Component	Overpressure (P_{so}) Level, psi				
	15,000	10,000	5,000	1,000	500
Stress	0.42	0.45	0.47	0.5	0.5
Acceleration	.044	.048	.067	.130	.204
Velocity	.029	.030	.039	.074	.100
Displacement	.029	.030	.039	.074	.100

Table 4. Peak horizontal displacement and velocity for crater-induced ground shock

Overpressure Level P_{so} psi	Peak Horizontal Displacement d_h ft	Peak Horizontal Velocity V_h ft/sec
15,000	4.5	1.6
10,000	2.9	1.2
5,000	1.4	0.7
1,000	.3	0.2
500	.1	0.1

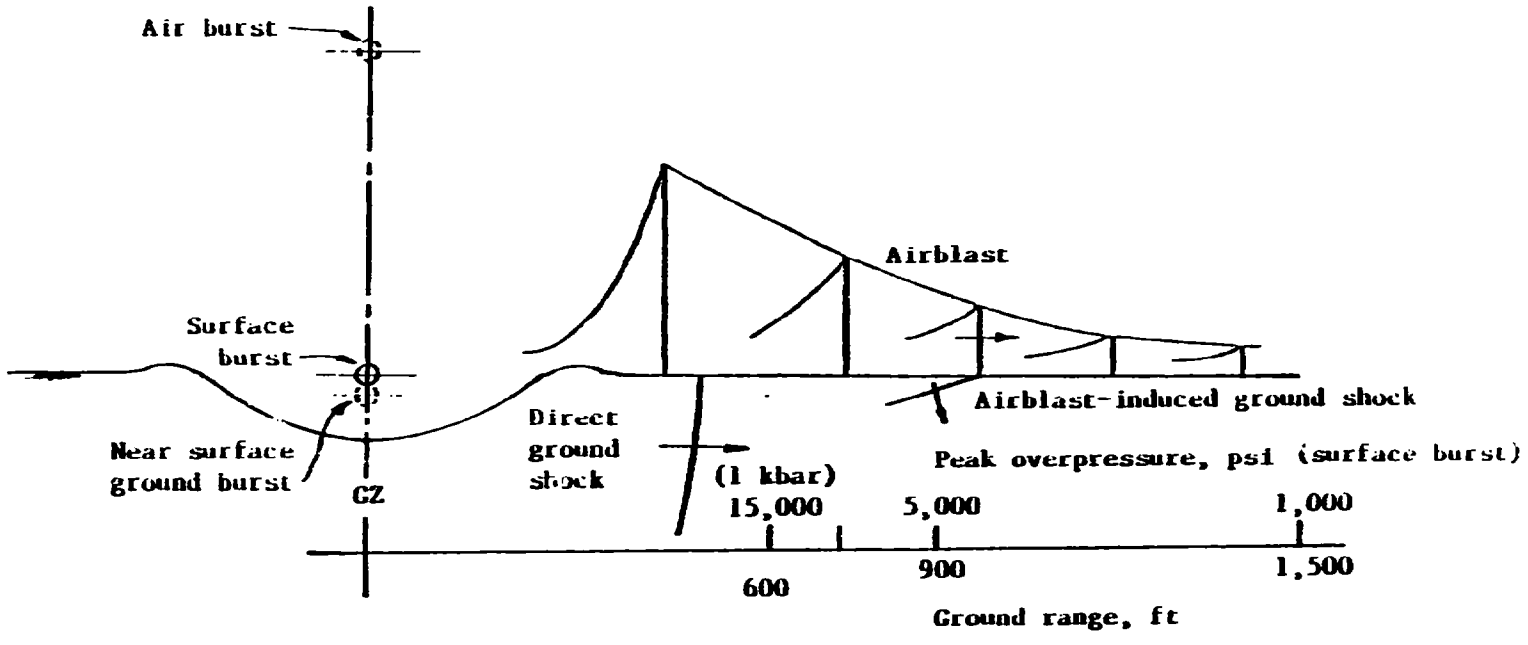

Figure 3. Burst conditions of interest and peak overpressure versus range for a 1-MT surface burst.

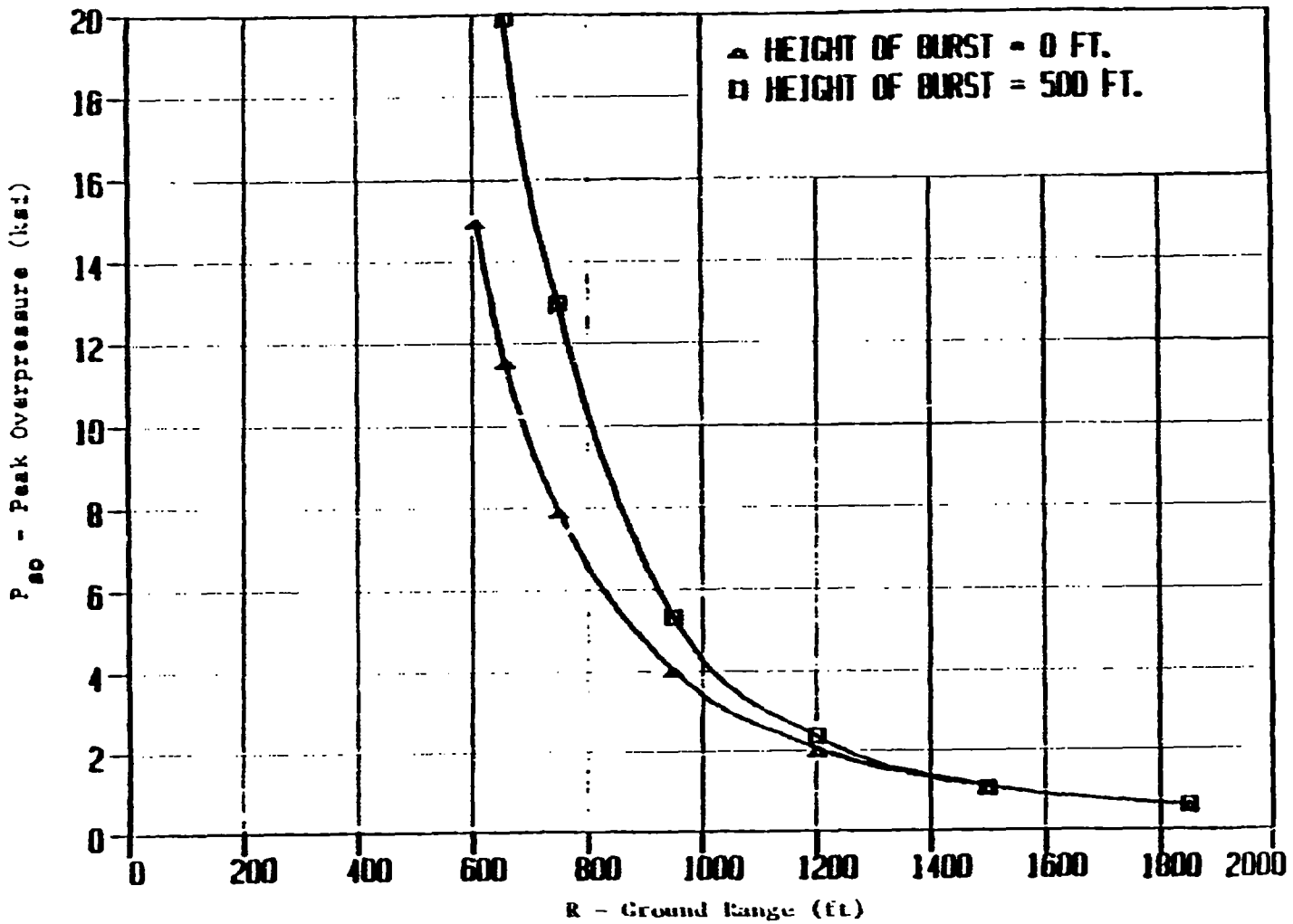

Figure 4. Peak ground surface air overpressure with range, 1-MT weapon, HOB = 0 and 500 ft.

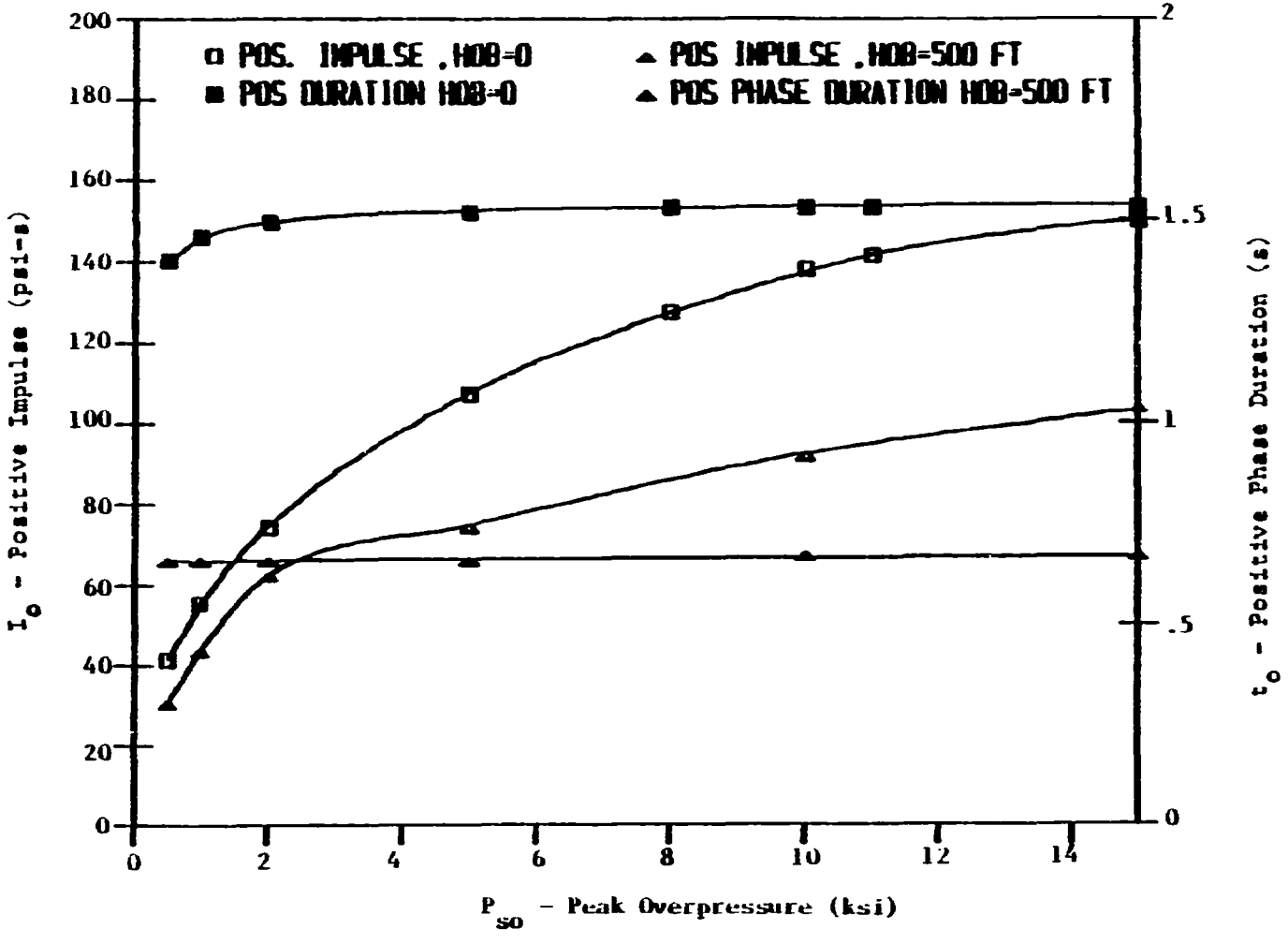

Figure 5. Positive phase duration and impulse, 1-MT weapon. HOB = 0 and 500 ft.

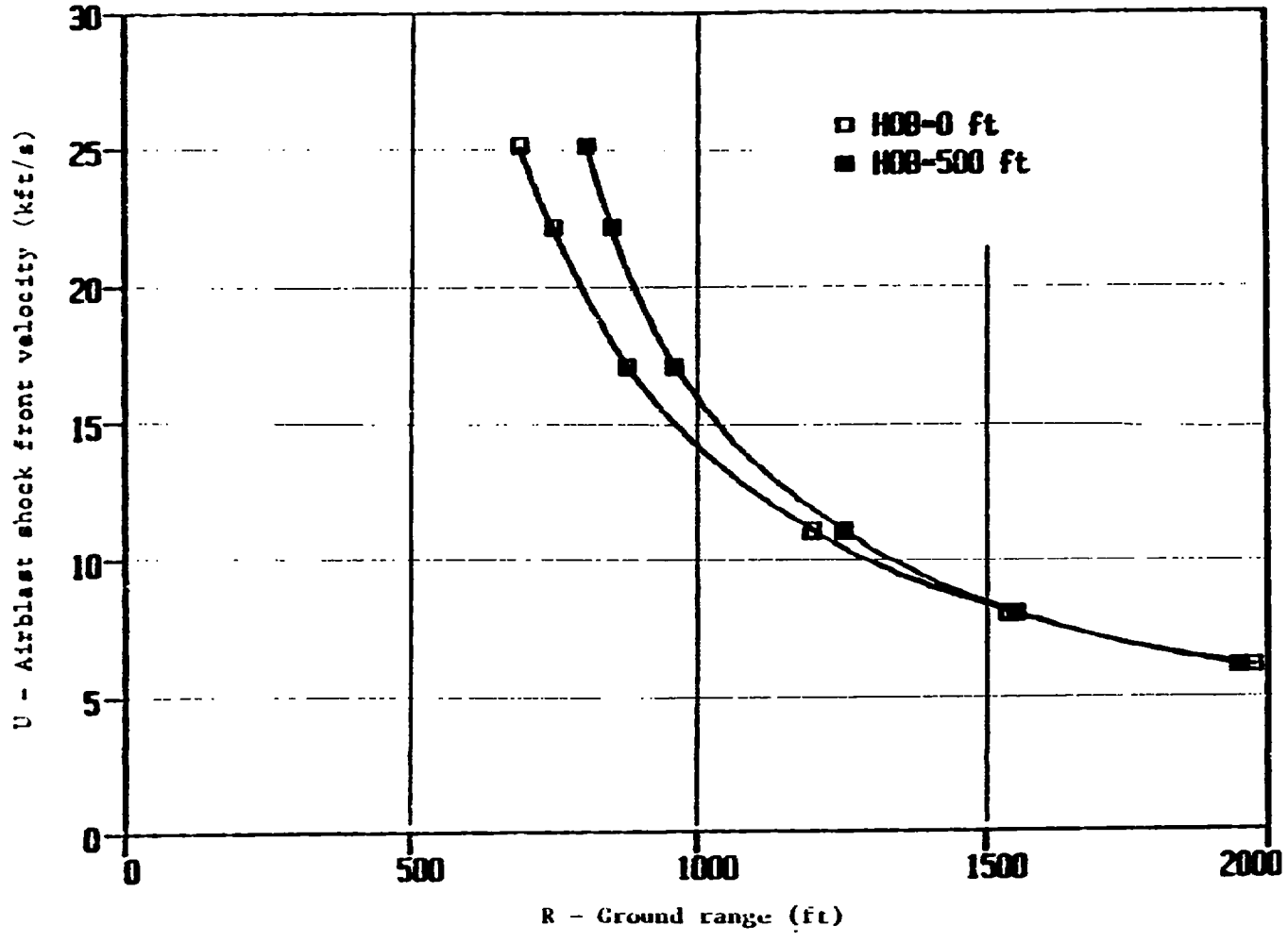

Figure 6. Airblast shock front velocity with range, 1-MT weapon, HOB = 0 and 500 ft.

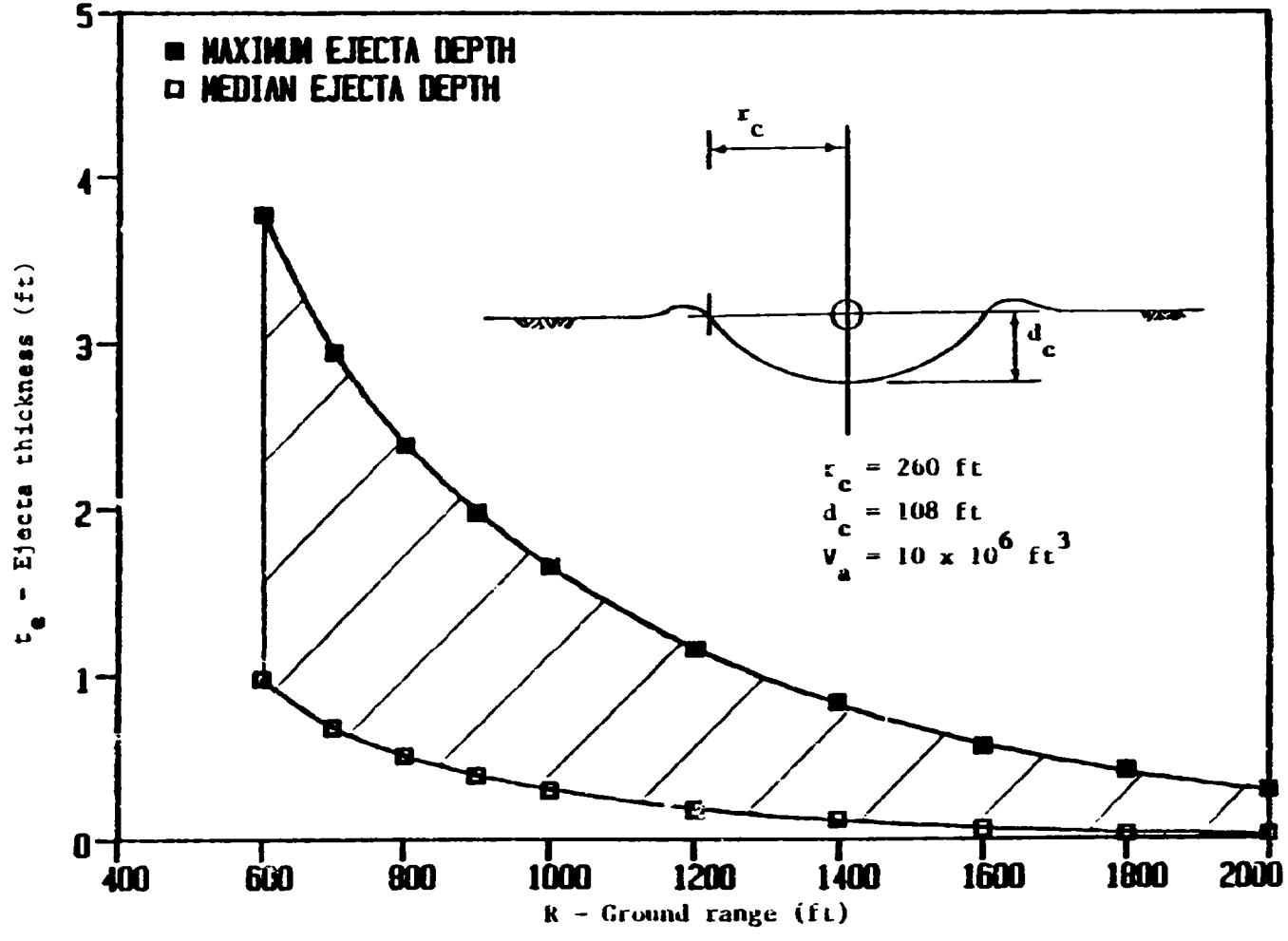

Figure 7. Crater radius, depth and apparent volume including maximum and median ejecta depth with range, 1-MT weapon, HOB = 0.

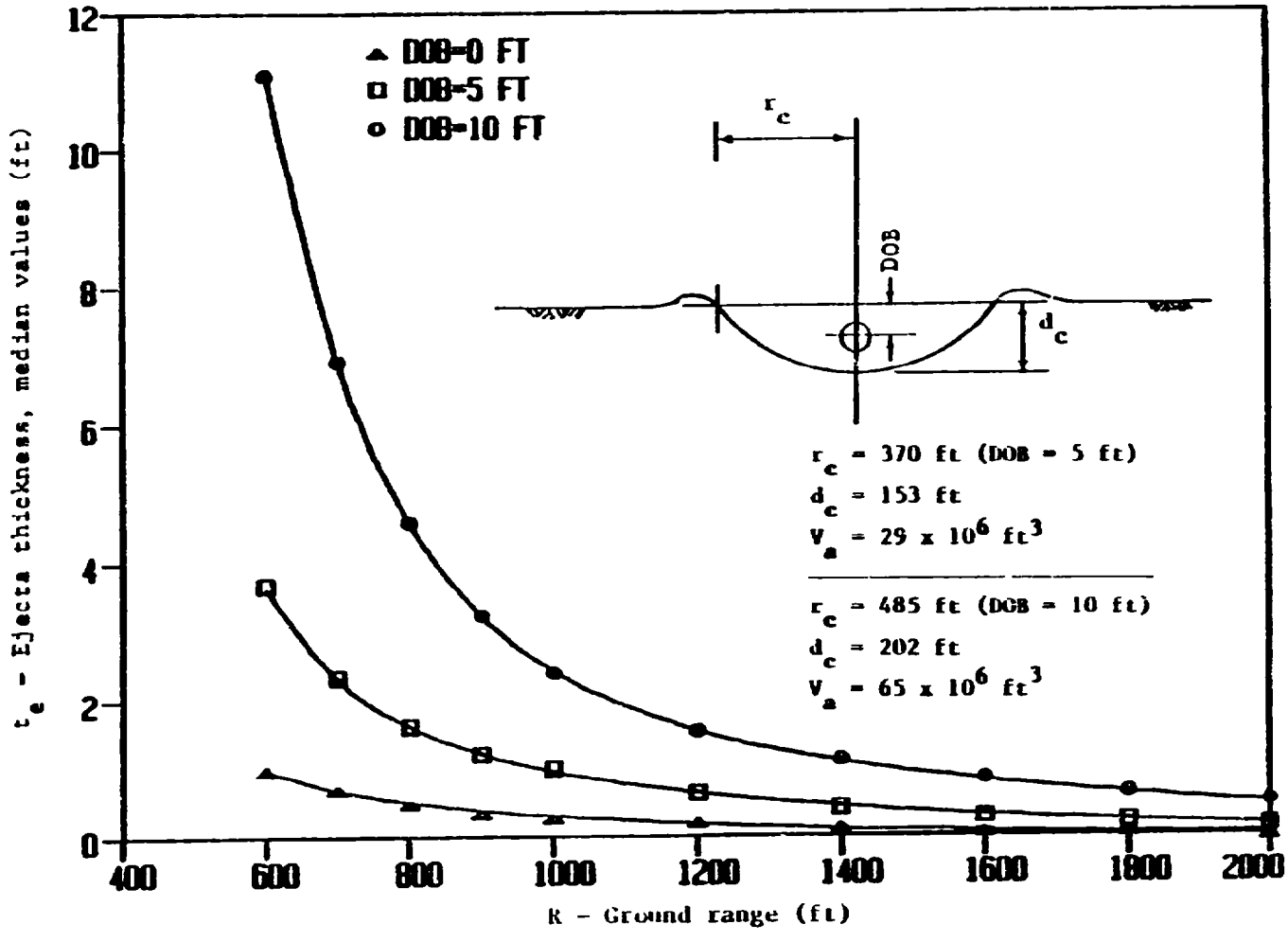

Figure 8. Crater radius, depth and apparent volume including median ejecta depth with range, 1-MT weapon, HOB - 5 and 10 ft.

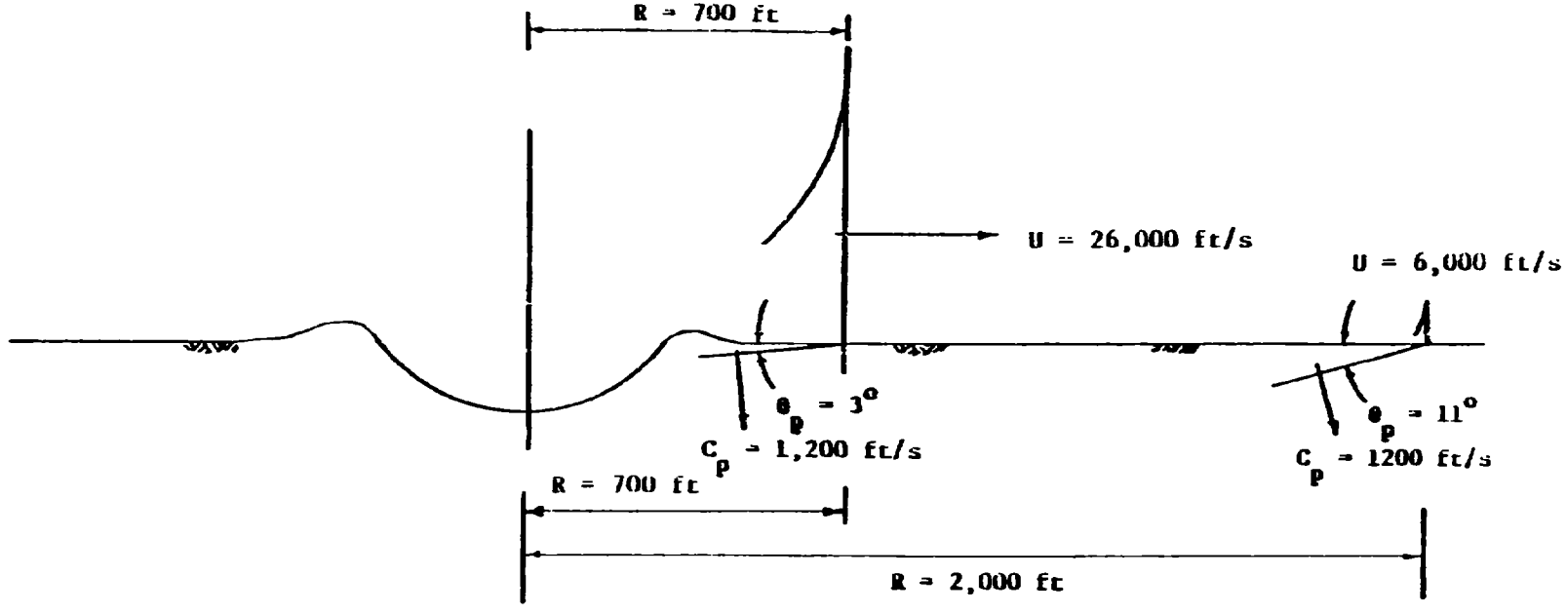

Figure 9. Angle dilatational wave makes with the ground surface at 700- and 2,000-ft ranges.

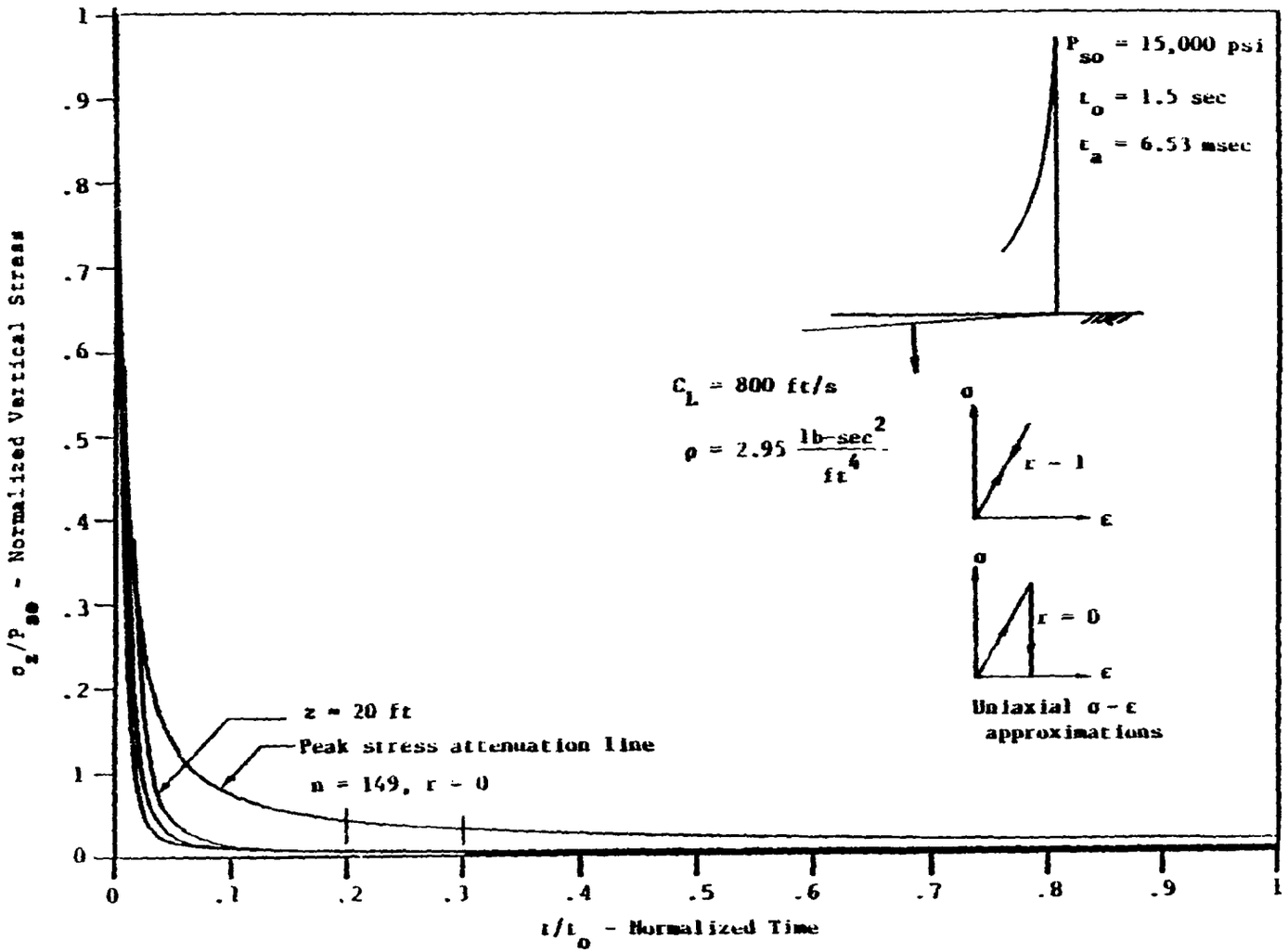

a. Normalized vertical stress at depths of 5, 10 and 20 ft for peak overpressure of 15,000 psi, airblast-induced ground shock, 1-MT weapon, HOB = 0 ft.

Figure 10. Normalized solutions for peak overpressure of 15,000 psi.

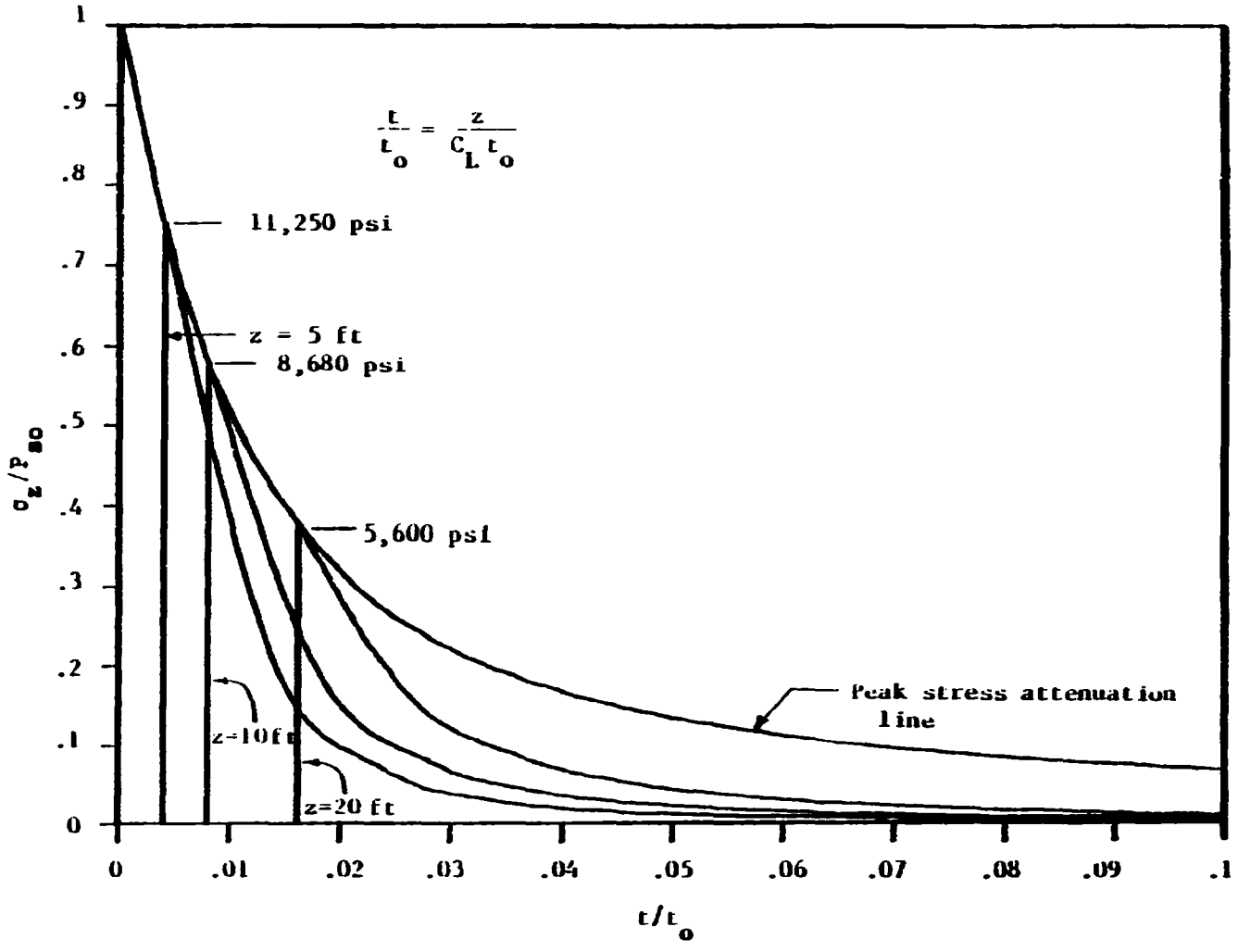

b. Expanded time scale - stress.

Figure 10. Normalized solutions for peak overpressure of 15,000 psi (continued).

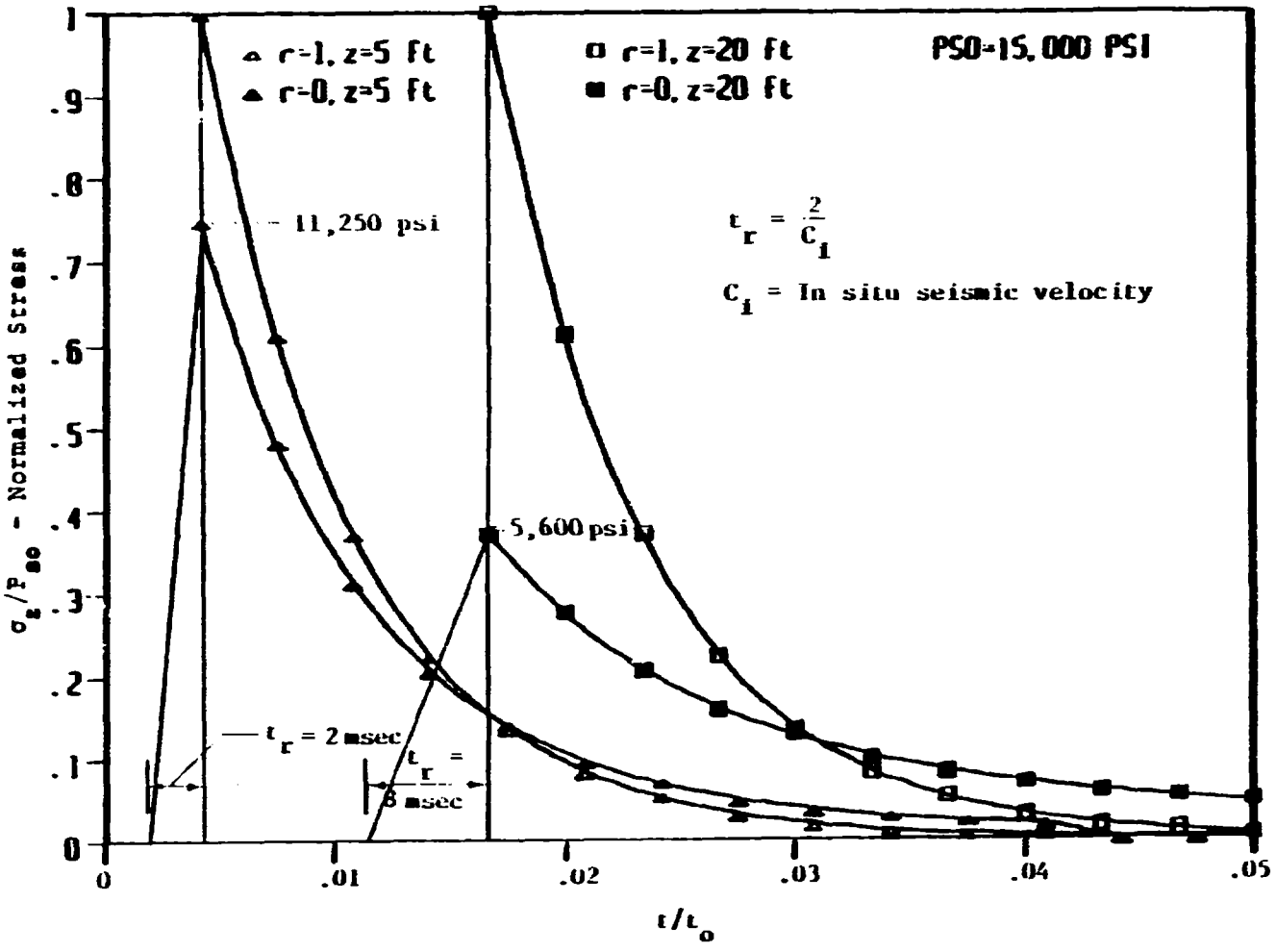

c. Normalized vertical stress as a function of strain recovery at depths of 5 and 20 ft, airblast-induced ground shock, 1-MT weapon, HOB = 0 ft.

Figure 10. Normalized solutions for peak overpressure of 15,000 psi (continued).

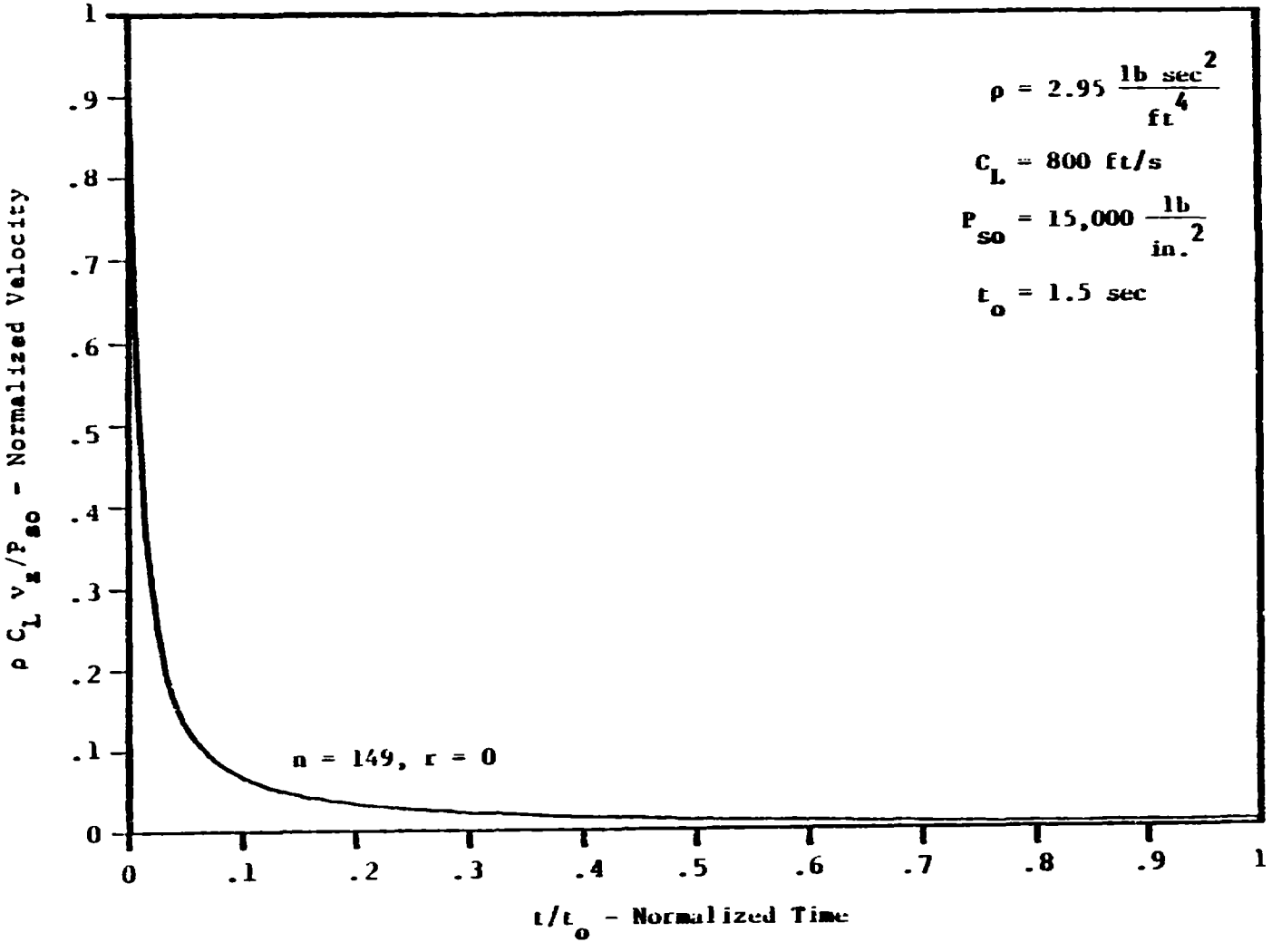

d. Normalized vertical particle velocity for peak overpressure of 15,000 psi airblast-induced ground shock, 1-MT weapon, HOB = 0 ft.

Figure 10. Normalized solutions for peak overpressure of 15,000 psi (continued).

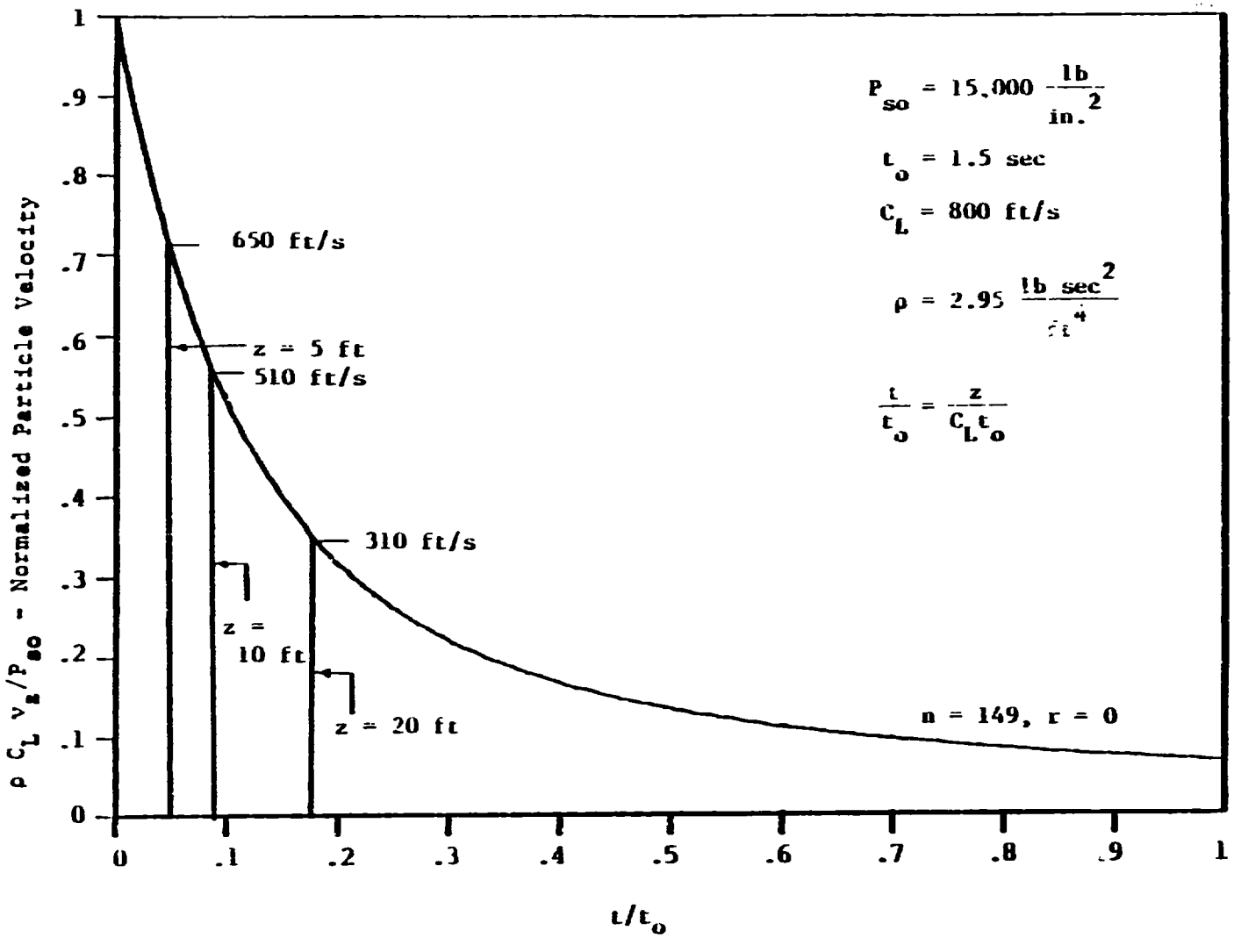

c. Expanded time scale - velocity.

Figure 10. Normalized solutions for peak overpressure of 15,000 psi (continued).

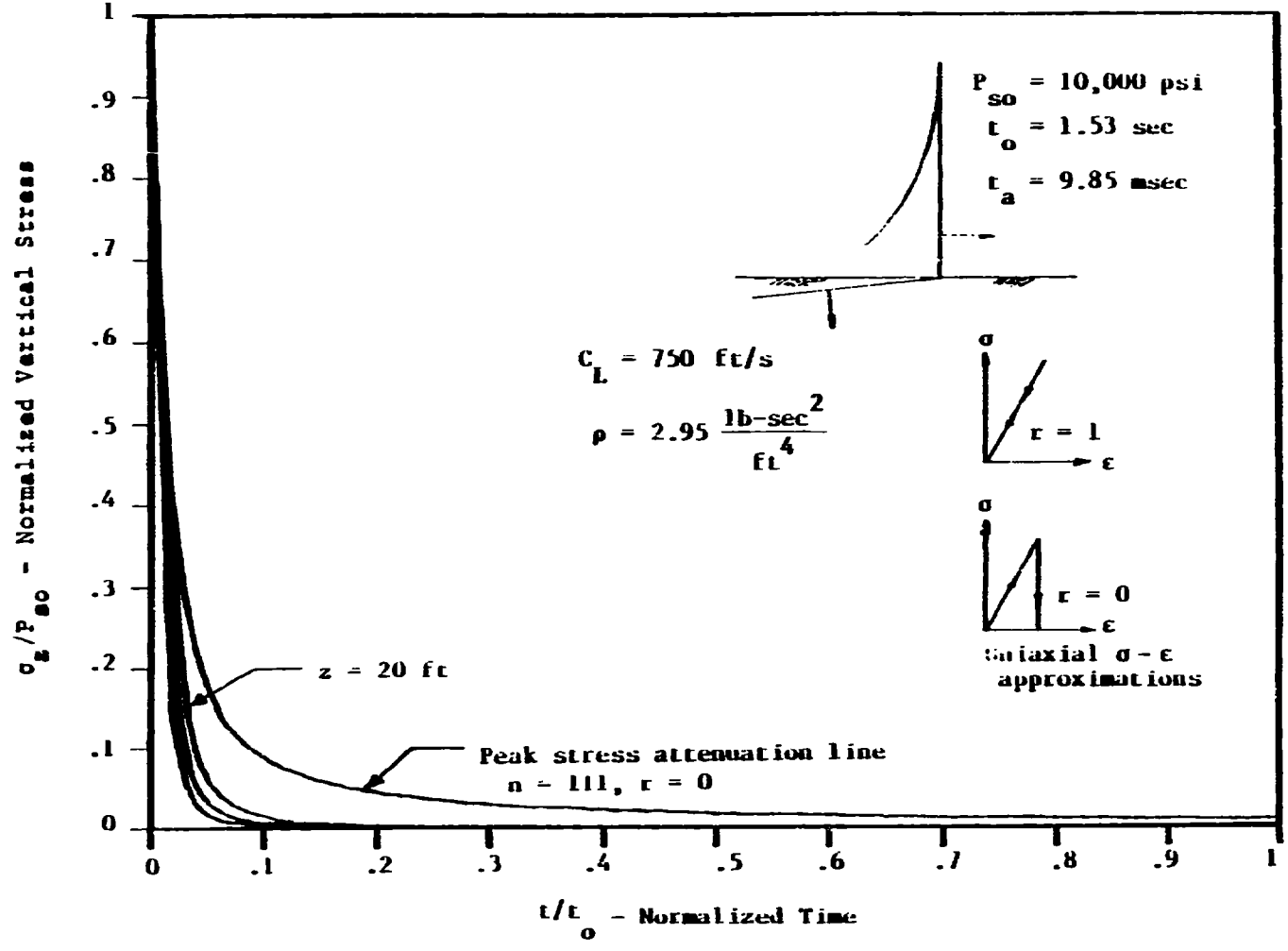

a. Normalized vertical stress at depths of 5, 10 and 20 ft for peak overpressure of 10,000 psi, airblast-induced ground shock, 1-MT weapon, HOB = 0 ft.

Figure 11. Normalized solutions for peak overpressure of 10,000 psi.

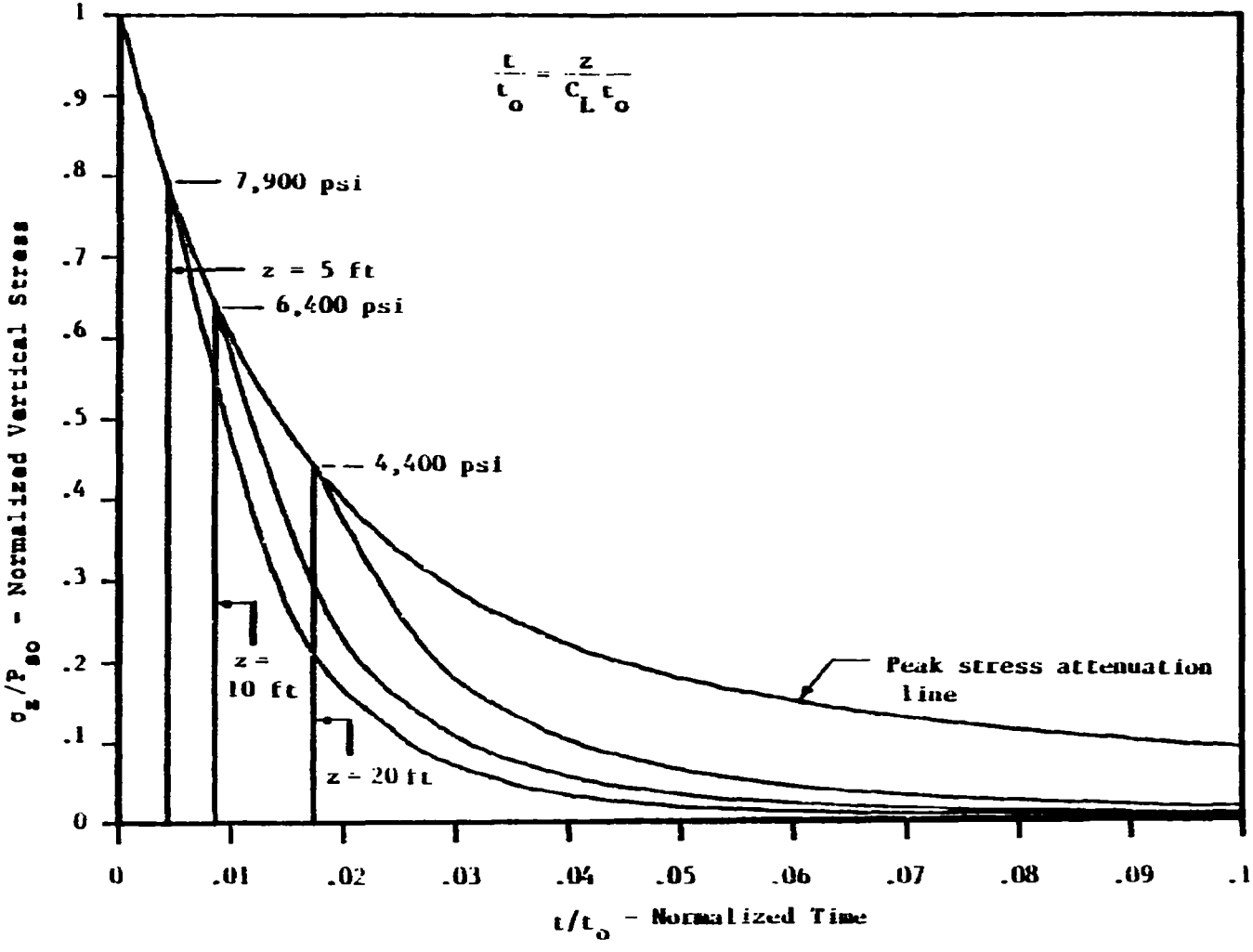

b. Expanded time scale - stress.

Figure 11. Normalized solutions for peak overpressure of 10,000 psi (continued).

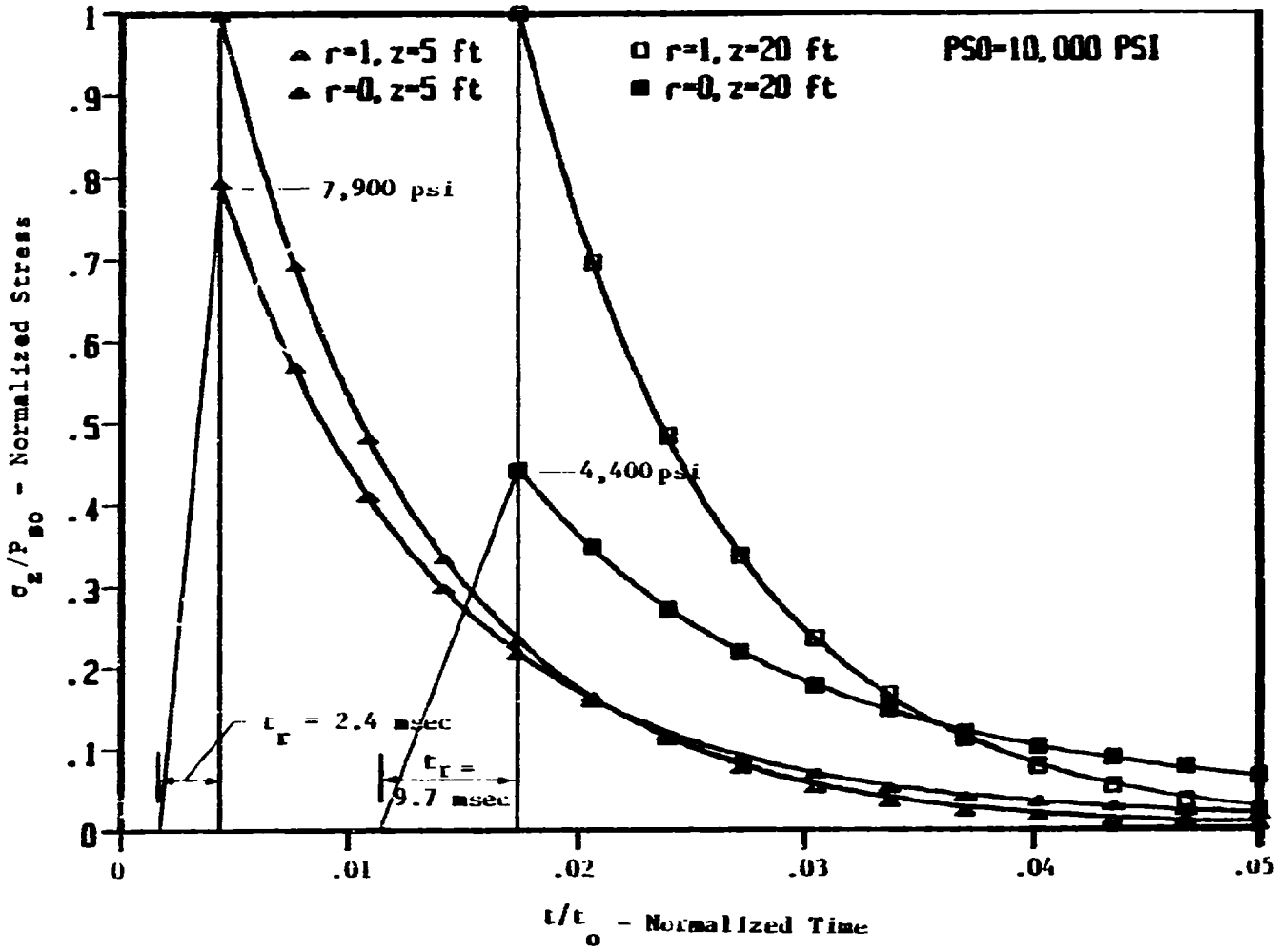

c. Normalized vertical stress as a function of strain recovery at depths of 5 and 20 ft, airblast-induced ground shock, 1-MT weapon, HOB = 0 ft.

Figure 11. Normalized solutions for peak overpressure of 10,000 psi (continued).

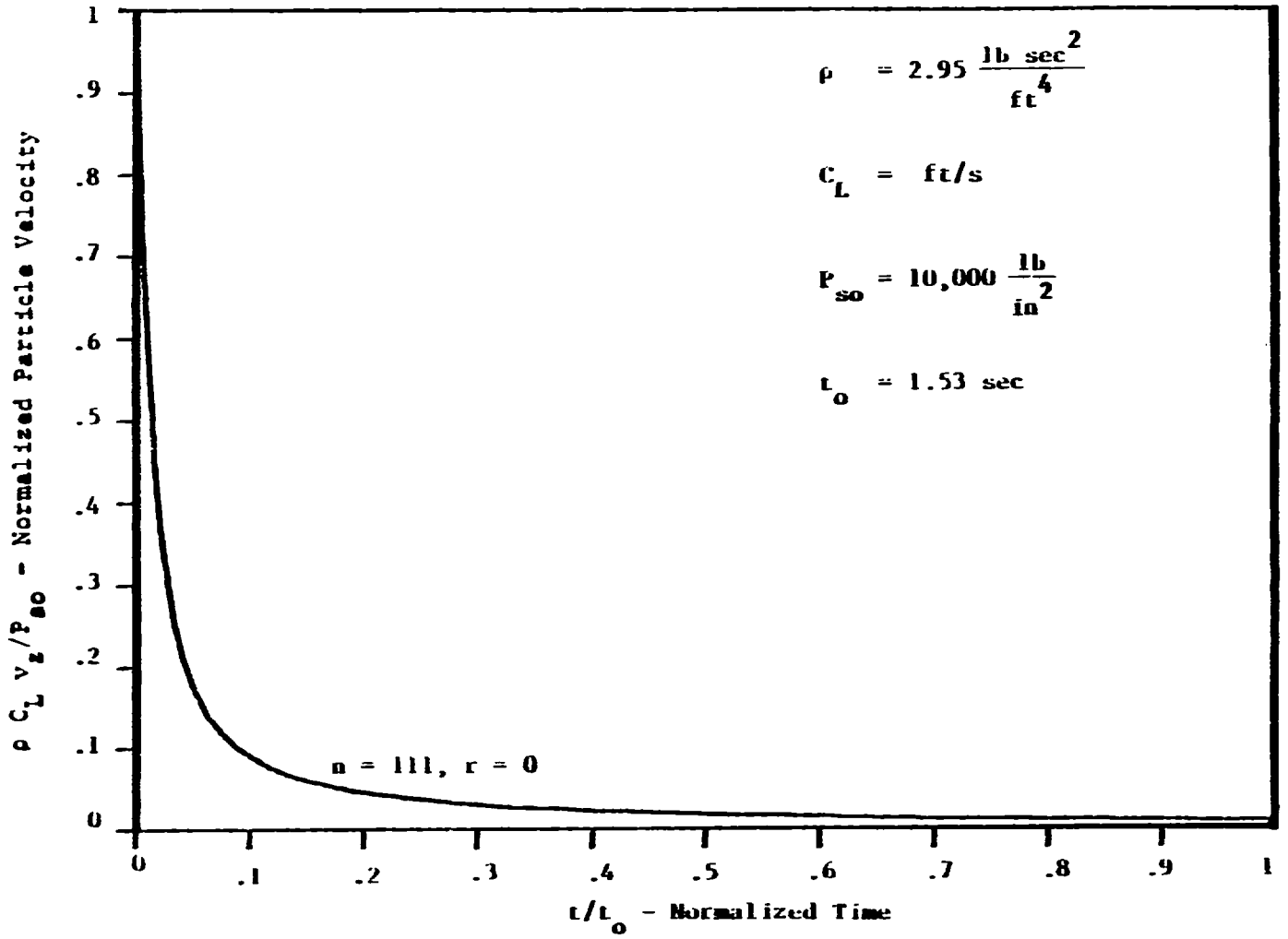

d. Normalized vertical particle velocity for peak overpressure of 10,000 psi, airblast-induced ground shock, 1-Mt weapon, HOB = 0 ft.

Figure 11. Normalized solutions for peak overpressure of 10,000 psi (continued).

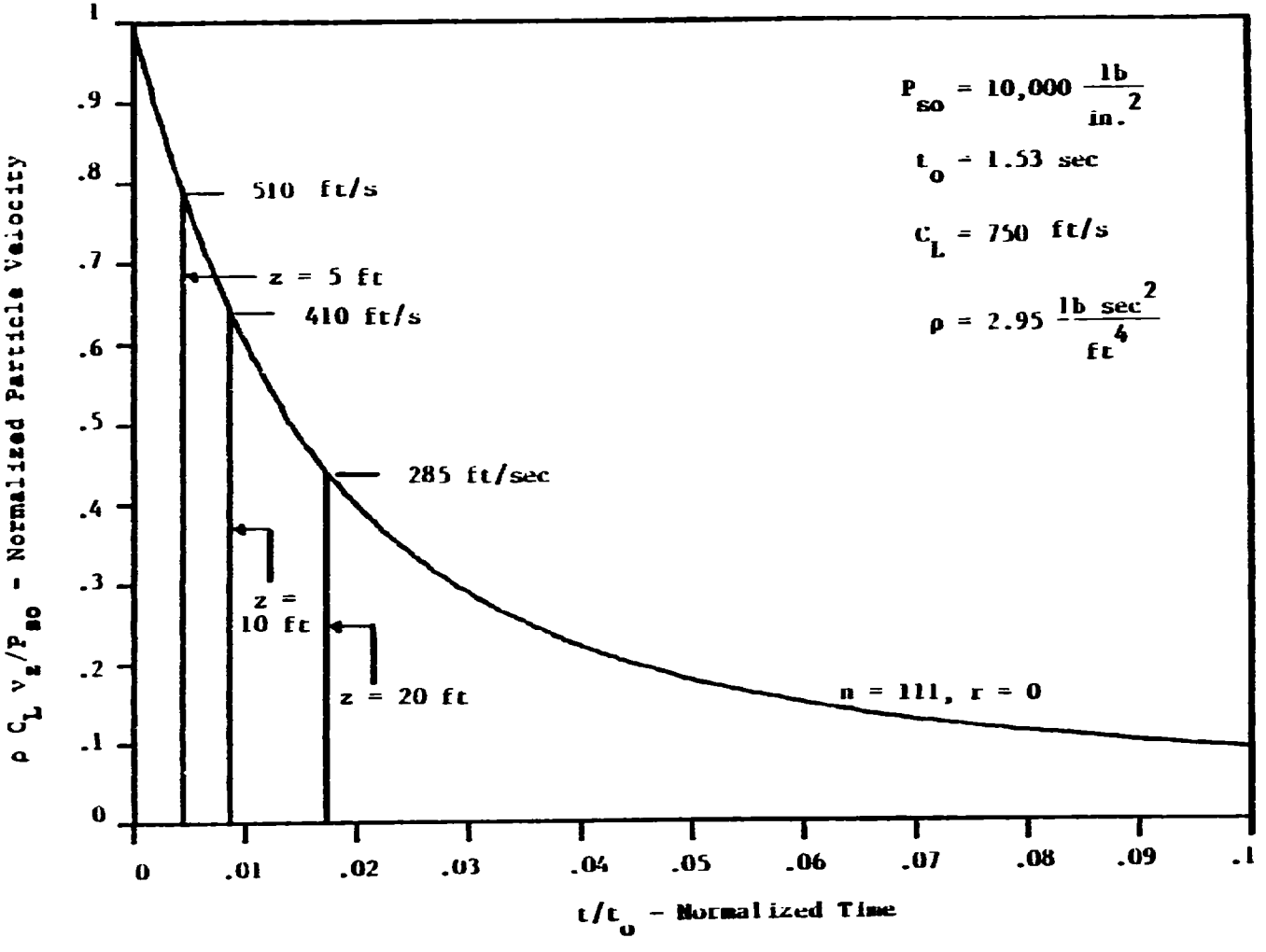

e. Expanded time scale - velocity.

Figure 11. Normalized solutions for peak overpressure of 10,000 psi (continued).

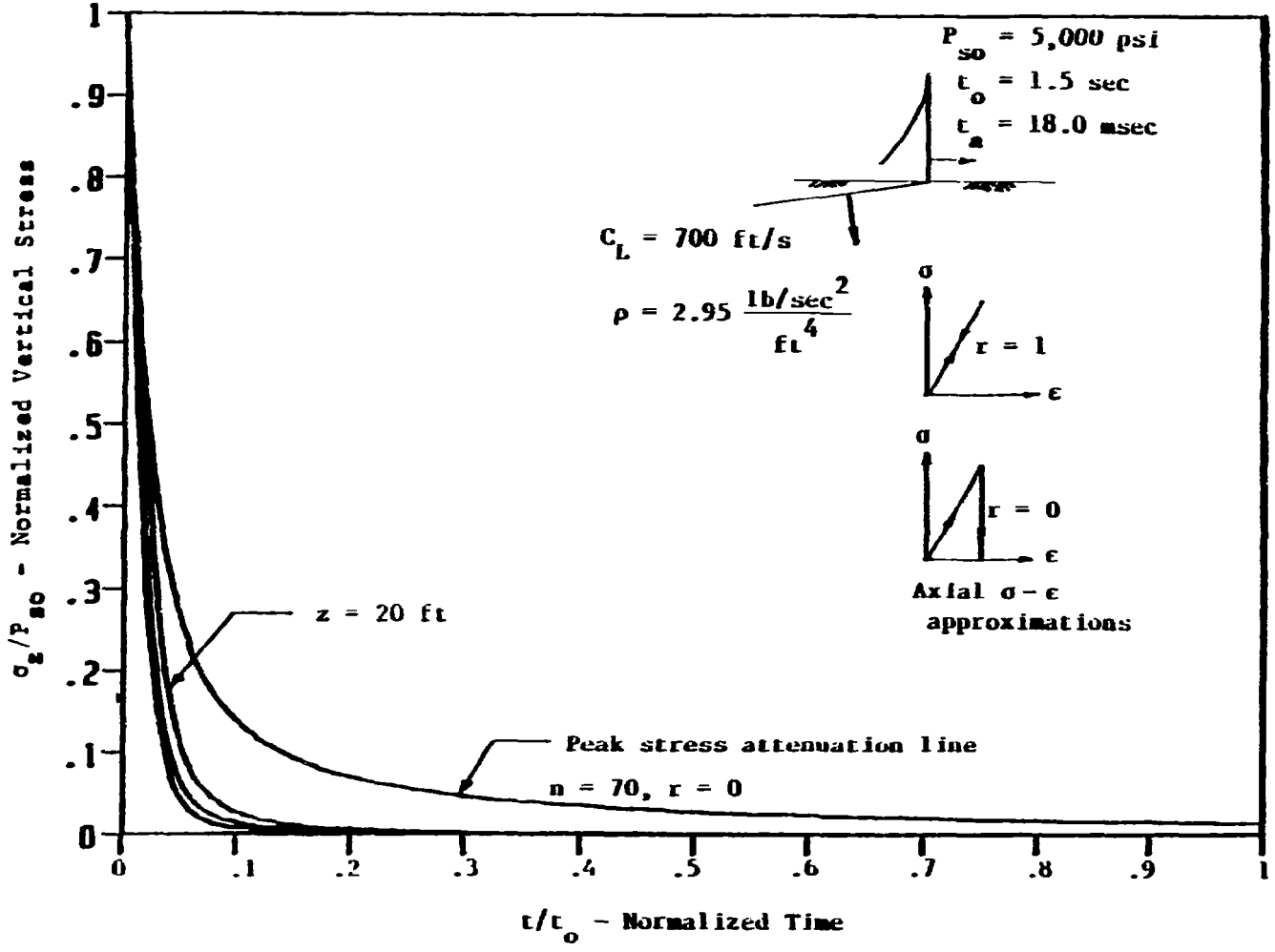

a. Normalized vertical stress at depths of 5, 10 and 20 ft for peak overpressure of 5,000 psi, airblast-induced ground shock, 1-MT weapon, HOB = 0 ft.

Figure 12. Normalized solutions for peak overpressure of 5,000 psi.

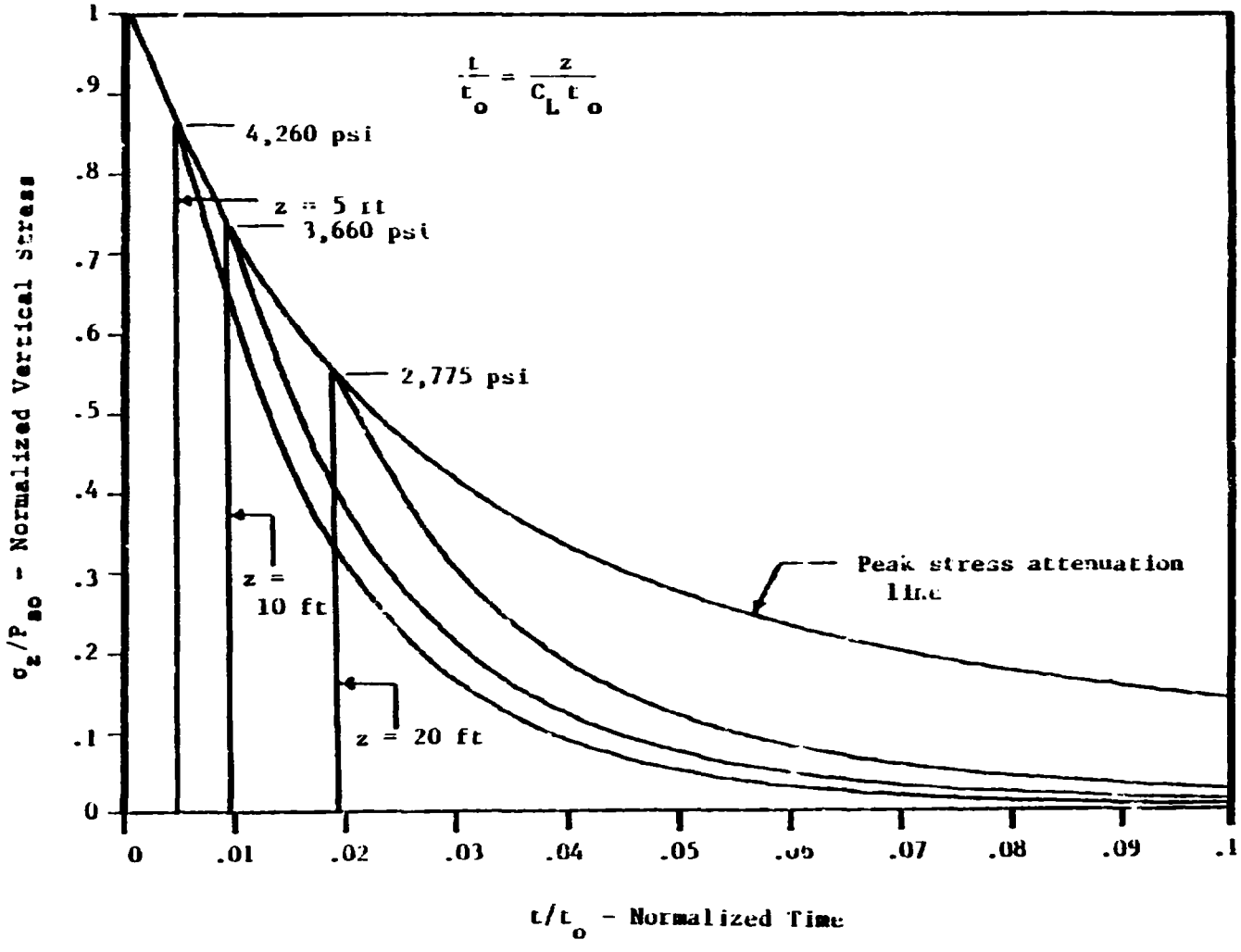

b. Expanded time scale - stress.

Figure 12. Normalized solutions for peak overpressure of 5,000 psi (continued).

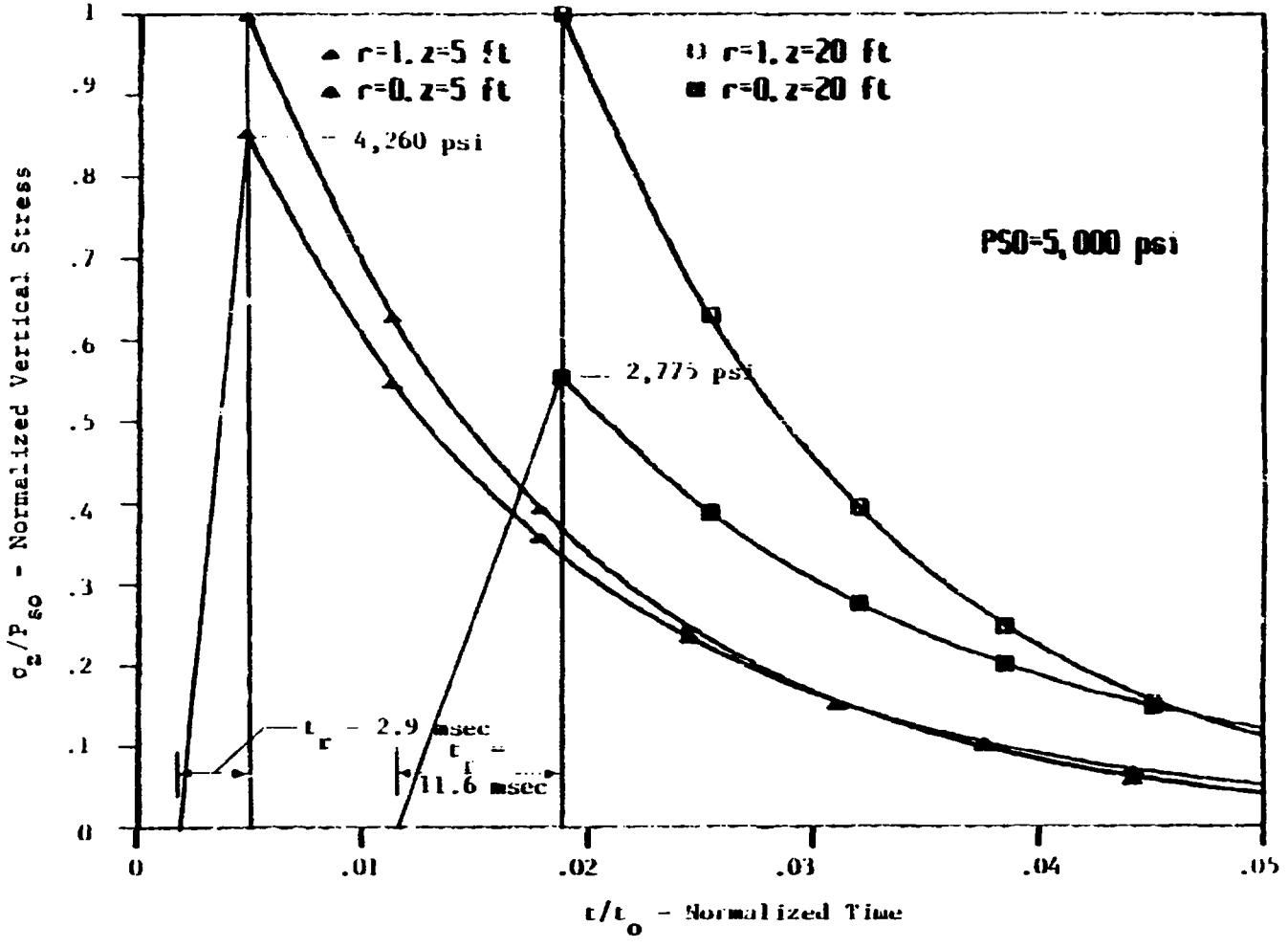

c. Normalized vertical stress as a function of strain recovery at depths of 5 and 20 ft, airblast-induced ground shock, 1-MT weapon, HOB = 0 ft.

Figure 12. Normalized solutions for peak overpressure of 5,000 psi (continued).

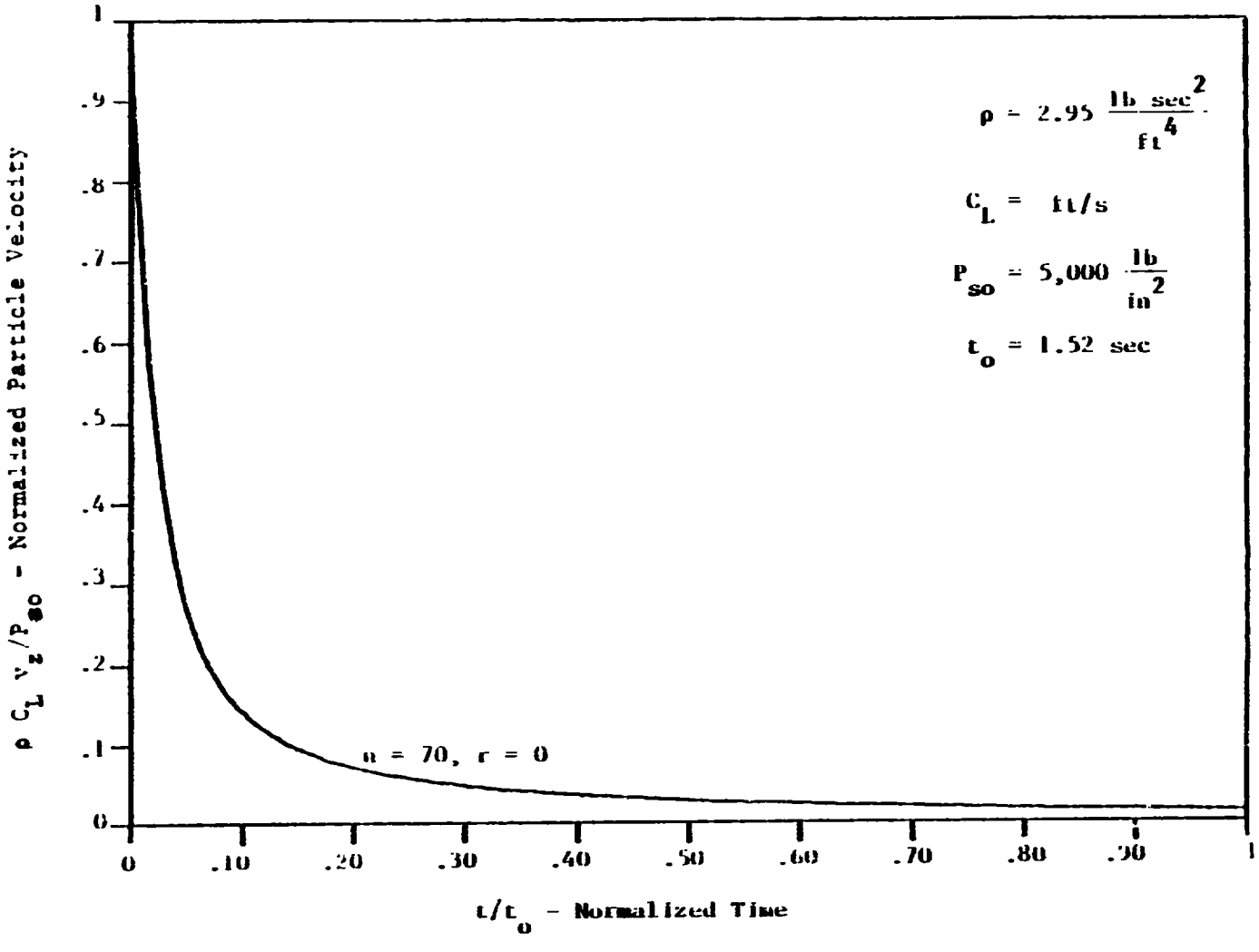

d. Normalized vertical particle velocity for peak overpressure of 5,000 psi, airblast-induced ground shock, 1-MT weapon, HOB = 0 ft.

Figure 12. Normalized solutions for peak overpressure of 5,000 psi (continued).

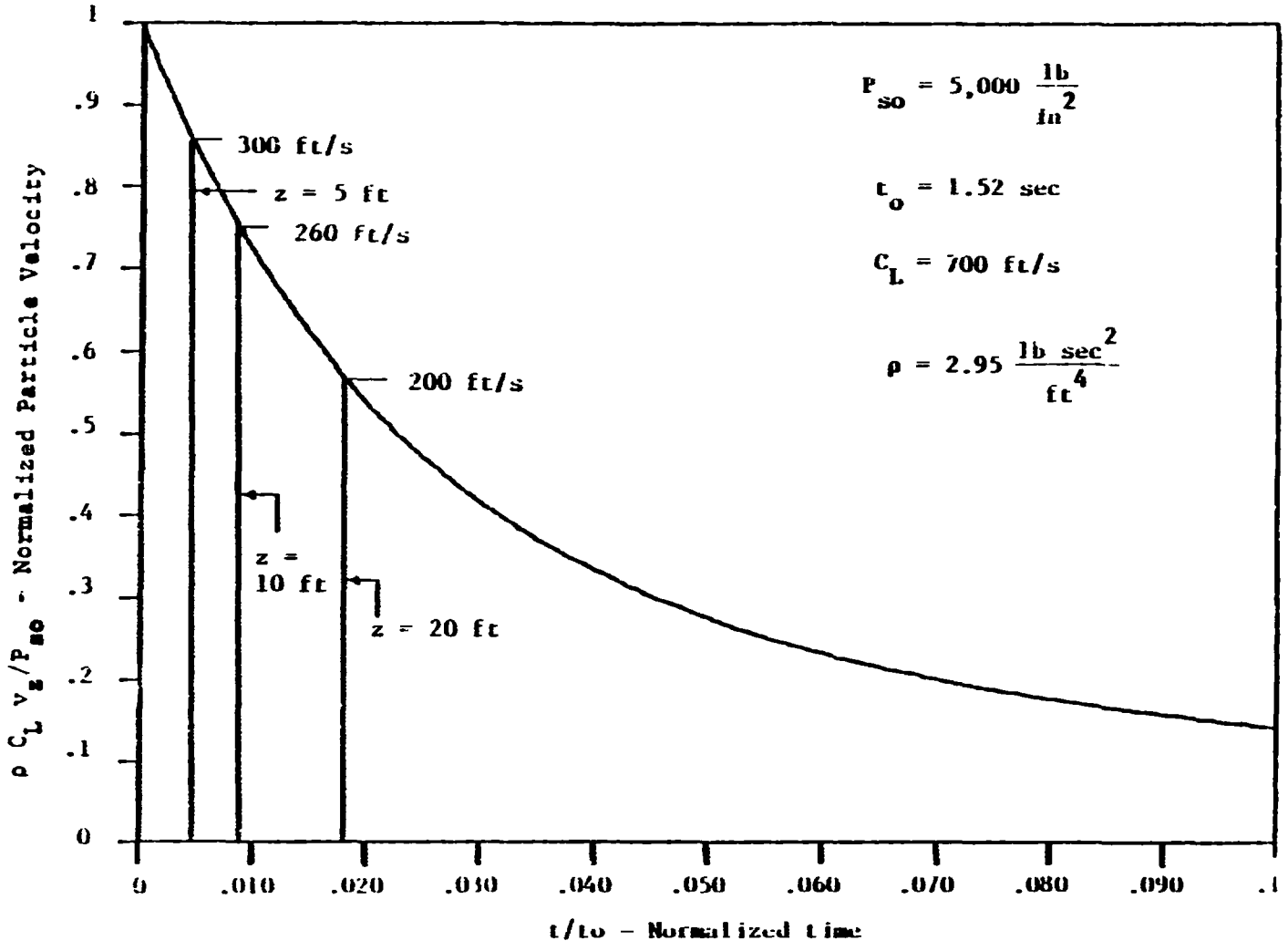

e. Expanded time scale - velocity.

Figure 12. Normalized solutions for peak overpressure of 5,000 psi (continued).

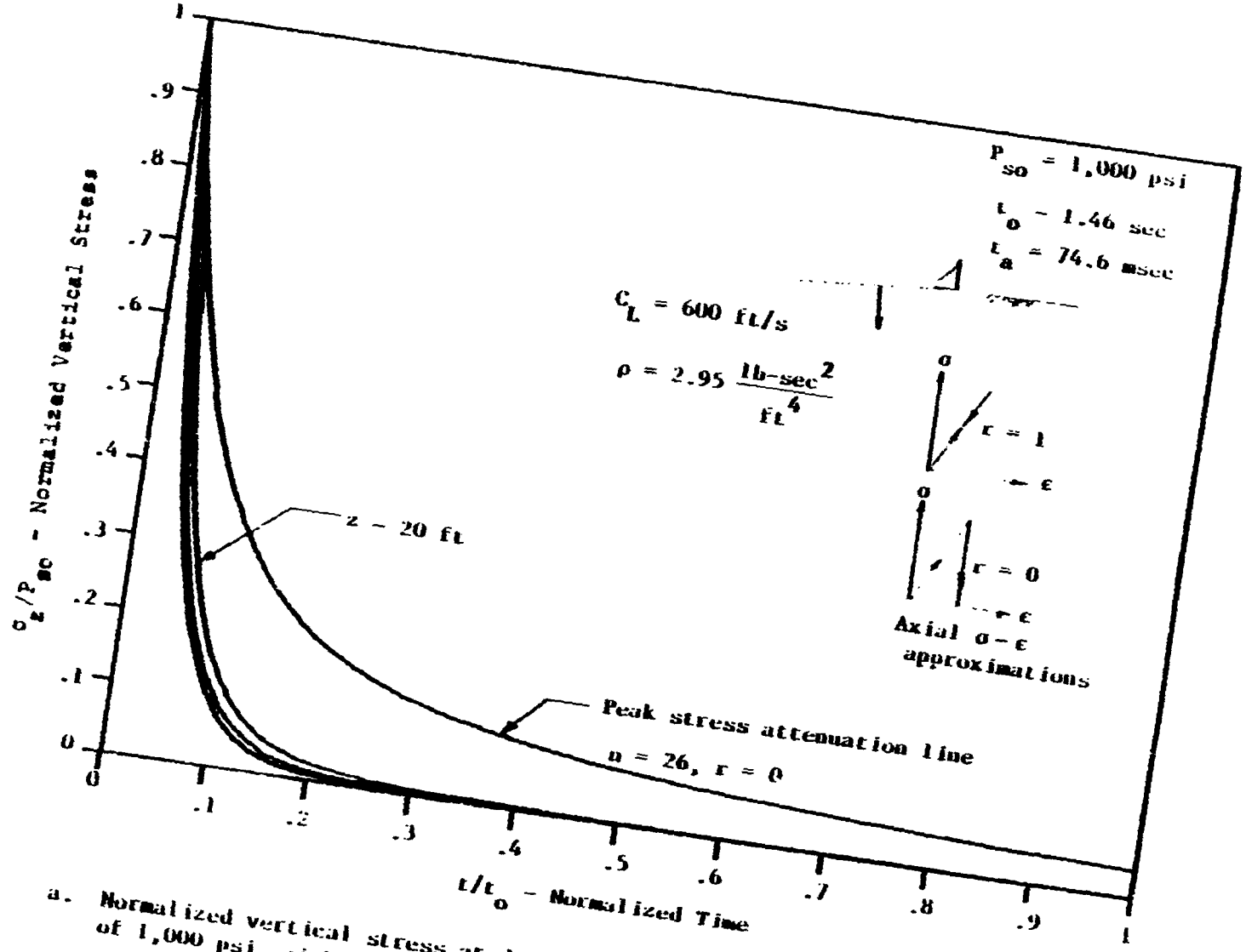

a. Normalized vertical stress at depths of 5, 10 and 20 ft for peak overpressure of 1,000 psi, airblast induced ground shock, 1-MT weapon, HOB = 0 ft.

Figure 13. Normalized solutions for peak overpressure of 1,000 psi.

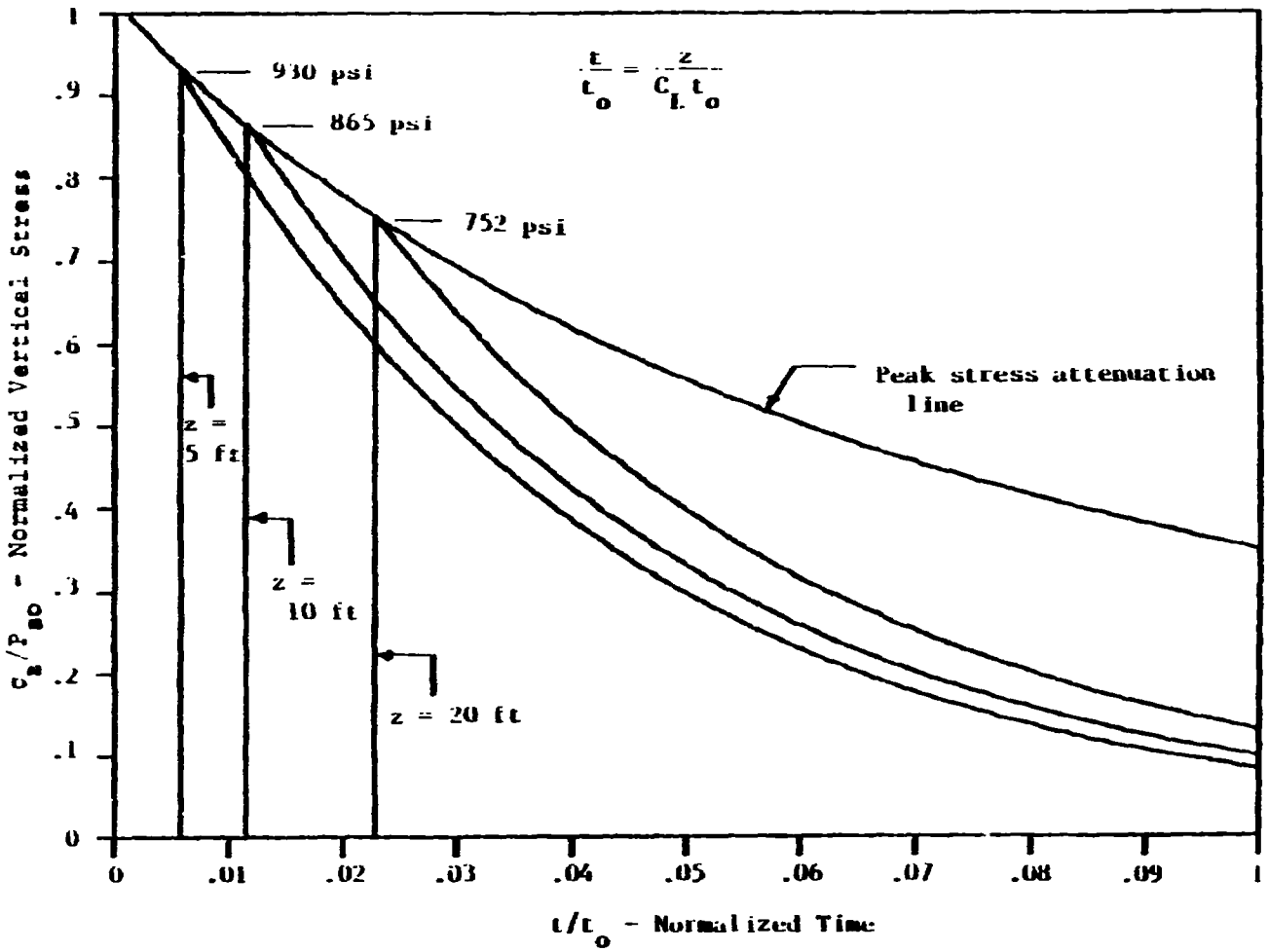

b. Expanded time scale - stress.

Figure 13. Normalized solutions for peak overpressure of 1,000 psi (continued).

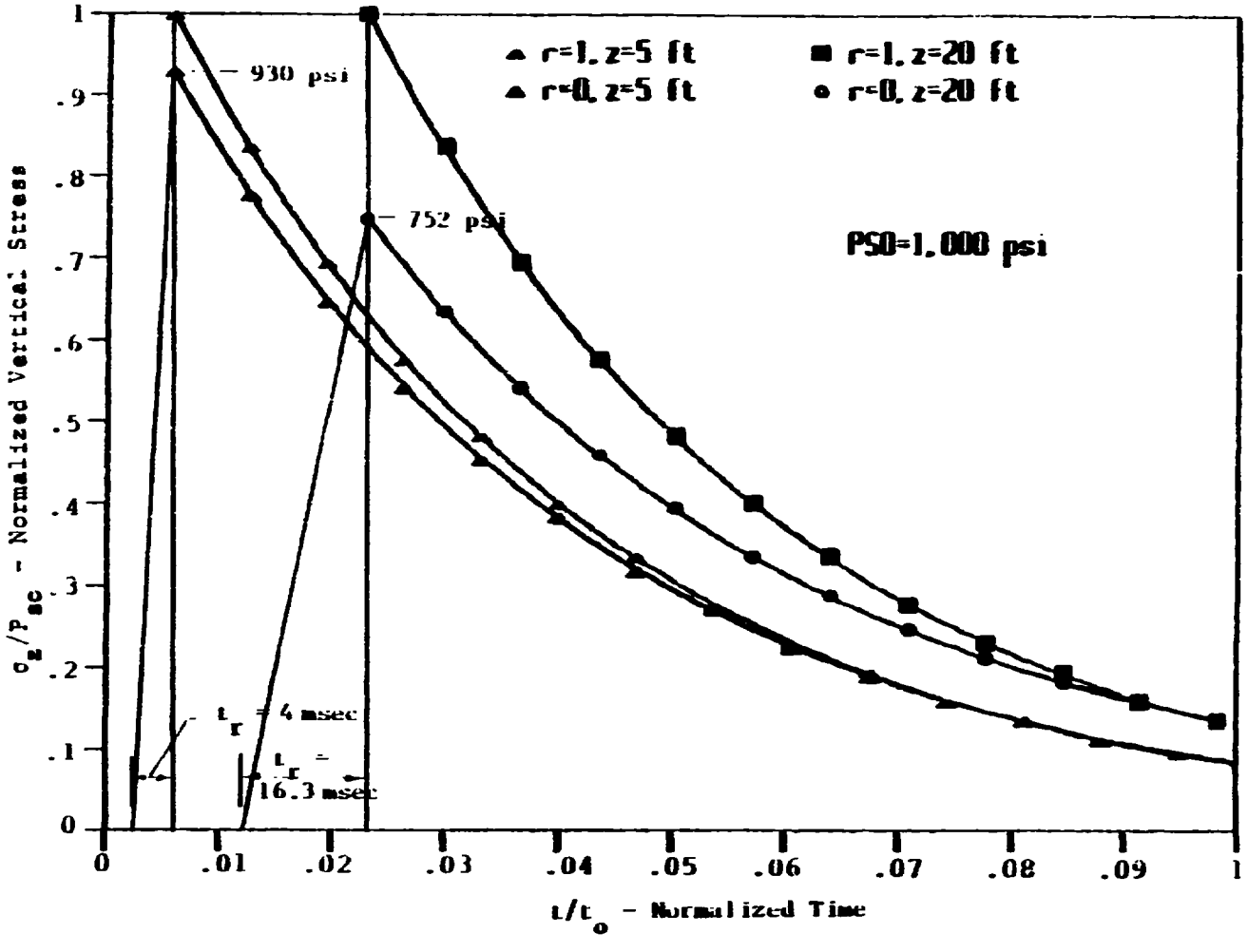

c. Normalized vertical stress as a function of strain recovery at depths of 5 and 20 ft, airblast-induced ground shock, 1-MT weapon, HOB = 0 ft.

Figure 13. Normalized solutions for peak overpressure of 1,000 psi (continued).

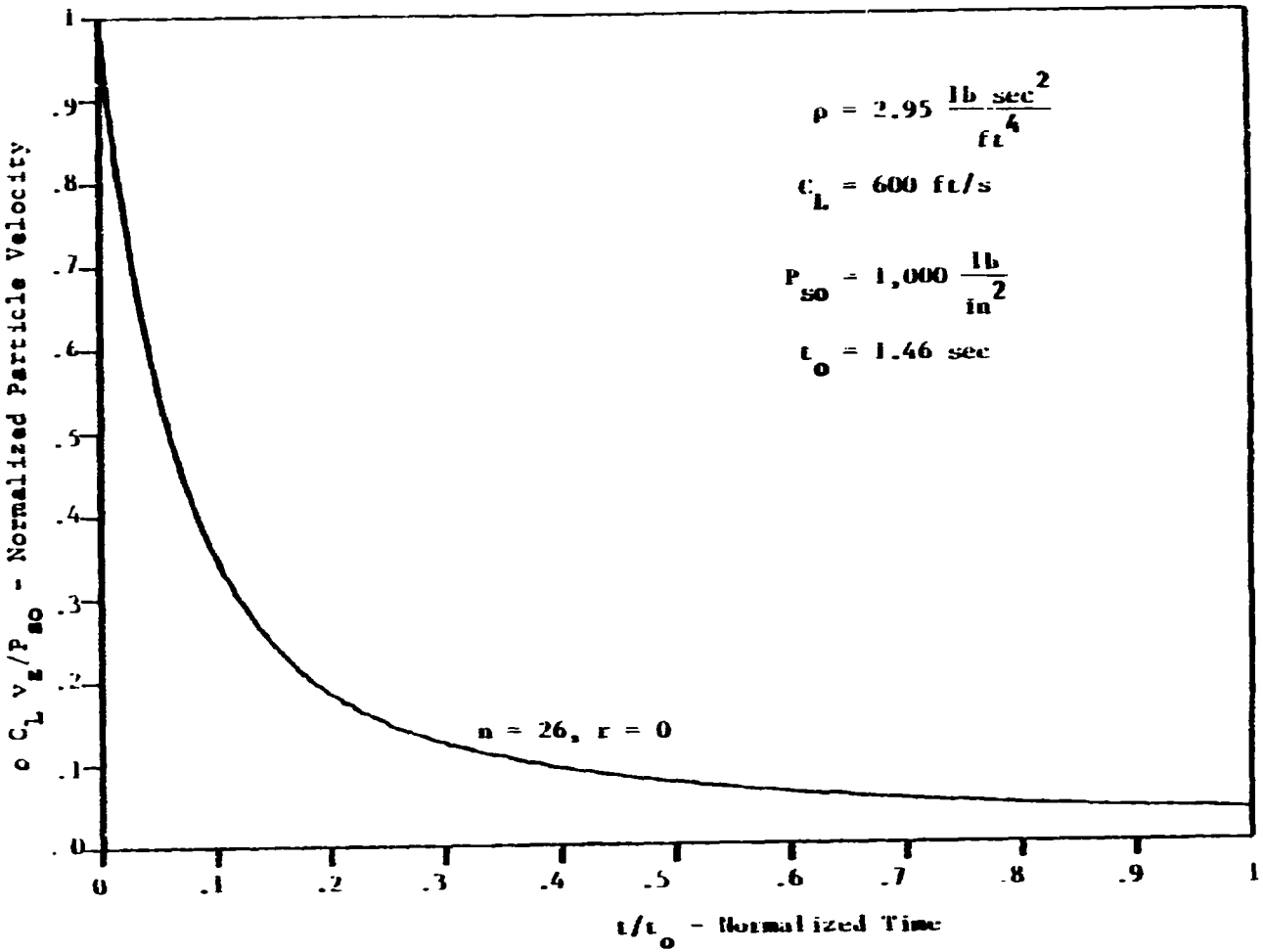

d. Normalized vertical particle velocity for peak overpressure of 1,000 psi, airblast-induced ground shock, 1-MT weapon, HOB = 0 ft.

Figure 13. Normalized solutions for peak overpressure of 1,000 psi (continued).

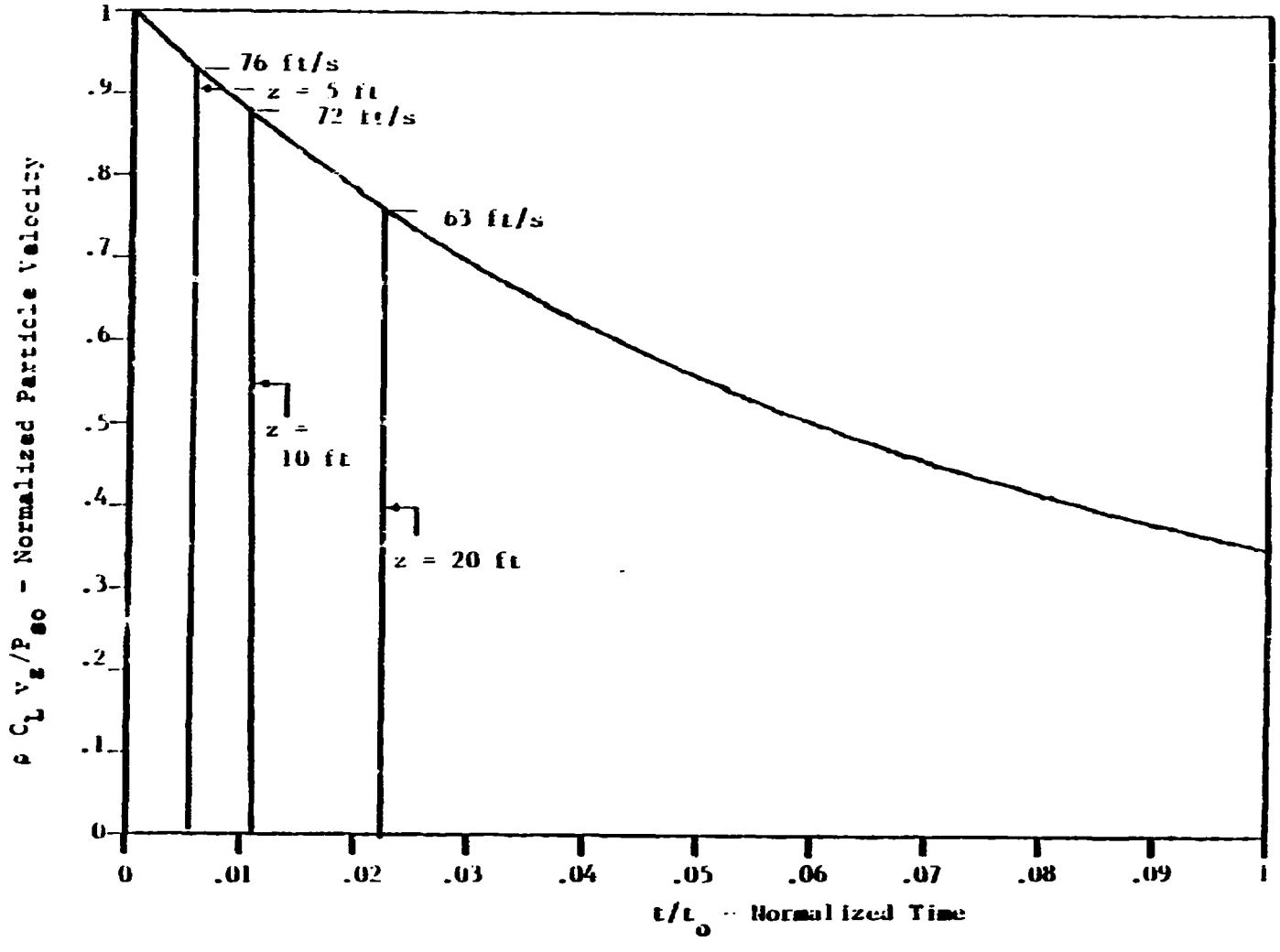

e. Expanded time scale - velocity.

Figure 13. Normalized solutions for peak overpressure of 1,000 psi (continued).

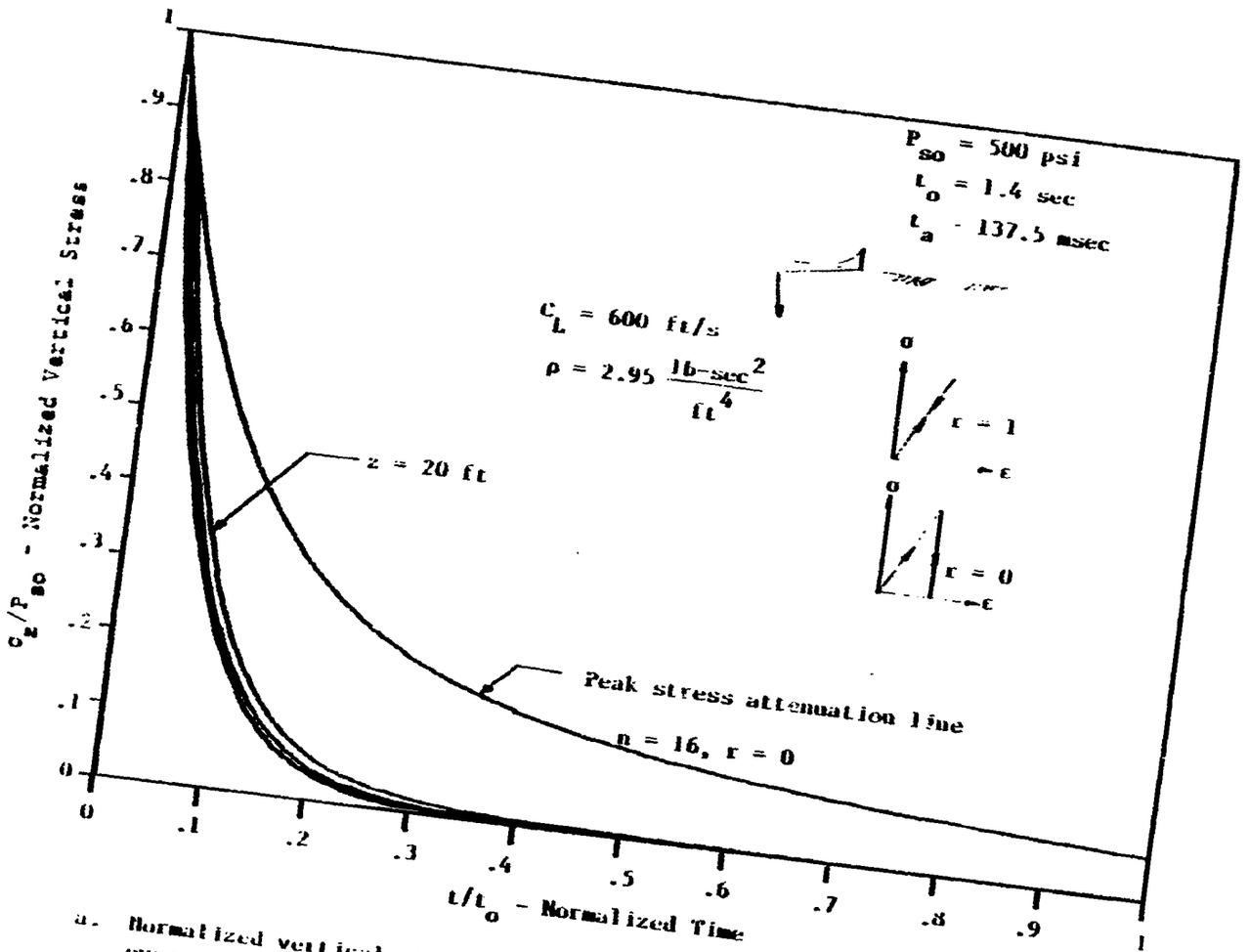

a. Normalized vertical stress at depths of 5, 10 and 20 ft for peak overpressure pf 500 psi, airblast-induced ground shock, 1-MT weapon, HOB = 0 ft.

Figure 14. Normalized solutions for peak overpressure of 500 psi.

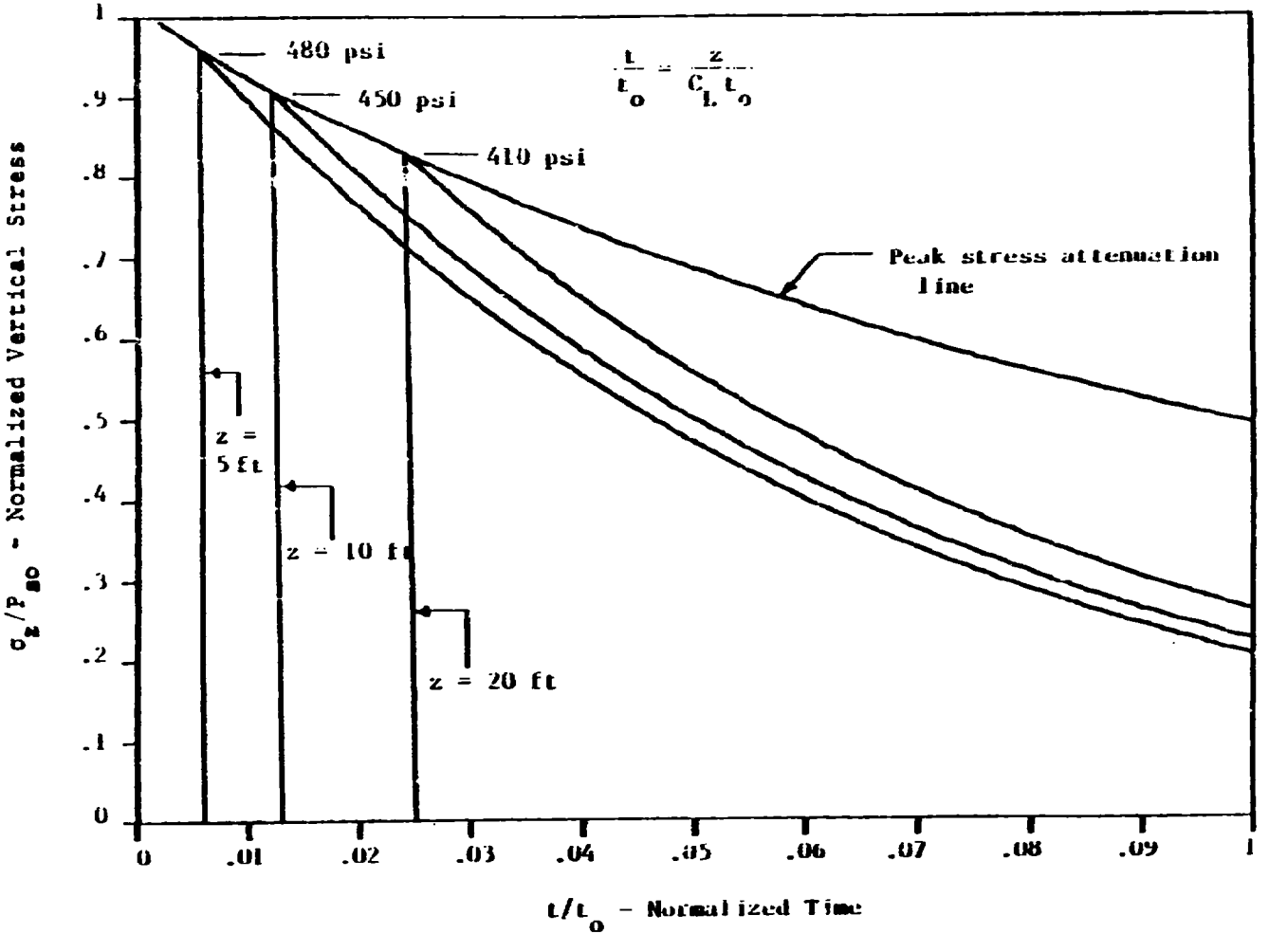

b. Expanded time scale - stress.

Figure 14. Normalized solutions for peak overpressure of 500 psi (continued).

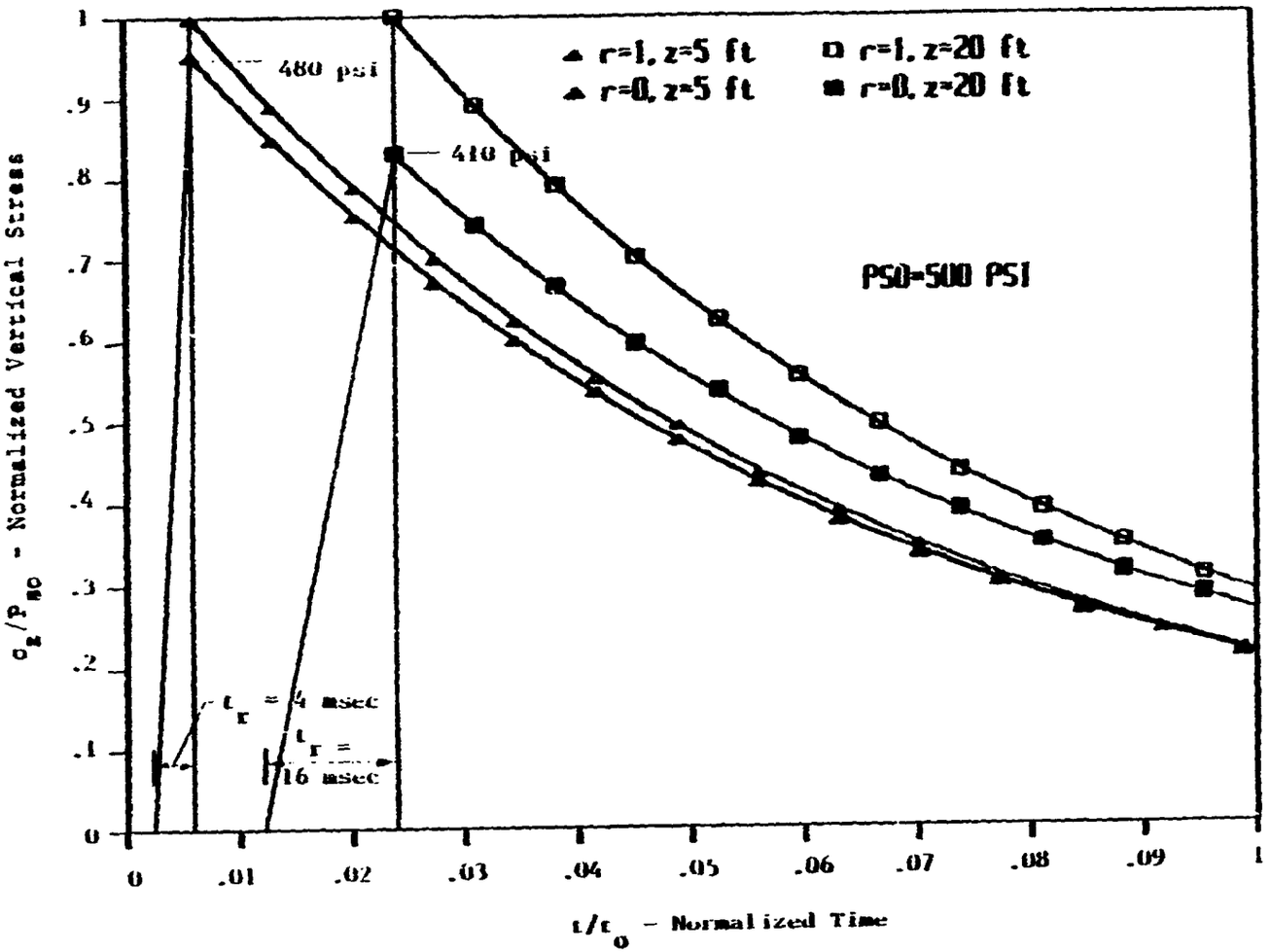

c. Normalized vertical stress as a function of strain recovery at depths of 5 and 20 ft, airblast-induced ground shock, 1-MT weapon, HOB = 0 ft.

Figure 14. Normalized solutions for peak overpressure of 500 psi (continued).

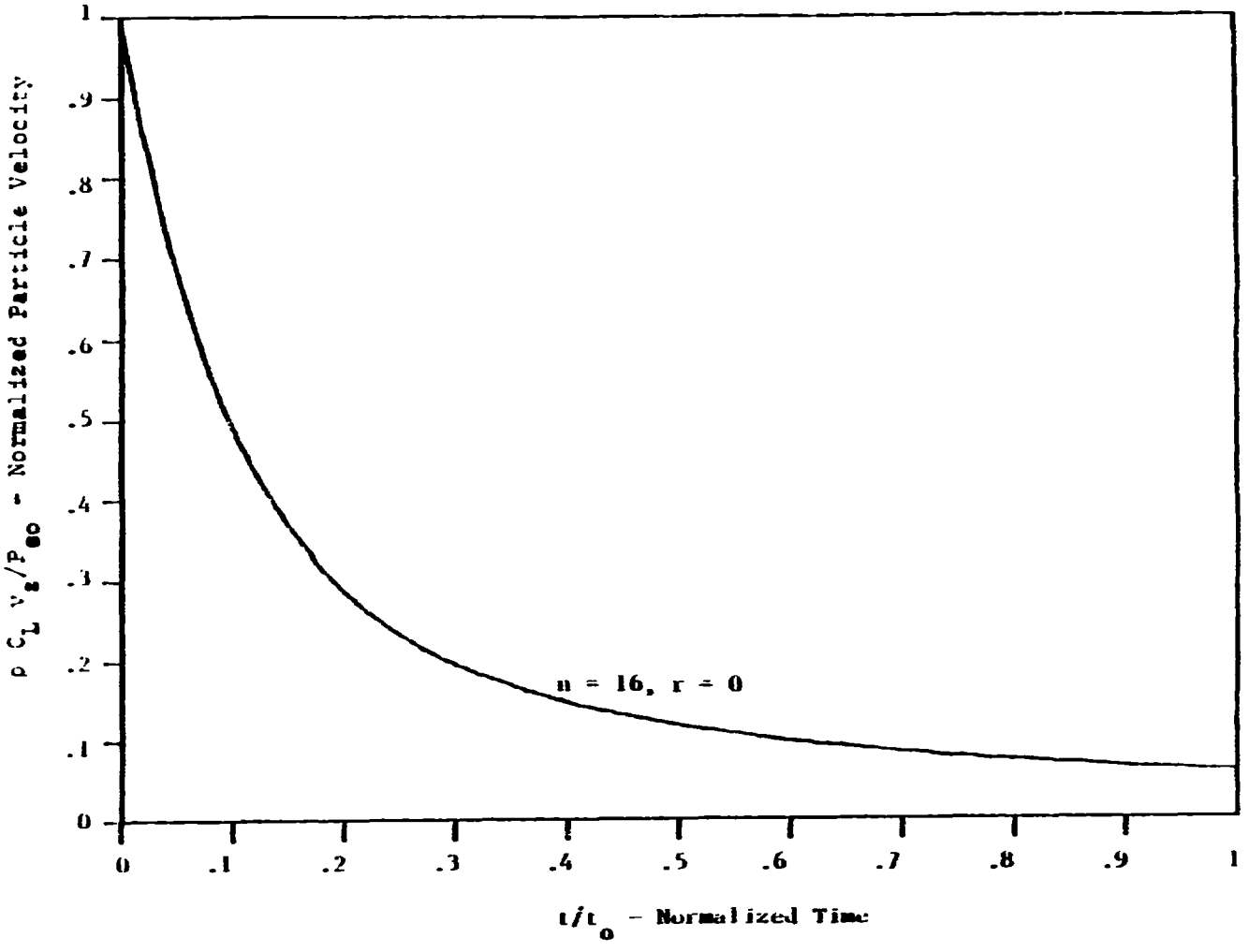

d. Normalized vertical particle velocity for peak overpressure of 500 psi, airblast-induced ground shock, I-MT weapon, HOB = 0 ft.

Figure 14. Normalized solutions for peak overpressure of 500 psi (continued).

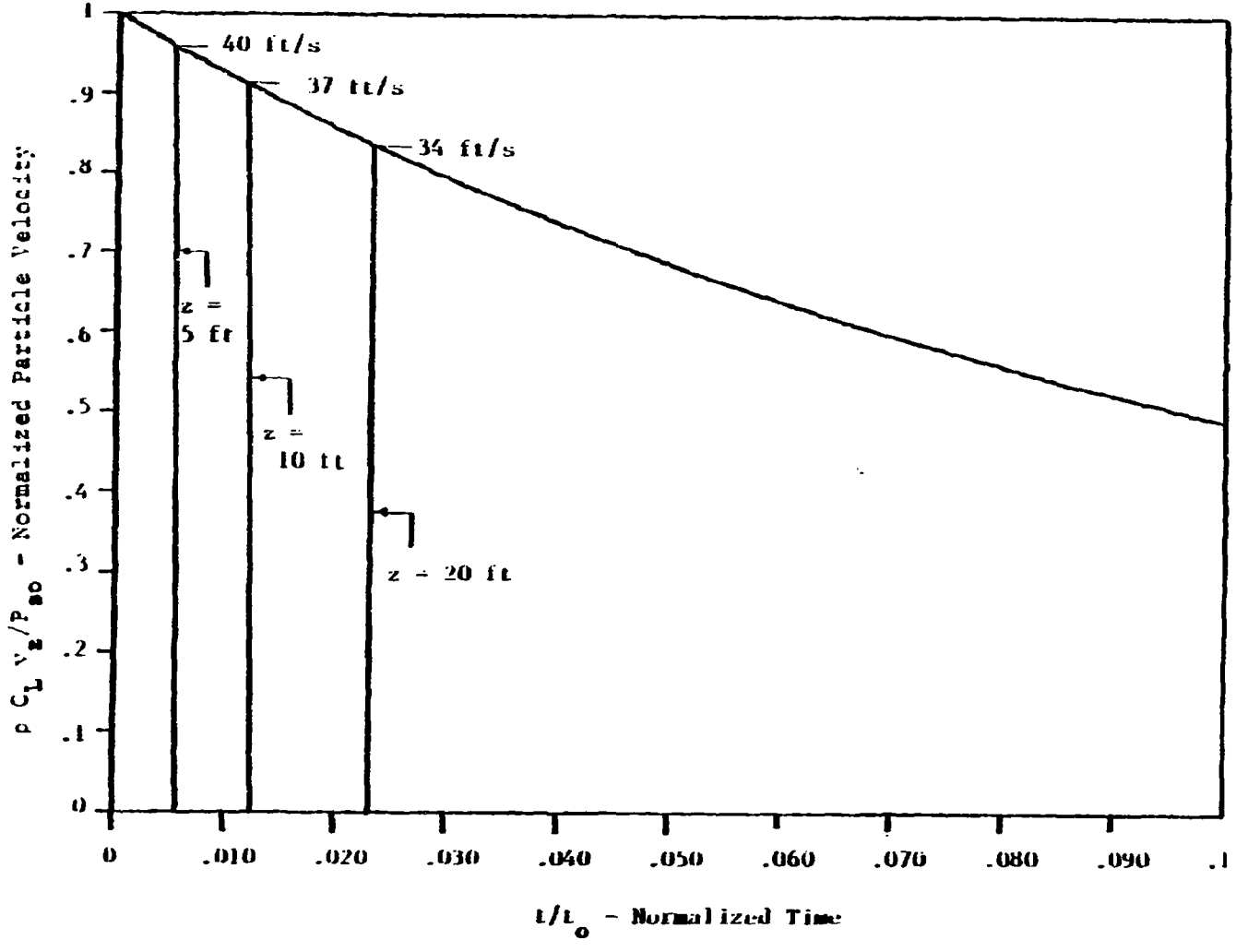

e. Expanded time scale - velocity.

Figure 14. Normalized solutions for peak overpressure of 500 psi (continued).

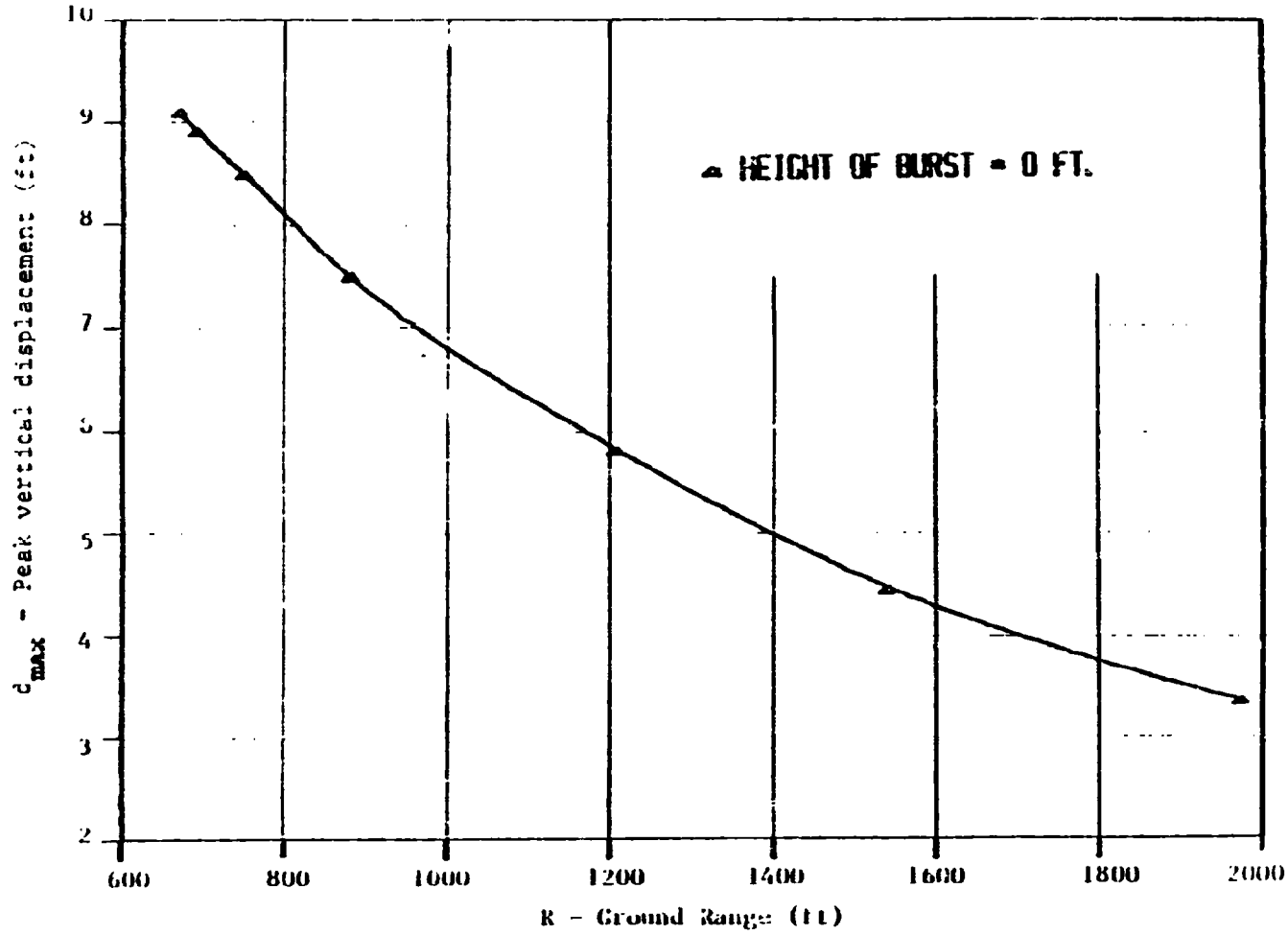

Figure 15. Peak vertical displacement versus range for airblast-induced ground shock, 1-MT weapon, HOB = 0 ft.

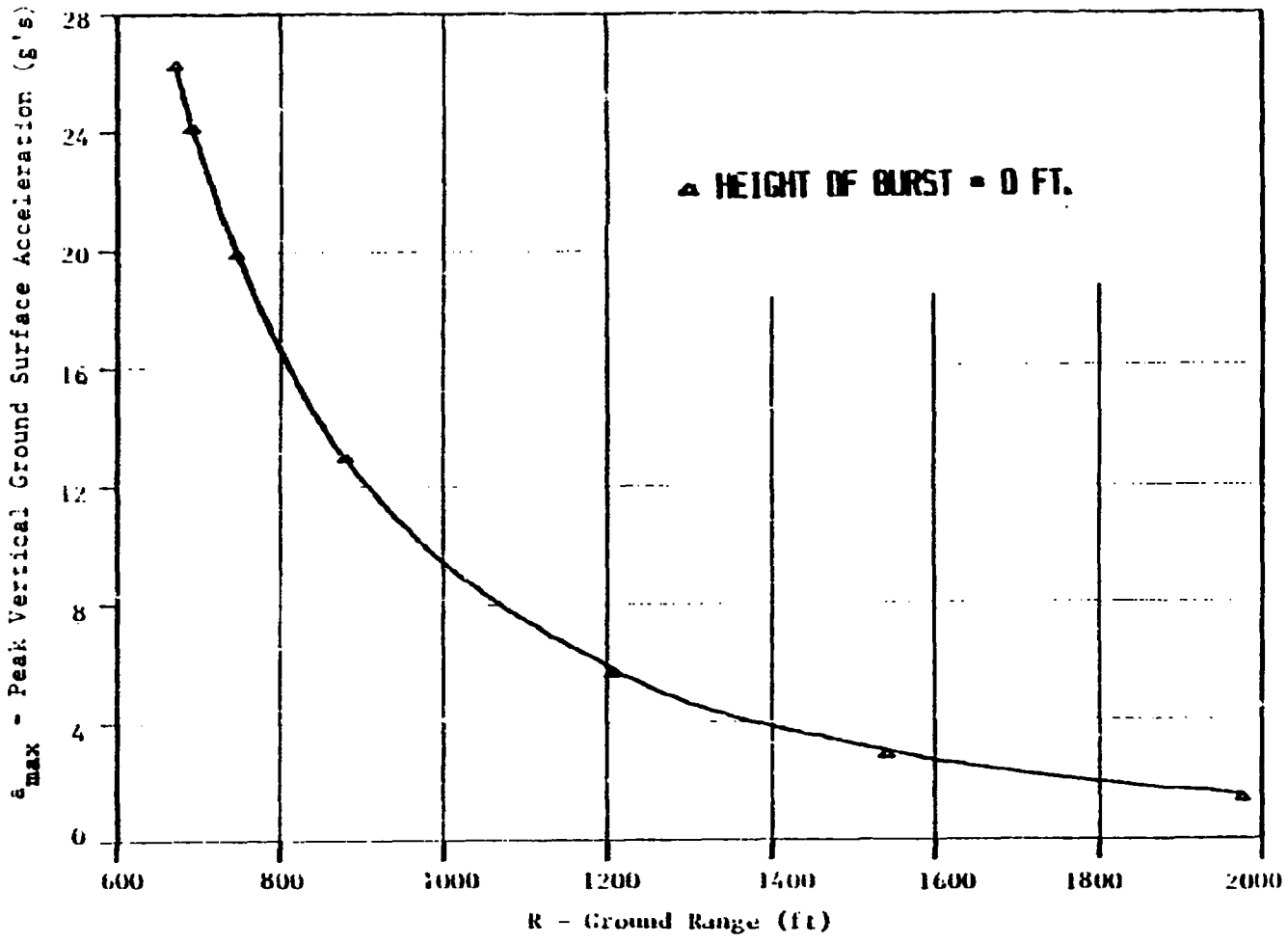

Figure 16. Peak vertical surface acceleration versus range for airblast-induced ground shock, 1-Mt weapon, HOB = 0.

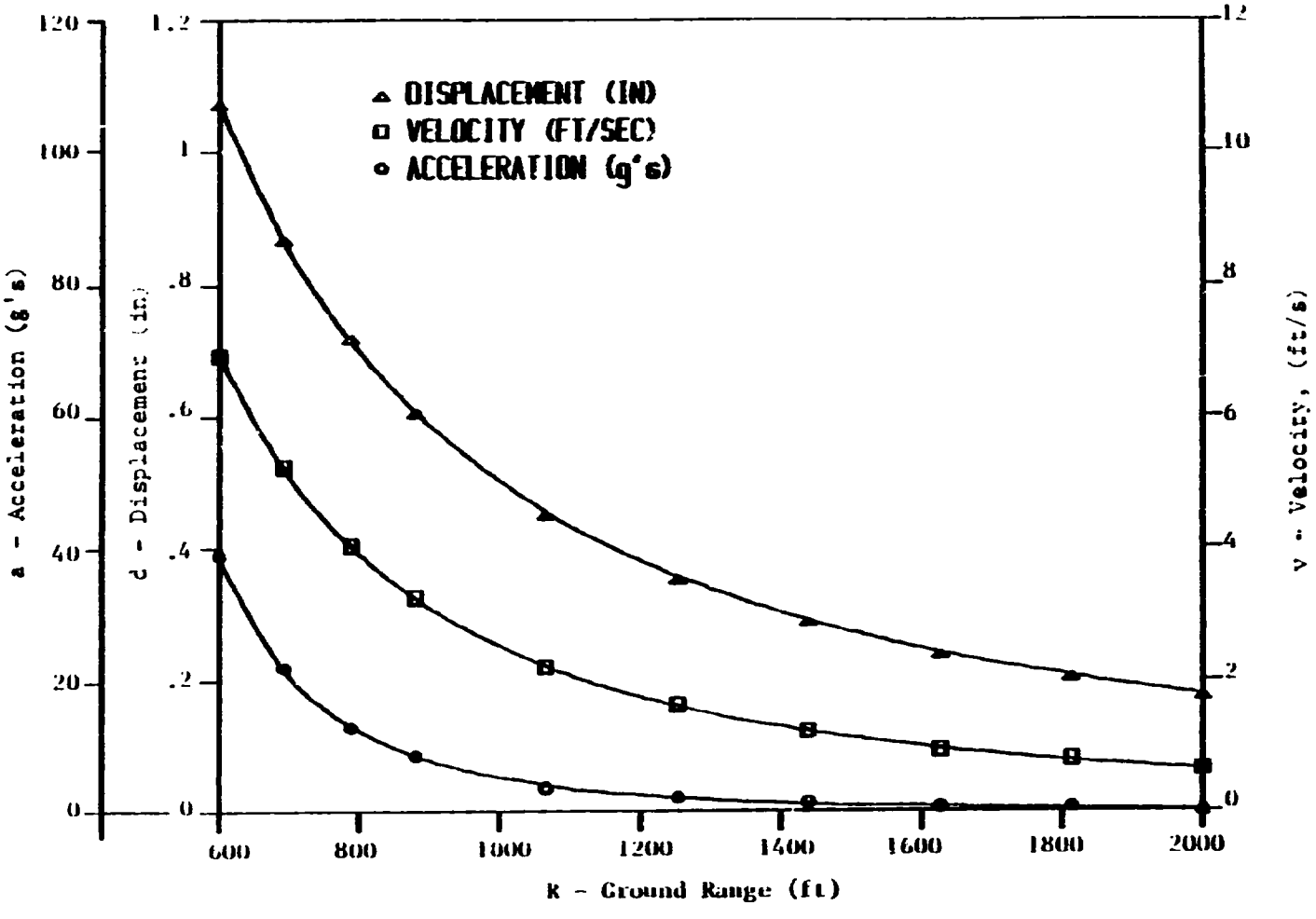

Figure 17. Peak near-surface horizontal displacement, velocity and acceleration for direct-induced ground shock, 1-MT weapon, HOB = 0.

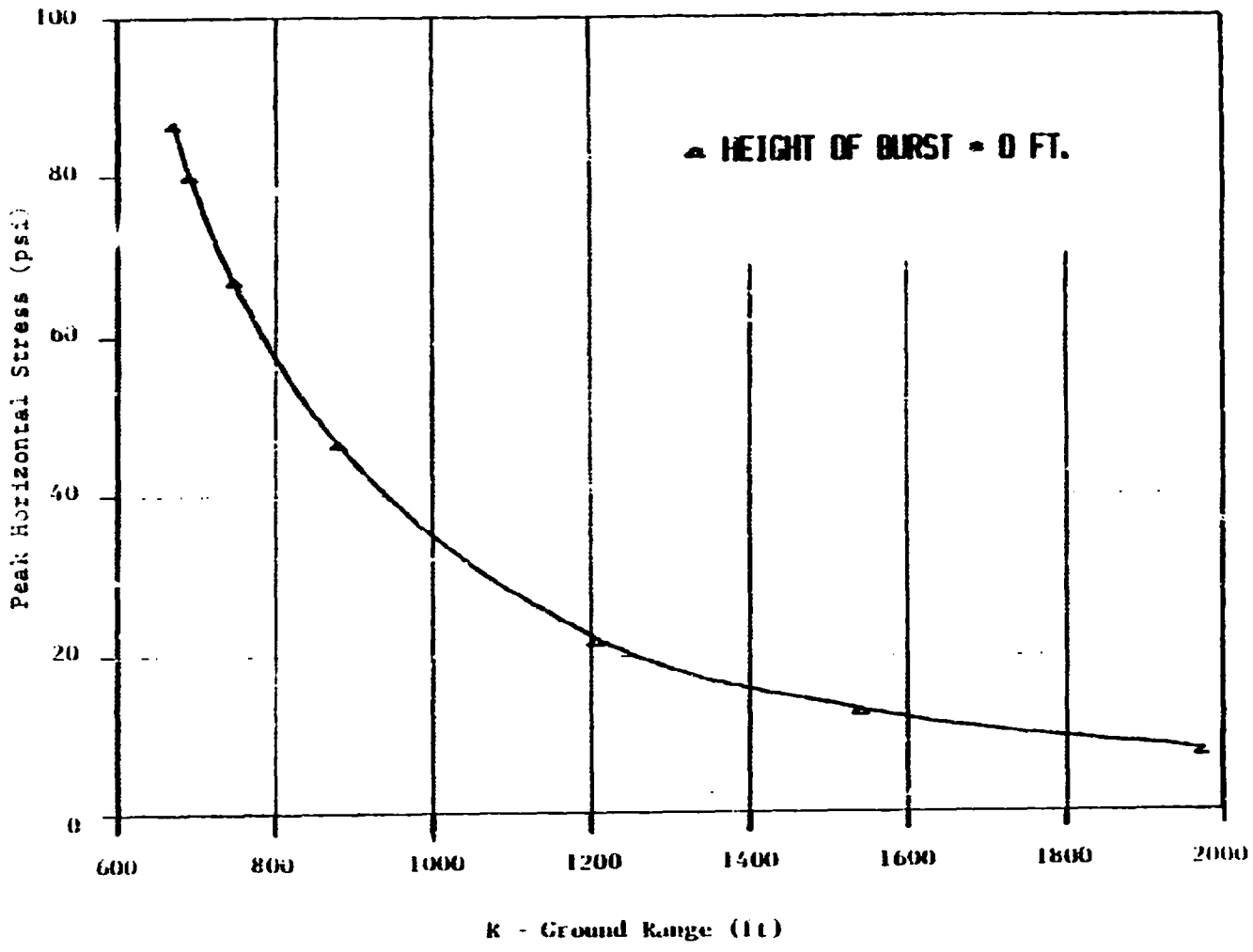

Figure 18. Peak near-surface horizontal stress for direct-induced ground shock, 1-MT weapon, HOB = 0.

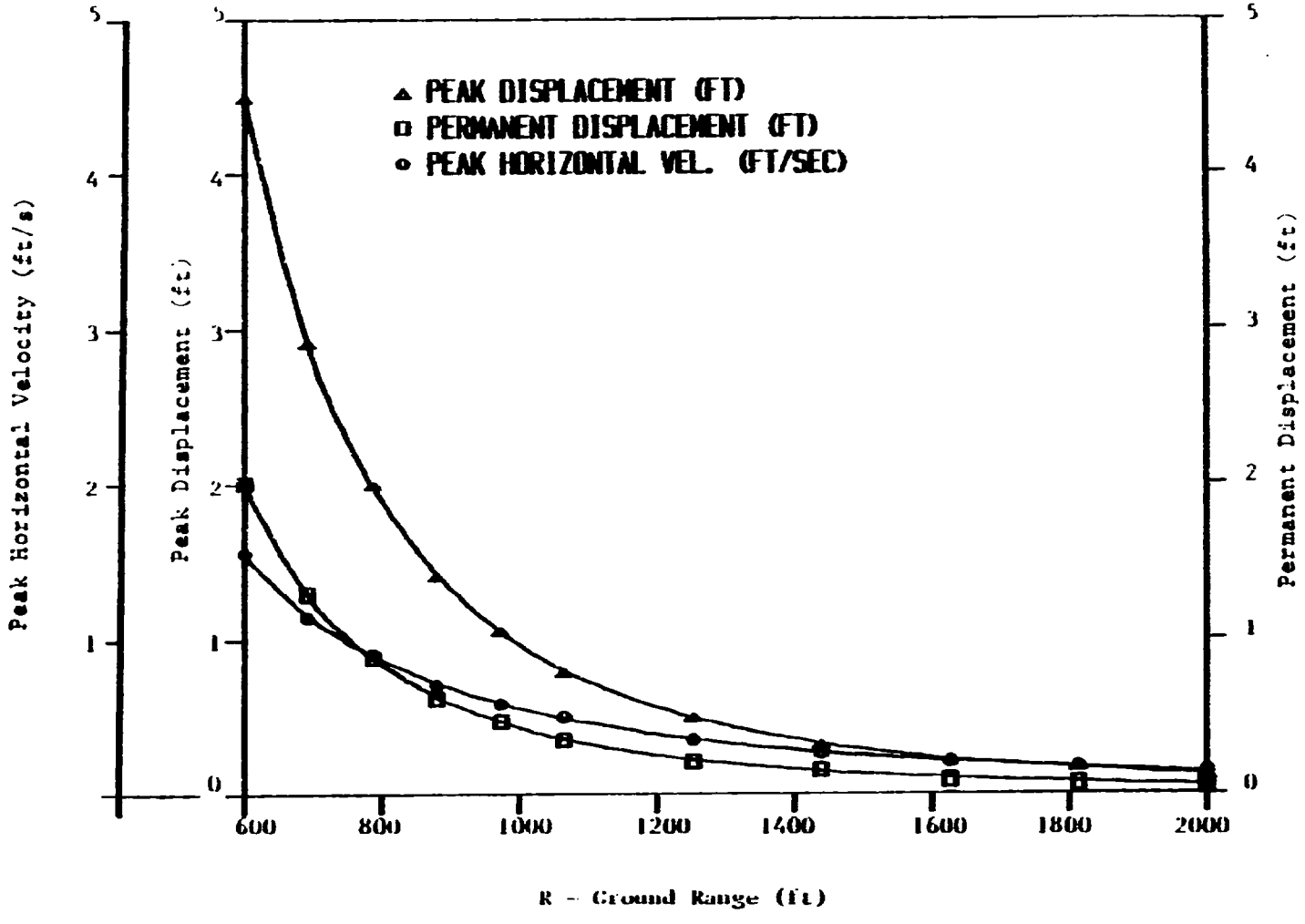

Figure 19. Peak near-surface horizontal displacement, permanent displacement and horizontal particle velocity, crater-induced ground shock, 1-MT weapon, HOB = 0.

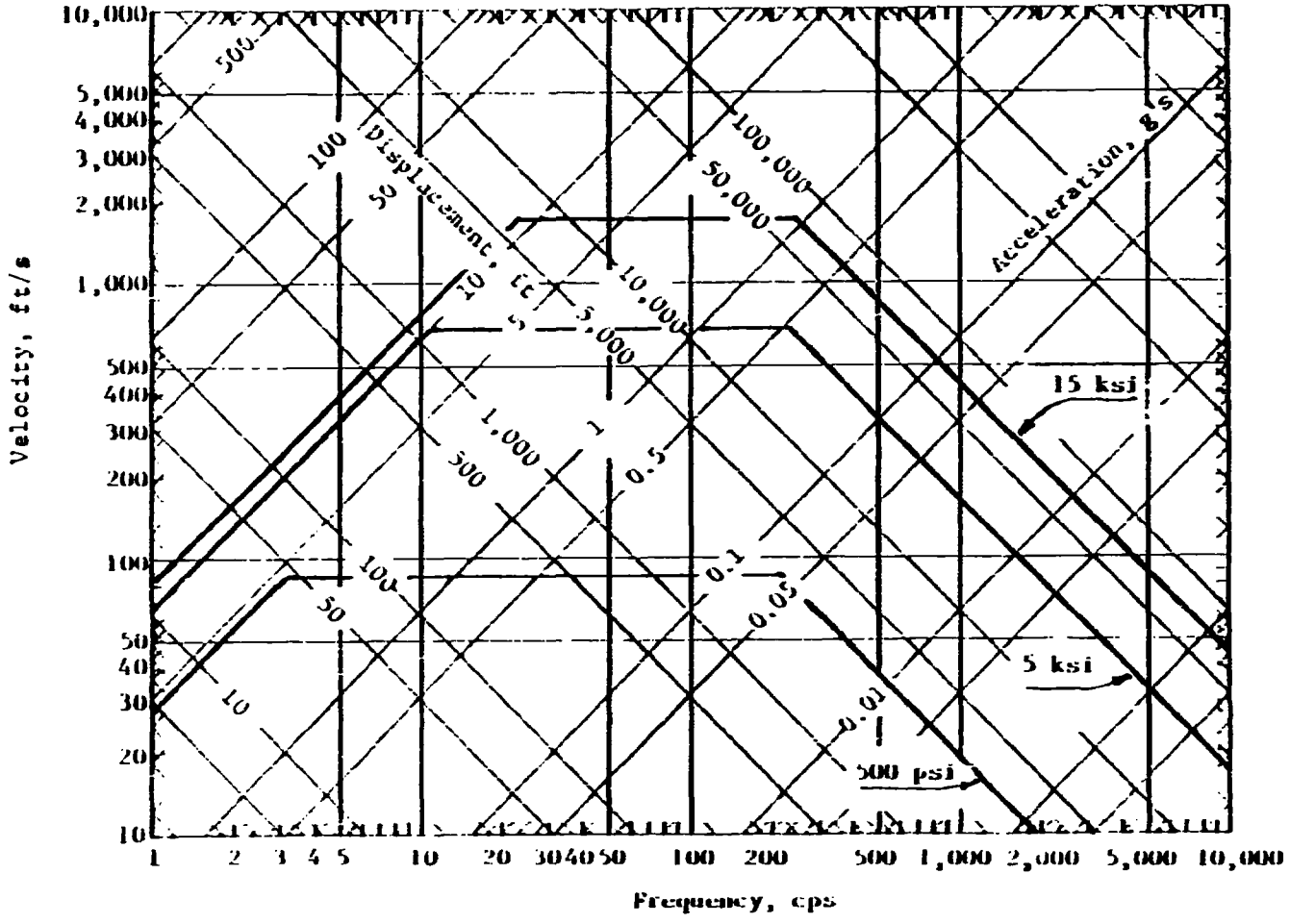

Figure 20. Vertical response spectrum for airblast-induced shock loading for three overpressures, 1-MT surface burst.

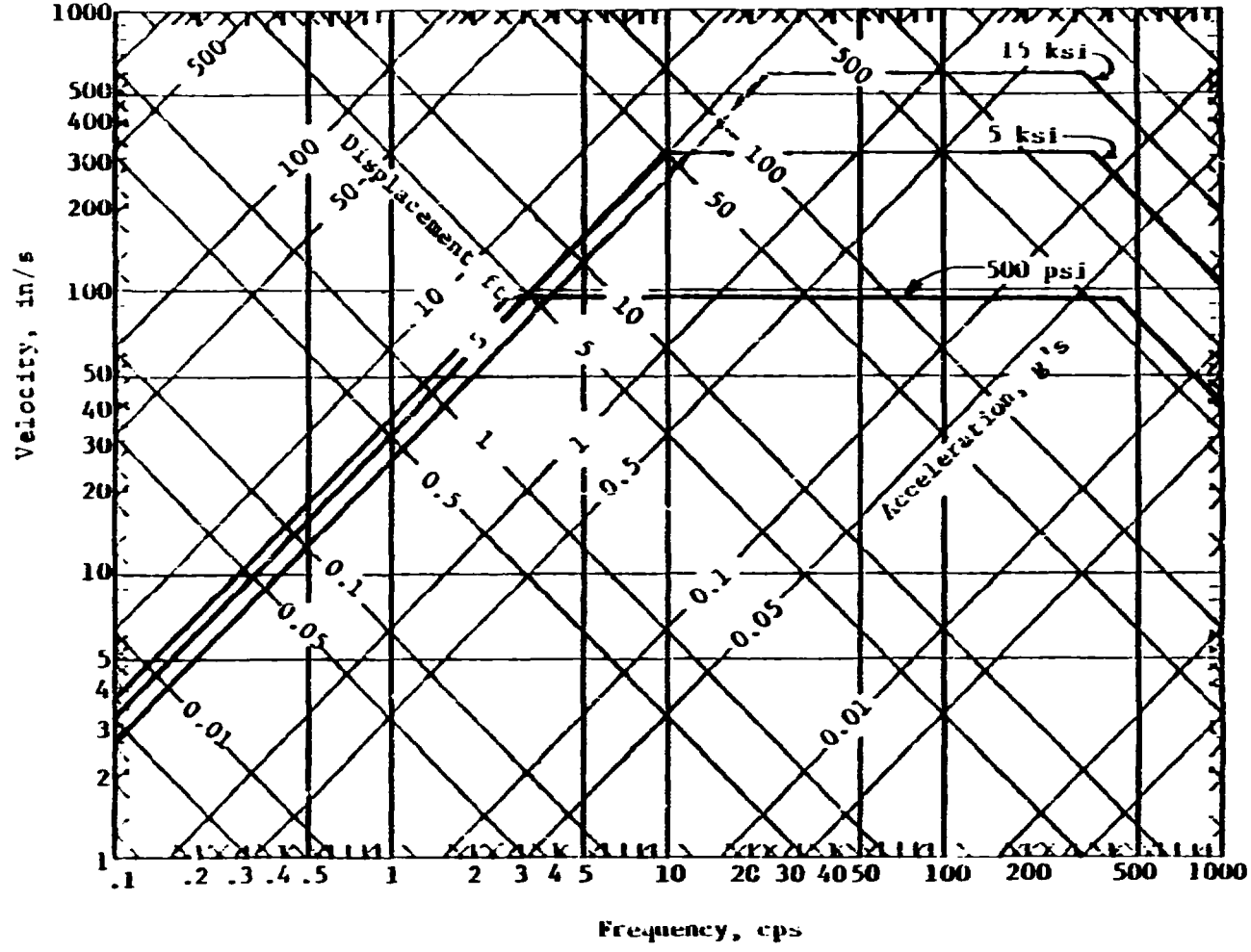

Figure 21. Horizontal response spectrum for airblast-induced shock loading for three overpressures, 1-MT surface burst.

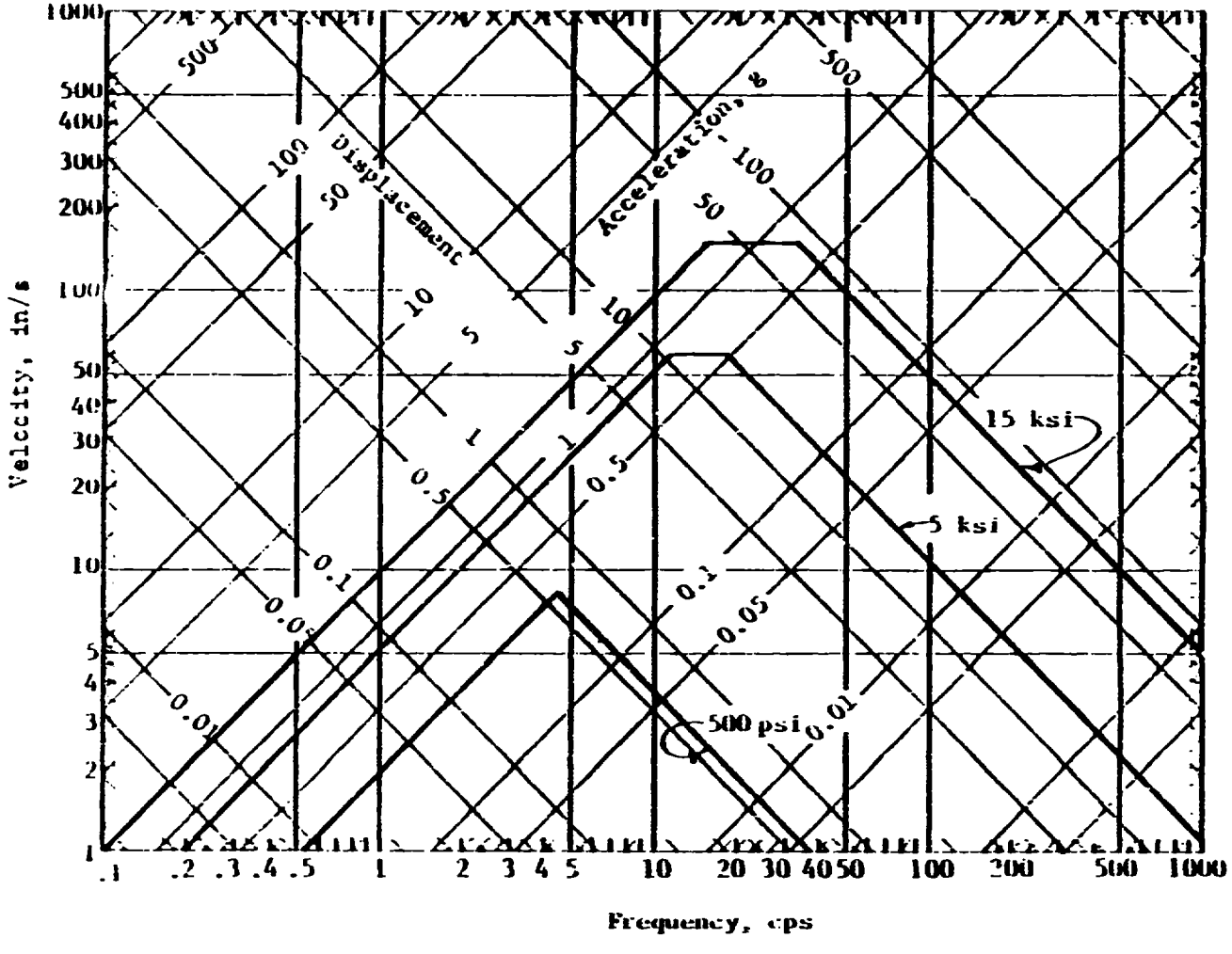

Figure 22. Horizontal response spectrum for direct-induced shock loading for three overpressures, 1-MT surface burst.

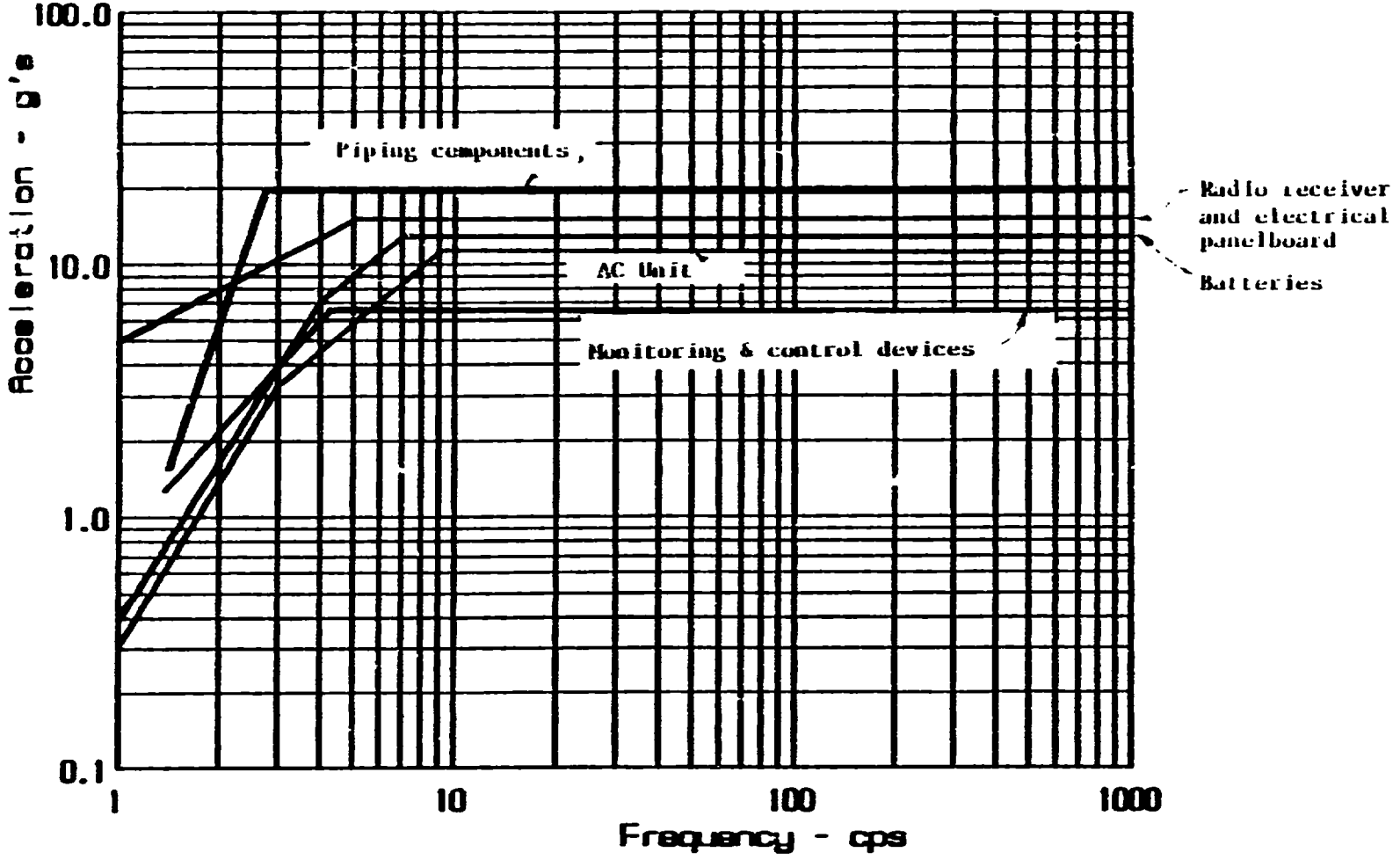

Figure 23. "Sure safe" vertical and horizontal shock spectra for internal components, 5 percent damping (Reference 7).

SECTION 3
TYPICAL ELEMENTS FOR HARDENED ANTENNA STRUCTURES

The hardened antenna structures will be buried flush with the ground surface to take advantage of the favorable loading condition produced by the interaction of the structure with the surrounding soil and the elimination of significant airblast reflections as no structural obtrusions will exist above the ground surface.

In addition to placing structures to achieve favorable loading conditions, efficient structural geometries and materials will also be selected. Flush-buried, silo-type structures are ideally suited to effectively resist combinations of vertical and horizontal loading conditions.

In this section, we shall describe ways of performing initial designs or sizing for a hardened structure to house antennae located at ground surface overpressure levels ranging from about 15,000 to 500 psi generated by a 1-MT burst. The elements of interest are the closure, the silo and the base slab to support the silo as well as concepts for lifting the closure and antennae.

3.1 SLAB-TYPE CLOSURES.

A significant number of tests on closures have been conducted and empirical equations have been formulated to describe the response of a variety of closure types (References 1, 4, 7, and 11). An empirical shear model for the static resistance of a steel/concrete composite closure is presented in Reference 2. For our purposes, the closure can be considered to be circular or square and span a circular opening. The general configuration of a composite closure is shown in Figure 24.

3.1.1 Static Resistance.

The static resistance (P_s) of tub-type closures using two different equations is presented. The total equivalent thickness (D_e) of the composite closure shown in Figure 24 was determined by transforming the thickness of the bottom steel plate to an equivalent thickness of concrete (Reference 2):

$$D_e = D - \left(\frac{E_s}{E_c} - 1\right) t_b \qquad (3.1)$$

where:

E_s = Modulus of elasticity of steel.

E_c = Modulus of elasticity of concrete.

t_b = Thickness of bottom steel plate.

The modulus of elasticity of concrete (E_c) can be reasonably estimated (Reference 8) from the following expression:

$$E_c = 33\, w^{1.5} \sqrt{f'_c}\ , \text{ psi} \qquad (3.2)$$

where:

w = Weight of concrete, lb/ft^3 .

f'_c = Compressive strength of concrete, psi.

The static resistance (P_s) can be determined empirically for span-to-depth (S/D) ratios from 3.5 to 7, and steel plate thicknesses greater than 1 percent of the span using the following expression (Reference 2):

$$P_s = K \sqrt{f'_c}\ \frac{\frac{4\, D_e}{S}}{1 - \left(\frac{D_e}{S}\right)} \qquad (3.3)$$

where:

f'_c = Compressive strenght of contrete.

$K = (27 - \frac{2S}{D})\ psi^{1/2}$.

The 1 percent requirement for the steel plate is sufficient to provide adequate confinement and subsequent increase resistance to shear. For values less than 1 percent, the shear resistance is reduced appreciably and, hence, so is the static resistance of the slab. If the confining steel is increased to 2 percent, there is about a 20 percent increase in resistance.

Using Equation 3.3, curves presented in Figure 25 have been prepared showing the static resistance of closures having the configuration shown in

Figure 24. The curves were prepared for three concrete strengths and have been extended to a S/D ratio of 2 which somewhat exceeds the lower limit of 3.5 for the test data upon which Equation 3.3 was based.

A study (Reference 16) examined a set of closures under static loading conditions. A regression analysis of the test data was performed and the following empirical formula was developed for the static resistance (P_s) in kips/in^2:

$$P_s = 0.4 + 4.9 \left[\frac{t_s}{S} f_y\right] + 2.3 \left[\frac{t_b}{S} f_y\right] + 0.23 f'_c \qquad (3.4)$$

where:

f_y = Yield strength of steel, ksi.

t_s = Thickness of side plate, inches.

The equation is applicable for the following limits:

$$1.35 \leq \frac{S}{D} \leq 3.5$$

$$0.001 \leq \frac{t_b}{S} \text{ and } \frac{t_s}{S} \leq 0.03$$

$$36 \text{ ksi} \leq f_y \leq 70 \text{ ksi}$$

$$3 \text{ ksi} \leq f'_c \leq 12 \text{ ksi}$$

The closure geometry shown in Figure 24 is also applicable for Equation 3.4. It should also be noted that Equation 3.4 is applicable for deeper slabs than described by Equation 3.3.

Shown in Figure 26 is the static resistance for tub closures based on Equation 3.4. By using a high percentage of steel plate and concrete having a compressive strength of at least 10,000 psi, it is possible to achieve a static resistance up to 15,000 psi. This probably represents the upper level of resistance for tub-type closures. To resist higher pressures it is more efficient to use other configurations such as closures with integral grids or other geometries to achieve an increase in strength.

3.1.2 Natural Period.

The natural periods for any of the closures of interest, especially the thicker ones, will be relatively small in comparison to the duration of the airblast load associated with a 1-MT detonation. We shall assume that a square slab over a circular opening will behave very close to that of a circular slab over a circular opening. Expressions have been developed (Reference 13) for the natural period (T_N) of clamped and simply supported circular plates as follows:

$$T_N = \frac{2\pi}{B_{c \text{ or } s}} \sqrt{\frac{\rho\, S^4\, (1 - \nu^2)}{E\, D^2}}, \text{ sec} \qquad (3.5)$$

where:

E = Modulus of elasticity, lb/in^2.

D = Thickness of slab, inches.

ρ = Mass density, $lb\text{-}s^2/in^4$.

S = Diameter of circular plate, inches.

B_c = 11.84, first mode, edges clamped.

B_s = 5.9, first mode, simple supports at edge.

ν = Poisson's ratio.

Assuming a compressive strength (f'_c) of concrete of 10,000 psi, the natural periods (T_N) for different slab thicknesses and spans are shown in Figures 27 and 28 for the cases where the edges are clamped (B_c) and simply supported (B_s), respectively. For concrete, assume Poisson's ratio to be 1/5 (Reference 21).

3.1.3 Ductility Factors.

The ductility of stiff closures is important when considering the energy absorbing capacity of such systems. For deep reinforced concrete slabs without bottom and side plates having span-to-thickness (S/t) ratios of 1.89, 2.6, and 3.5, the ductility factor varied from approximately 2 to 3 (Reference 1). The slabs responded in shear with the center portion of the slabs being crushed, i.e. little ductility.

For composite slabs, i.e. reinforced concrete slabs having steel plate bottoms and sides, the response under load is a combination of shear and membrane action. In a test program (Reference 11), composite, rectangular closures over rectangular openings having clear S/D ratios of about 2 were evaluated. From these tests it appears that the ductility factor varied from about 8 to 10 or perhaps even greater than 10.

For design purposes for the tub-type closures considered in this study, we shall use ductility factors of 2 and 5 that should represent a conservative range of values.

3.1.4 Effect of Strain Rate.

The strength characteristics of steel and concrete are dependent upon strain rate and states of stress, i.e. uniaxial, biaxial and triaxial. In this section, we shall consider only the influence of strain rate. If we assume strain rate is a function of the natural period, say, the peak strain (0.002) is reached in a time equal to $T_N/4$, then a conservative strain rate can be estimated (Reference 10).

It is also assumed the period of the structure will be a value between that for the clamped and simply supported cases. Strain rate values have been estimated for S/D ratios of 2, 3, 4, 6, and 8 for three span lengths, as shown in Table 5. Also shown are the ratios relating dynamic to static strength for concrete and steel based on Reference 10. For all strain rate values greater than 10 in/in/s, an increase factor (IF) of 2 was assumed as an upper limit.

3.1.5 Dynamic Analysis.

A dynamic analysis using an exponentially decaying airblast curve (Reference 14) was conducted for a SDOF representation of the closures. The static resistance (P_s) shown in Figure 25 and the average natural period (T_N) and dynamic strength IF's shown in Table 5 were used as inputs in the dynamic analysis. However for the static resistance (P_s) for the S/D ratio of 2, it was assumed that the bottom plate thickness-to-span (t_s/S) ratio is approximately 0.015 to correspond more closely to Equation 3.4 (see Figure 26). The static resistance is greater for higher strain rates because of the increase in material strength. As the static resistance is

directly proportional to concrete strength, the static resistance (P_s) can be multiplied by the strain rate IF to determine a revised static resistance. Shown in Figure 4 are the peak ground surface air overpressures for a 0- and 500-foot HOB. Note that the 15,000-psi ground surface overpressure occurs at ground ranges of 600 and 700 feet, respectively, for the 0- and 500-foot HOB's. The positive phase durations are shown in Figure 5; note that the durations for the "0" HOB are about twice that for the 500-foot HOB.

For design purposes the "0" HOB was selected. This means if a structure was designed to resist 15,000 psi corresponding to a range of 600 feet for a surface burst, it would need to be at a range of 700 feet, which is the 15,000-psi level for a 500-foot HOB. The large differences in duration for the two burst conditions affect the response very little as the durations for either case are large with respect to the natural period of the closure. Using ductility factors (μ) of 2 and 5, the results of the dynamic analysis are shown in Table 6. The results also compare favorably with those when using response charts shown in Reference 12 based on a Brode-Speicher airblast input loading. The results are also shown in Figures 29 and 30 that relate S/D ratios versus allowable peak overpressure for a 1-MT weapon, HOB = 0, for ductility factors of 2 and 5, respectively.

3.1.6 Bearing Capacity.

A dynamic analysis of the composite slab closure was performed to determine the dynamic reaction or shear load delivered to the bearing area at the upper end of the silo. It is this shear load that must be carried by the bearing ring and dictates the needed bearing area for the closure. The analysis was made for a square plate either fixed or simply supported over a circular opening equal to the inside diameter of the silo. The general expression (Reference 5) for the dynamic reaction (V) for a square plate is as follows:

$$V = 0.39\ F + 0.16\ R \qquad (3.6)$$

where:

F = Total dynamic force, pounds.

R = Total resistance, pounds.

The total dynamic force and resistance can be determined for the slab closures described in Table 6. Since the time-to-maximum response of the closure is very short with respect to the duration, the peak overpressure (P_{so}) will be used in the calculation of the dynamic reaction (V). Equation 3.6 can be more conveniently expressed as:

$$V = (0.09\ P_{so} + 0.16\ P_s)(2\ R_o)^2 \tag{3.7}$$

Equation 3.7 was developed for a square slab and will be somewhat conservative for a circular slab but adequate for design purposes. The bearing stress for a circular slab can thus be expressed as:

$$P_b = \frac{(0.09\ P_{so} + 0.16\ P_s^{\,1})\ (2\ R_o)^2}{\pi \left[R_o^{\,2} - \frac{S^2}{4}\right]} \tag{3.8}$$

The allowable bearing capacity (P_{ba}) of the steel/concrete composite closure is dependent on the concrete bearing strength, shear resistance on the bottom plate, and the friction force between the uncracked concrete and the side steel plate. The expression (Reference 2) for the allowable bearing capacity is as follows:

$$P_{ba} = f'_c \left\{ K \left(\frac{R_i}{R_o}\right)\left(\frac{t_s}{R_o}\right) + \frac{R^2 - R_i^{\,2}}{R_o^{\,2}}\left[1 + K\,\frac{t_s}{R}\,N_\phi\right] - 2\,\mu_s\,K\,\frac{t_s}{R_o^{\,2}}\left[D - (R - R_i)\,N_\phi\right]\right\} \tag{3.9}$$

where:

f'_c = Compressive strength of concrete, psi.

$K = f_y/f'_c$.

R_i = Radius of opening, inches; $S = 2\ R_i$.

R_o = Radius of closure, inches.

t_s = Steel thickness, inches.

D = Closure thickness, inches.

$N_\phi = \tan^2 (45 + \phi/2)$.

$R = R_o - t_s$.

ϕ = Angle of internal friction.

μ_s = Coefficient of friction, steel on concrete.

In Equation 3.9, the angle of internal friction for concrete (ϕ) was selected as 45 degrees and the coefficient of friction (μ_s) was taken to be 0.6. These reasonable values are given as recommendations (Reference 2) for use if exact values are not available.

Both Equations 3.8 and 3.9 are dependent on the value of R_o which also establishes the bearing width. Therefore, an iteration was performed by varying the value of R_o until the values of P_b and P_{ba} were equal. In determining P_b, the resistance and overpressure shown in Table 6 for the $\mu = 2$ case were used. In the determination of P_{ba}, a steel t_s/S ratio of 0.01 was assumed as well as dynamic strength values of concrete and steel.

It should be noted that for t_s/S ratios greater than 0.01, the required bearing width would be less for a given S/D ratio. Shown in Figure 31 is the required bearing width ratio as a function of S/D ratio for concrete strengths of 5,000 and 10,000 psi, and for a t_s/S ratio of 0.01. The analysis shows that as the S/D ratio decreases, the required bearing width increases rapidly with a bearing width of 17 percent of the span necessary for an S/D ratio of 2. For S/D ratios greater than 4, it is shown that bearing widths less than 5 percent of the span are acceptable. However, based upon experimental data (Reference 9) and practical purposes, it is recommended that the bearing width be no less than 5 percent of the span (S).

3.2 DOME-TYPE CLOSURES.

Domes offer the promise of being an effective closure for silo-type structures housing dished and telescoping whip-type antennae. Mechanically, the dome can be designed in quarter sections that open like the petals of a flower. There are possibilities that the dome could be designed to shed some of the load delivered to the silo supporting the dome. The overpressure engulfing the top or exposed part of the dome is transmitted at the wave speed of the dome material to the reaction region at the top of the silo. The air-induced ground shock then engulfs the dome at a rate dictated by the wave speed in soil. Hence, the soil-induced part of the load arrives at the reaction region at a later time at which the peak reaction load from the direct-induced airblast has had a chance to decay.

For design purposes, it was assumed that the dome was made of reinforced concrete and responded in a uniform compression mode. Initially, the dome will probably experience some bending but on complete load engulfment will seek a uniform compression mode of response. The load engulfment of the dome closure supported by a silo and the idealized loading conditions assumed for design are shown in Figure 32.

3.2.1 Static Resistance.

The static resistance (Reference 8) of a reinforced concrete dome in uniform compression can be expressed as:

$$P_c = (1.7\ f'_c + 2\ p_t\ f_y)2D/S \qquad (3.10)$$

where:

P_c = Compression mode resistance, psi.

D = Thickness of dome, inches.

S = Inside diameter of dome, inches.

p_t = Total steel ratio based on gross cross sectional area.

f'_c = Compressive strength of concrete, psi.

f_y = Yield strength of steel, psi.

The static resistance (P_c) for various S/D values, for concrete strengths (f'_c) of 5,000 and 10,000 psi, steel yield strength of 60,000 psi, and a total steel ratio (p_t) of 1 percent are shown in Figure 33.

3.2.2 Natural Period.

The natural period of vibration (Reference 8) of a dome for the uniform compression mode can be expressed as follows:

$$T_N = 2\pi \sqrt{\frac{\rho\ (1 - \nu)\ \frac{S^2}{4}}{2E}} \qquad (3.11)$$

where:

ρ = Mass per unit volume of dome.

ν = Poisson's ratio.

The natural periods for domes having concrete strengths (f'_c) of 5,000 and 10,000 psi are shown in Table 7.

3.2.3 Effect of Strain Rate.

The strain rate effects for the dome-type closure are computed in a similar manner as was done for the slabs. If the peak strain (0.002) is reached in a time equal to $T_N/4$, then a conservative strain rate may be estimated. Strain rate values have been calculated for the three dome diameters, each for two concrete strengths. Also determined are the ratios relating dynamic to static strength for concrete based on Reference 10. Again, for all strain rate values greater than 10 in/in/s, an IF of 2 was assumed as an upper limit. The strain rates of interest and dynamic increase factors are also shown in Table 7.

3.2.4 Dynamic Analysis.

A dynamic analysis of the dome closure was next performed where the dome was treated as a SDOF system. The previous calculations, including static resistance (P_c), the natural period (T_N) and the strength IF were used as inputs in the analysis. A ductility factor (μ) of 2 was assumed. The results are shown in Table 8.

The results have also been plotted in Figure 34 that shows the peak overpressure capacity of the dome closure for various S/D ratios. It is probable that some type of steel domed closure would be more satisfactory than a reinforced concrete one. If a reinforced concrete dome is considered, it is recommended that the inside surface be formed with steel plates. For calculation purposes to determine the static resistance, the thickness of the plate should be considered as an equivalent thickness of concrete. The inside plate will not only serve as a form when placing concrete, but also for attaching studs to help induce confinement. A steel framework would also be essential for a dome that is fabricated in, say, four equal quadrants so that it can open like the petals of a flower.

3.3 SILOS.

The loading of a buried silo is complex. The airblast load collected by the closure is dumped to the silo walls (assumed to be concrete) in a short period of time and the stress wave travels at roughly the speed of sound in concrete. The load being transmitted through the soil surrounding the silo travels at a speed approximately 1/10 to 1/15 of that travelling through the structure. At cross sections below the closure level, the time-to-maximum response of the silo in vertical compression occurs before the horizontal, hoop-type compression load arrives through the soil. During this early time, the skin friction developed at the silo-soil interface will tend to resist the downward movement of the silo. After the soil stress wave arrives, this procedure can reverse, i.e. the skin friction force caused by the soil stress wave causes a downward movement of the silo. Hence, initially the silo responds in a vertical compression mode. At a later time it responds to a combination of vertical and hoop compression (horizontal) modes causing a significant triaxial state of stress. Under such states of stress, it is possible for the silo system to accept much greater loads than possible for uniaxial or biaxial states of stress.

It was estimated (Reference 22) that maximum vertical strain occurs at a level approximately equal to 40 percent the length of the silo for the silos investigated and for the overpressures considered. Based on this observation, a section 5 feet from the top of the silo was selected for design purposes.

3.3.1 Static Resistance.

The static resistance of a silo will first be calculated for axial compression and then for hoop compression. It is anticipated that for most cases if the silo can withstand the axial forces it will probably also resist the hoop compressive forces.

3.3.1.1 Axial (Vertical) Compression. Since the overpressure region of interest is superseismic, it is reasonable to assume a static overpressure (P_s) that interacts vertically with the silo. Based on this assumption, the expression for the static resistance (P_s) for an unlined silo is as follows:

$$P_s = \frac{f'_c \left[\frac{S}{t} + 1\right]}{\frac{1}{4}\left(\frac{S}{t}\right)^2 + \frac{S}{t} + 1} \qquad (3.12)$$

where:

f_c = Compressive strength of concrete.

S = Inside diameter of silo.

t = Thickness of silo wall.

The static resistance (P_s) has been determined for various S/t ratios and concrete strengths (f'_c of 5,000 and 10,000 psi, see Figure 35.

The resistance of the silo can be enhanced by including an internal steel liner. This liner also helps to restrain or confine the silo which in turn also increases the resistance. The axial static resistance (P_s) for a silo including an internal steel liner is expressed as follows:

$$P_s = \frac{f'_c \left[\left[\frac{S}{t} + 1\right] + \frac{f_y}{f'_c}\left(\frac{S}{t}\right)\left(\frac{a}{t}\right)\right]}{\frac{1}{4}\left(\frac{S}{t}\right)^2 + \left[\frac{S}{t} + 1\right]} \qquad (3.13)$$

where a is the thickness of the steel liner.

Using this equation, the static resistance has been determined and shown in Figure 36 for various S/t ratios, for concrete strengths of 5,000 and 10,000 psi, and liner-to-wall thickness ratios of 1/32 and 1/64 as shown in Figure 36. Also, the yield strength (f_y) of steel was assumed to be 60,000 psi.

The resistance of the silo can be enhanced even more by including both inner and outer steel liners. The axial static resistance (P_s) for a silo having both <u>internal and external steel liners</u> is as follows:

$$P_s = \frac{f'_c \left[\left(\frac{S}{t} + \frac{2a}{t} 1 \right) + \frac{2 f_y}{f'_c} \left(\frac{a}{t} \right) \left(\frac{S}{t} + 1 \right) \right]}{\frac{1}{4} \left(\frac{S}{t} \right)^2 + \left(\frac{S}{t} + 1 \right)} \qquad (3.14)$$

Shown in Figure 37 is the static resistance of silos with internal and external liners. It can be observed by comparing Figures 35, 36, and 37 that steel liners enhance appreciably the static axial load-carrying capacity of silos.

<u>3.3.1.2 Hoop (Horizontal) Compression</u>. It will be assumed based on experimental observations that the silo behaves in a hoop compression mode. The static resistance (P_c) of an <u>unlined silo</u> for a uniformally applied inward loading is as follows:

$$P_c = \frac{f'_c \left(\frac{t}{S} \right)}{\frac{1}{2} + \left(\frac{t}{S} \right)} \qquad (3.15)$$

where the terms are the same as shown in Figure 35.

The static resistance (P_c) in hoop compression was determined for various S/t ratios and concrete strengths (f'_c) of 5,000 and 10,000 psi (see Figure 38).

If an <u>inner steel liner</u> is used, the hoop resistance of the silo including the influence of the liner can be estimated as follows:

$$P_c = \frac{f'_c \left[\left(\frac{t}{S}\right) + \frac{f_y}{f'_c} \left(\frac{a}{S}\right) \right]}{\frac{1}{2} + \frac{t}{S}} \qquad (3.16)$$

Using this equation, the static resistance has been determined for various S/t ratios, concrete strengths of 5,000 and 10,000 psi, and steel liner thicknesses (a) of 1/64 and 1/32 as shown in Figure 39. The yield strength of steel was assumed to be 60,000 psi.

If <u>inner and outer liners</u> are used, the hoop resistance can be estimated as follows:

$$P_c = \frac{f'_c \left[\frac{t}{S} + \frac{2 f_y}{f'_c} \left(\frac{a}{S}\right) \right]}{\frac{1}{2} + \frac{t}{S}} \qquad (3.17)$$

Using this equation, the static hoop resistance has been determined and is shown in Figure 40. It can be observed by comparing Figures 38, 39, and 40 that steel liners enhance the static hoop resistance of silos.

3.3.2 Natural Periods and Influence of Strain Rate.

Presented are expressions for the silo acting in axial compression and in hoop compression modes. These modes should be reasonable for the axial load caused directly by airblast and the horizontal loading induced by soil stress. Also presented is the influence of strain rate on concrete strength for both modes.

<u>3.3.2.1 Axial (Vertical) Compression Mode</u>. The natural period (Reference 9) in axial compression can be expressed as follows:

$$T = 30\ell\sqrt{\frac{1}{E}}, \text{ msec} \qquad (3.18)$$

where:

ℓ = Length of silo, inches.

E = Modulus of elasticity, psi.

Shown in Table 9 is the natural period in axial compression for a silo having different lengths and concrete strengths (f'_c) of 5,000 and 10,000 psi. Also shown is the strain rate and corresponding dynamic-to-static strength ratio.

3.3.2.2 Hoop (Horizontal) Compression Mode. The natural period (Reference 8) in the hoop compression mode is expressed as follows:

$$T = 2\pi \sqrt{\frac{\nu \left(\frac{S}{2}\right)^2}{E\, g}} \qquad (3.19)$$

where:

γ = Weight density.

S = Inside diameter.

E = Modulus of elasticity.

g = Acceleration due to gravity.

The expression is for circular rings where the thickness is small compared to the radius (S/2). The periods in hoop compression for silos having various diameters (S) and concrete strengths of 5,000 and 10,000 psi are shown in Table 10. Also shown is strain rate and the corresponding dynamic-to-static strength ratio. For S/t values of 2 and 4, the calculated periods using Equation 3.19 are in error by 25 and 16 percent, respectively. As the calculated periods are very small with respect to the duration time of the load, the error in the period is insignificant for response predictions.

3.3.3 Influence of State of Stress of Concrete.

Concrete is used primarily for its compressive strength characteristics, hence, the uniaxial compressive strength (f'_c) is an important factor in defining the strength of concrete. However, when considering the response of buried silo-type structures, the influence of a triaxial state of stress is significant. The increase in load-carrying capacity under triaxial conditions can be significant as demonstrated by the normalized triaxial compression data shown in Figure 41.

For the biaxial state when $\sigma_3 = 0$ and $\sigma_2 = 0.2\sigma_1$, it can be observed that the normal compressive stress, σ_1, is about 30 percent greater than the compressive strength of concrete ($\sigma_r = f'_c$). For slight increases in σ_3, the value for σ_1 increases appreciably. Under triaxial states of stress the behavior of concrete is much more ductile than under uniaxial or biaxial states of stress; hence, the energy absorbing capacity of the material is also increased.

If we consider a horizontal section of a silo below the closure, the directly transmitted shock through the structure will arrive before the airblast-induced ground shock. During the lag time between the arrival of the two shock fronts, the induced stresses in the silo are caused only by the shock directly transmitted through the structure. However, even for this case, steel liners and reinforcing steel in the silo can create a confined condition that should produce a beneficial state of stress thereby increasing the load-carrying capacity of the silo. When the horizontal component of the ground shock arrives, it couples with the directly induced stresses in the concrete silo causing a much more beneficial state of stress. Both of these conditions are discussed in the following sections. A section 5 feet from the top of the silo was selected for design purposes, see Section A of Figure 42.

3.3.3.1 Directly Transmitted Shock through Silo Only. The silo under this condition is loaded only by the directly induced shock through the structure, i.e. the airblast-induced ground shock has not yet arrived at the section of interest, Figure 42 ($t = t_1$). Also, if inside and outside steel liners are used, the stress wave will travel faster in the steel and arrive at Section A before the stress wave travelling through the concrete sandwiched between the two plates arrives. This should tend to induce horizontal compressive stresses in the concrete at Section A. The stress wave in the concrete arrives a short time later (less than about 1 ms for the structures considered in this report). The axial compressive stress (σ_1) induces a hoop compressive stress (σ_2) based on Poisson's ratio (υ). The strain in the radial direction is constrained by lateral rebars (ties) in combination with the steel liners if they are present as well as the

passive action of the surrounding soil. Hence, the radial stress component (σ_3) can also be in compression. Thus, if the three components of stress are in compression, a favorable condition exists, see Figure 42.

Based on Reference 2, the confinement provided by hoop steel in circular columns can increase the axial compressive strength up to, say, 40 percent, depending on the amount of confining steel. If inner and outer steel liners are used in conjunction with confining steel, the axial compressive strength will even be greater (Reference 2). From calculations made for the case of rigid liners, it was found that the axial strength for thick-walled silos was increased by a factor greater than four. For design purpose, we will assume the following conditions for the three silo geometries of interest:

$$\text{Silo with no liners, } \sigma_1 = 1.2\ \sigma_r \tag{3.20}$$

$$\text{Silo with inner liner, } \sigma_1 = 1.5\ \sigma_r \tag{3.21}$$

$$\text{Silo with inner and outer liners, } \sigma 1 = 2.0\ \sigma_r \tag{3.22}$$

where $\sigma_r = f'_c$, see Figure 41.

3.3.3.2 Directly Transmitted Shock through Silo Coupled with Airblast-Induced Ground Shock. It should be noted that the relationships shown in Figure 41 are based on the following assumption:

$$\sigma_1 > \sigma_2 > \sigma_3$$

Depending on the ground range from GZ, i.e. P_{so} from 15,000 to 500 psi, various combinations of stress can exist. For example, if the radial soil stress is greater than the axial stress shown in Figure 42, then the following relationships are possible:

$$\sigma_1 = \sigma_{hoop}$$

$$\sigma_2 = \sigma_{radial}$$

$$\sigma_3 = \sigma_{axial}$$

If the axial stress is greater than the radial soil stress, the following relationships are possible:

$$\sigma_1 = \sigma_{hoop}$$

$$\sigma_2 = \sigma_{axial}$$

$$\sigma_3 = \sigma_{radial}$$

Shown in Figure 42 at $t = t_2$ is the arrival of the airblast-induced ground shock loading at Section A. The horizontal component of this soil stress creates a fairly uniform radial stress at this section. Also at this time, the shock front in the concrete silo has probably reflected off the bottom, travelled upward, and may have even passed Section A, depending on the length of the silo. Regardless, the peak axial compressive stress has had time to decay.

To determine the triaxial state of stress for Section A at $t = t_2$, the axial load on the silo at that time must first be calculated. The axial load at time $t = t_2$ was found by evaluating the expression for overpressure, $p(t)$, with time using the following relationship from Reference 8:

$$p(t) = P_{so}(1 - r)(ae^{-\alpha r} + be^{-\beta\gamma} + ce^{-\gamma r}) \qquad (3.23)$$

Shown in Table 11 are the ground surface air overpressure, $p(t_2)$, at a time equal to t_2 for overpressure levels ranging from 15,000 to 500 psi determined by using Equation 3.23. Having determined the peak pressure acting on the silo at time t_2, the axial stress at time t_2 is determined by the following expression:

$$\sigma_{axial} = p(t_2)\left[\frac{\frac{s^2}{4} - st + t^2}{st - t^2}\right] \qquad (3.24)$$

Shown in Figures 10 through 14 are normalized vertical stresses (σ_z) with depth for the linearly elastic case (r = 1) and the linear loading case with no recovery (r = 0). The actual stress is between the two values and for our calculations will be assumed to be the average of the two cases. The horizontal or radial soil stress is determined from the following relationship:

$$\sigma_{radial} = k\ \sigma_z \tag{3.25}$$

From Table 3 and for depths up to, say, 20 feet, a reasonable and average value for k is 0.42 and has been used in determining the radial stress.

The <u>hoop</u> compressive stress is related to the radial stress as follows:

$$\sigma_{hoop} = \frac{\left[\frac{S}{2} + t\right] \cdot \sigma_{radial}}{t} \tag{3.26}$$

Shown in Tables 12, 13, and 14 are the relationship of σ_1/σ_1 and σ_2/σ_r based on Figure 41 for peak ground surface overpressure levels of 15,000, 10,000 and 5,000 psi, respectively. Equations 3.24, 3.25 and 3.26 describing the <u>axial</u>, <u>radial</u> and <u>hoop</u> stresses were used in the development of the tables. For design purposes, it is believed reasonable to use the following values:

$$\sigma_1/\sigma_r = 4 = \sigma_2/\sigma_r \tag{3.27}$$

The effective duration, Δt , of the <u>axial</u> stress before engulfment of the <u>radial</u> stress can be determined as follows and is shown in Table 11:

$$\Delta t = t_1 - t_2 \tag{3.28}$$

where:

$$t_1 = \frac{5\ ft \times 10^3}{C_c} = 0.5\ ms$$

$$t_2 = \frac{5 \text{ ft} \times 10^3}{C_L}, \text{ ms}$$

3.3.4 Sidewall Friction.

The increased load-carrying capacity of the silo resulting from sidewall friction has been calculated. It has been determined that the increase is negligible in comparison to the loads the silos are expected to resist. For example, a 10-foot silo will generate only about 1 psi and a 20-foot silo only 2 psi in sidewall friction. Therefore, the effects of sidewall friction in the analysis will not be considered.

3.3.5 Dynamic Analysis.

A dynamic analysis was made using a SDOF representation of the buried silo in axial (vertical) and hoop (horizontal) compression modes. The response was determined for silos having S/t ratios from 2 to 8. The static resistances (P_s and P_c) shown in Figures 35 and 37, the natural periods (T_N) and the dynamic IF's shown in Tables 9 and 10 were required inputs in the analysis. The response of the SDOF system was made for two conditions: before and after radial soil engulfment, with the critical condition being before. The analysis was made for the unlined silo, the inner steel lined silo, and for the silo having both inner and outer steel liners. In all cases, the steel liner thickness (a) was assumed to be 1/64 of the concrete thickness (t). A ductility factor (μ) of 2 for the elastic-perfectly plastic system was assumed.

3.3.5.1 Axial (Vertical) Compression Mode. The analysis of the silo at Section A in axial compression was made for the case before soil engulfment. It should be noted that the silo will be strengthened significantly after the engulfment, thus greatly increasing its load-carrying capacity.

Response charts have been developed (Reference 12) by numerically integrating the nondimensional equations of motion for the undamped SDOF model. The input loading used in developing the charts was an analytical approximation to the actual nuclear burst. The duration associated with the loading is dependent upon the wave speeds in the soil (C_L) and concrete

(C_c). A value of 10,000 ft/s was used as the wave speed in the concrete (C_c). For calculation purposes, values of C_L of 800, 750, 700, 650, and 600 ft/s were used at overpressure ranges of 15,000, 10,000, 5,000, 1,000, and 500 psi, respectively.

The results of the analysis are shown in Tables 15, 16, and 17 for the unlined-, single- and double-lined silos, respectively. The results are presented graphically in Figures 43, 44, and 45 which show more clearly the benefits of the steel liners.

3.3.5.2 Hoop (Horizontal) Compression Mode. Shown in Figures 10 through 14 are normalized vertical stresses as a function of strain recovery (r) and overpressure with depth. These figures, coupled with Table 3 which relates horizontal to vertical stresses, define the state of stress for a section of the silo. For consistency with previous calculations, an IF has been chosen and used for all overpressure and S/t ratios. For this section, a factor of 4 will be used. For analysis purposes, a recovery ratio of 1/2 and a depth of 5 feet were chosen. A dynamic analysis was performed on the silo in hoop compression to determine the silo's capacity to resist horizontally applied loads. The radial (horizontal) capacity of the silo is denoted by σ_{radial} and is related to the vertical stress (σ_z) by the k factor given in Table 3. In this section, k will be assumed constant and equal to 0.42. A relationship between σz and P_{so} has been determined via Figures 10 through 14 and shown as follows:

$$\sigma_z = .87\ P_{so}$$

The results of the analysis are shown in Table 18 and are also shown graphically in Figure 46.

3.4 BASE SLAB.

Generally, the base slab is an integral part of the silo system and as such is designed to withstand the shear and bending loads imposed by the silo as well as the vertical soil stresses induced by the punching action of the soil. For design purposes, the configuration used for the closure will

also be adequate for the base slab. The only difference would be the detailing of reinforcing steel to provide sufficient moment and shear transfer at the silo slab intersection. Also, sufficient reinforcing steel should be placed in each face to maintain the integrity of the slab with the silo. An alternate concept that might prove beneficial for a communications structure located at overpressure levels greater than 5,000 psi is a floating base slab. The acceleration and motion imparted to the floating slab would be significantly reduced compared to that for a rigid slab. Thus, the floating slab itself helps to serve as a shock isolation system. However, before such a concept could be considered it would need to be checked out by conducting model tests in the field in a simulated nuclear blast environment.

3.5 LIFTING MECHANISM CONCEPTS INCLUDING LOADING CRITERIA.

Discussed in this section are the general power requirements to lift the slab and dome closures. Shown in Table 19 are the design ejecta depths associated with different overpressure ranges from GZ, lifting stroke requirements, the effective resistance force (weight of closure, ejecta and shear resistance of soil), and horsepower requirements based on a travel rate of 1 ft/min for both slab- and dome-type closures. Shown in Figure 47 are the power requirements associated with various ranges from GZ. For practical purposes, a minimum value of 3 hp will be assumed. Lifting concepts for slab- and dome-type antennae structures are discussed in the following sections.

3.5.1 Slab-Type Closures.

Two basic concepts for lifting or moving slabs were considered. For overpressure ranges, say, less than 2,000 psi where the anticipated ejecta thickness is a little more than 1 foot, the slab closure can be moved horizontally. For overpressure ranges closer to GZ where ejecta thicknesses up to 4 feet are anticipated, concepts to raise the closure vertically have been considered. An interesting study (References 17 and 18) was conducted that evaluated 11 different closure concepts for missile silos. After various evaluations, including some simple model studies, it was concluded

that the rise and rotate and single-hinge concepts offered the most promise. For both of these concepts, the actuators and other mechanical systems to lift and rotate were located external to the silo. For slab closures for antenna structures it is believed the rise and rotate and sliding concept offer the most promise. The lifting and/or pushing mechanisms can probably be located within the structure for both concepts. The concept for lifting and rotating the closure are for the deeper ejecta depths, whereas the sliding concept is for ejecta depths less than 1 foot.

3.5.2 Lifting Mechanism Concepts for Dome Closures.

The dome-covered hardened structure makes it possible to develop an interesting concept for dished antennae systems. For an actual design the hemispherical dome as shown in this report could be supplanted by a more "bullet"-shaped closure. However, the design concepts and relative costs described in this report should be adequate for different shaped domes as well. The dome structure is probably better suited for high-overpressure levels and the sliding slab-type closure for lower overpressure levels. The concept for lifting a domed closure is shown in Figure 48. Note that this concept is based on a dome that unpeels like an orange in four pieces. The dome system also has the advantage or option of being completely covered by soil. If a camouflaged site is desired, the dome structure is well suited. The dished antennae rides on the lifting mechanism and is directly beneath the closure. After the closure has been raised and the dome opened, the antennae can be raised or operated in place. Estimated rattlespace requirements for the internal support system are also shown in Figure 48.

3.5.3 Lifting Mechanism for Antennae.

The lifting mechanism for the various antennae of interest is relatively straightforward. The same power supplies that operate the lifting mechanisms for the closures can be used to operate the antennae after the closures have been opened or moved.

3.6 SPACE REQUIREMENTS WITHIN A HARDENED COMMUNICATIONS STRUCTURE.

Not only must the facility contain the racks housing the receiving and transmitting equipment necessary for communication, but the supporting equipment as well. The supporting equipment includes the alternate power supplies to operate the lifting mechanisms for both the closures and antennae and to operate the communication equipment. It is assumed that two hardwired lines enter the structure to provide power; however, if both lines are lost during an attack, two alternate power supplies will be available, i.e. batteries and a motor generator. In addition, air-conditioning is required to maintain a proper environment for the communications equipment. Also, a sump pump may be needed to keep the structure free of standing water should rain be a problem. Shown in Table 20 are general requirements (provided by Mr. James D. Cooper of the DNA) for three different types of communications terminals.

3.6.1 Design and Operational Assumptions.

The following design assumptions have been made that influence space and operational requirements within the structure:

a. Hardwire power will be available from at least one source, preferably two.

b. Backup battery power will be available to operate the closure system and erect the antenna with a capability to operate the communication equipment for about 7 hours. The motor generator will take over when the closure is opened and the antennae erected; however if the generator fails, the batteries will continue to operate the communication equipment.

c. A backup motor generator will be available and designed for propane operation (first choice) or diesel (second choice). The system will be designed for two options, i.e. the first considers operation for <u>one week</u>, the second for <u>one month</u>. The system will be provided with means to supply fresh air for combustion and removal of exhaust gases and heat. Generator to be started after opening and erection of antenna.

d. Communication equipment requires only reasonable over-under voltage protection (not sophisticated regulation).

e. A logic circuit in the control system will be provided to take a normal path if the generator starts and an emergency path if the

generator does not start or fails sometime after starting so that the battery power can be reinitiated.

f. Batteries must be provided with means to remove gas (explosive) given off during charging. This must be provided while the silo is closed as it is assumed that the charging will be done by the hardwire power source.

g. Most of the temperature control can be provided by installing a heat exchanger in the soil (or rock) near the bottom of the silo. However, this does not include the generator exhaust and, therefore, fans must be provided to exhaust generator gases and heat. Equipment can be grouped and air-cooled as required.

h. Pressure switch at surface with programmable delay will put the system into operation unless cancelled by hardwire control. Thus, if hardwire is lost due to a nearby explosion, the system will deploy.

i. A carrier current system can be used effectively on the power hardwire if distances are not excessive. This will allow control signals to be sent to the silo and condition of components inside to be measured and telemetered on the powerline. For example, battery voltage, temperature, humidity, and results of equipment exercising data can be obtained.

3.6.2 Layout for One-Week Operation.

A layout for a one-week operational period is shown in Figure 49. In this configuration, an attempt was made to minimize the interior diameter of the silo. The equipment is packed within a space 8 feet in diameter and 23.6 feet high. The layout was also based on the lift or break out situation described in Figure 48 for a domed closure configuration. The form for a slab closure configuration would be very similar. The space configuration is based on the assumption that approximately 60 ft^3 of batteries are required and that the propane fuel tanks (2 feet in diameter by 3 feet long) contain 70 gal of fuel per tank and that the fuel is expended at a rate of 2-1/4 gal/h. The motor generator and hydraulic pump system each occupy a 4- by 2-1/2- by 2-foot space. Each communication equipment rack occupies a 7- by 2- by 2-1/2-foot space. The control panel for the equipment, the battery charger, switch gear, battery inverter, air-conditioner, and exhaust fans are not shown on the drawings. However, it is believed there is ample space for locating these items as well as hydraulic and electrical lines in the remaining space shown in Figure 49.

3.6.3 Layout for One-Month Operation.

A layout for a one-month operational period is shown in Figure 50. Note that this configuration is based on a space 10 feet in diameter by 17.8 feet high. The 2-foot increase in diameter over the space shown in Figure 49 makes it possible to pack the equipment for a one-month operational period. If the configuration shown in Figure 49 were to require operating for one month, the stack would increase from the 23.6 feet shown to about 32 feet, or about twice the length for a 10-foot-diameter stacking arrangement shown in Figure 50.

Table 5. Strength increase ratios due to strain rate for slab-type closures.

S/D	Span in	Natural Period (T_N) Fixed msec	Free msec	Average msec	Strain Rate $\dot{\epsilon} = \frac{2}{T_N/4}$ in/in/s	Dynamic to Static Strength Ratio (IF) Concrete f'_{dc}/f'_c	Steel f_{dy}/f_y
2	144	0.9	1.8	1.4	6	1.8	1.8
	96	0.6	1.2	0.9	9	1.9	1.9
	48	0.3	0.6	0.45	18	2.0	2.0
3	144	1.4	2.7	2.0	4	1.6	1.6
	96	0.9	1.8	1.35	6	1.8	1.8
	48	0.5	0.9	0.7	11	2.0	2.0
4	144	1.8	3.7	2.75	3	1.5	1.5
	96	1.2	2.4	1.8	4	1.6	1.6
	48	0.6	1.2	0.9	9	1.9	1.9
6	144	2.7	5.5	4.1	2	1.4	1.4
	96	1.8	3.7	2.75	3	1.5	1.5
	48	0.9	1.8	1.35	6	1.8	1.8
8	144	3.7	7.4	5.5	1	1.4	1.4
	96	2.4	4.8	3.6	2	1.5	1.5
	48	1.2	2.4	1.8	4	1.6	1.6

Table 6. Allowable peak overpressures and time to maximum response for slab-type closures, 1-MT device, HOB = 0.

S/D	Span S in	Concrete Strength f'_c psi	Static Resistance P_s psi	Revised Static Resistance $P'_s = IF^* \times P_s$ psi	Natural Period T_N msec	$\mu = 5$ P_{so} psi	$\mu = 5$ t_m msec	$\mu = 2$ P_{so} psi	$\mu = 2$ t_m msec
2	144	5,000	6,500	11,700	1.4	10,500	2.4	8,900	.98
		10,000	9,200	16,600		14,900	2.4	12,500	.98
	96	5,000	6,500	12,350	0.9	11,100	1.5	9,300	.63
		10,000	9,200	17,500		15,700	1.5	13,200	.63
	48	5,000	6,500	13,000	0.45	11,700	.76	9,800	.31
		10,000	9,200	18,400		16,500	.76	13,900	.31
3	144	5,000	3,000	4,800	2.0	4,300	3.4	3,600	1.4
		10,000	4,200	6,700		6,000	3.4	5,000	1.4
	96	5,000	3,000	5,400	1.35	4,900	2.3	4,100	.95
		10,000	4,200	7,550		6,800	2.3	5,700	.95
	48	5,000	3,000	6,000	0.7	5,400	1.2	4,500	.49
		10,000	4,200	8,400		7,500	1.2	6,300	.49
4	144	5,000	1,800	2,700	2.75	2,400	4.7	2,000	1.9
		10,000	2,500	3,750		3,400	4.7	2,800	1.9
	96	5,000	1,800	2,900	1.8	2,600	3.0	2,200	1.2
		10,000	2,500	4,000		3,600	3.0	3,000	1.2
	48	5,000	1,800	3,400	0.9	3,000	1.5	2,600	.63
		10,000	2,500	4,750		4,300	1.5	3,600	.63

* See Table 3.1.

Table 6. Allowable peak overpressures and time to maximum response for slab type closures, 1-MT device, HOB = 0 (continued).

S/D	Span S in.	Concrete Strength f'_c psi	Static Resistance P_s psi	Revised Static Resistance $P'_s = IF^* \times P_s$ psi	Natural Period T_N msec	$\mu = 5$ P_{so} psi	$\mu = 5$ t_m msec	$\mu = 2$ P_{so} psi	$\mu = 2$ t_m msec
6	144	5,000	850	1,200	4.1	1,100	7.0	900	2.9
		10,000	1,200	1,700		1,500	7.0	1,300	2.9
	96	5,000	850	1,300	2.75	1,200	4.7	1,000	1.9
		10,000	1,200	1,800		1,600	4.7	1,300	1.9
	48	5,000	850	1,500	1.35	1,300	2.3	1,100	.95
		10,000	1,200	2,150		1,900	2.3	1,600	.95
8	144	5,000	500	700	5.5	600	9.4	500	3.9
		10,000	800	1,100		1,000	9.4	800	3.9
	96	5,000	500	800	3.6	700	6.1	600	2.5
		10,000	800	1,200		1,100	6.1	900	2.5
	48	5,000	500	800	1.8	700	3.0	600	1.3
		10,000	800	1,300		1,200	3.0	1,000	1.3

* See Table 3.1.

Table 7. Strength increase ratios due to strain rate for dome-type closures.

Span S in	Concrete Strength f'_c psi	Natural Period T_N ms	Strain Rate $\dot{\epsilon} = \frac{2}{T_N/4}$ in/in/s	Dynamic to Static Strength Ratio (IF)	
				Concrete f_d/f'_c	Steel f_{dy}/f_y
144	5,000	2.3	3	1.5	1.5
	10,000	1.9	4	1.6	1.6
96	5,000	1.5	5	1.7	1.7
	10,000	1.3	6	1.8	1.8
48	5,000	.75	11	2.0	2.0
	10,000	.63	13	2.0	2.0

Table 8. Allowable peak overpressures and time to maximum response for dome-type closures, 1-HF device, HOB = 0.

S/t	Span S in	Concrete Strength f'_c psi	Static Resistance P_c psi	Revised Static Resistance $P'_c = IF^* \times P_c$ psi	Natural Period T_N ms	$\mu = 2$ P_{so} psi	$\mu = 2$ t_m ms
3	144	5,000	6,000	9,000	1.9	6,800	1.3
		10,000	11,700	18,800		14,200	1.3
	96	5,000	6,000	10,200	1.3	7,700	.91
		10,000	11,700	21,000		15,800	.91
	48	5,000	6,000	12,000	.63	9,000	.44
		10,000	11,700	23,400		17,600	.44
4	144	5,000	4,500	6,700	1.9	5,100	1.3
		10,000	8,800	14,100		10,600	1.3
	96	5,000	4,500	7,600	1.3	5,700	.91
		10,000	8,800	15,800		11,900	.91
	48	5,000	4,500	9,000	.63	6,800	.44
		10,000	8,800	17,600		13,300	.44
6	144	5,000	3,000	4,500	1.9	3,400	1.3
		10,000	5,900	9,400		7,100	1.3
	96	5,000	3,000	5,100	1.3	3,900	.91
		10,000	5,900	10,600		8,000	.91
	48	5,000	3,000	6,000	.63	4,500	.44
		10,000	5,900	11,800		8,900	.44

*See Table 7

Table 8. Allowable peak overpressures and time to maximum response for dome-type closures, 1-MT device, HOB = 0 (continued).

S/t	Span S in	Concrete Strength f'_c psi	Static Resistance P_c psi	Revised Static Resistance $P'_c = IF^* \times P_c$ psi	Natural Period T_N ms	$\mu = 2$ P_{so} psi	$\mu = 2$ t_m ms
8	144	5,000	2,300	3,400	1.9	2,600	1.3
		10,000	4,400	7,000		5,300	1.3
	96	5,000	2,300	3,900	1.3	2,900	.91
		10,000	4,400	7,900		5,900	.91
	48	5,000	2,300	4,600	.63	3,500	.44
		10,000	4,400	8,800		6,600	.44

*See Table 7

Table 9. Strength increase ratios due to strain rate for silos in axial compression.

Length ft	Concrete Strength psi	Natural Period ms	Strain Rate in/in/s	Dynamic to Static Strength (IF) Ratio
10	5,000	5.45	1	1.4
	10,000	4.62	2	1.4
15	5,000	8.18	1	1.4
	10,000	6.93	1	1.4
20	5,000	10.9	.7	1.4
	10,000	9.23	1	1.4

Table 10. Strength increase ratios due to strain rate for silos in hoop compression.

Span (S) ft	Concrete Strength psi	Natural Period ms	Strain Rate in/in/s	Dynamic to Static Strength (IF) Ratio
4	5,000	1.09	8	1.9
	10,000	.92	9	1.9
8	5,000	2.18	4	1.6
	10,000	1.84	4	1.6
12	5,000	3.27	2	1.4
	10,000	2.76	3	1.5

Table 11. Peak pressure at time, $t = t_2$.

P_{so} ksi	C_L ft/s	t_2 ms	$\tau = \frac{t_2}{t_o}$	a	b	c	α	β	γ	$P(t_2)$ ksi
15	800	5.75	.0038	.015	.160	.825	7.0	55	1,000	2.5
10	750	6.17	.0041	.022	.170	.808	5.4	44	660	2.2
5	700	6.64	.0044	.040	.190	.770	3.9	28	340	1.9
1	600	7.83	.0052	.150	.30	.550	2.9	21	130	.7
.5	600	7.83	.0052	.250	.37	.380	2.6	20	100	.4

Table 12. Triaxial stress relationships for unlined silo after soil stress engulfment, P_{so} = 15,000 psi .

S/t	σ_{axial} psi	σ_{hoop} psi	σ_{radial} psi	σ_3/σ_1	σ_2/σ_1	σ_2/σ_r	σ_1/σ_r
2	3,250	11,000	5,500	.29	.50	5.6	10.8
3	3,800	13,750	5,500	.28	.40	4.3	10.4
4	4,350	16,500	5,500	.26	.33	3.0	9.4
5	4,950	19,250	5,500	.26	.28	2.2	9.0
6	5,600	22,000	5,500	.25	.25	1.7	8.6
7	6,200	24,750	5,500	.22	.25	1.6	7.8
8	6,800	27,500	5,500	.20	.25	1.6	6.1

Table 13. Triaxial stress relationships for unlined silo after soil stress engulfment, P_{so} = 10,000 psi .

S/t	σ_{axial} psi	σ_{hoop} psi	σ_{radial} psi	σ_3/σ_1	σ_2/σ_1	σ_2/σ_r	σ_1/σ_r
2	2,900	8,000	4,000	.36	.50	6.8	13.0
3	3,400	10,000	4,000	.34	.40	5.3	12.2
4	3,900	12,000	4,000	.32	.33	4.1	11.6
5	4,400	14,000	4,000	.28	.32	3.1	10.2
6	5,000	16,000	4,000	.25	.31	2.6	9.2
7	5,600	18,000	4,000	.22	.31	2.2	8.2
8	6,100	20,000	4,000	.20	.30	2.1	6.6

Table 14. Triaxial stress relationships for unlined silo after soil stress engulfment, P_{so} = 5,000 psi .

S/t	σ_{axial} psi	σ_{hoop} psi	σ_{radial} psi	σ_3/σ_1	σ_2/σ_1	σ_2/σ_r	σ_1/σ_r
2	2,500	4,300	2,150	.50	.60	10.4	17.0
3	3,000	5,400	2,150	.40	.56	8.0	14.4
4	3,400	6,450	2,150	.33	.53	6.2	12.4
5	3,900	7,500	2,150	.29	.52	5.2	11.2
6	4,300	8,600	2,150	.25	.50	4.5	9.4
7	4,800	9,650	2,150	.22	.50	4.1	8.4
8	5,250	10,750	2,150	.20	.49	3.6	7.3

Table 15. Allowable peak overpressures and time to maximum response for unlined silos responding in axial compression prior to arrival of radial soil stress.

S/t	Concrete Strength f'_c psi	Static Resistance P_s psi	Revised Static Resistance $P'_s = P_s \times 1.4 \times 1.2$ psi	Natural Period T_N ms	Pulse Duration t_d ms	$\mu = 2$ P_{so} psi	$\mu = 2$ t_m ms
2	5,000	3,750	6,300	8.2	6.4	7,050	4.5
	10,000	7,500	12,600	7.0	5.8	13,800	4.1
3	5,000	3,200	5,400	8.2	6.5	6,000	4.6
	10,000	6,400	10,750	7.0	6.0	11,700	4.2
4	5,000	2,800	4,700	8.2	6.6	5,200	4.6
	10,000	5,600	9,400	7.0	6.2	10,100	3.7
5	5,000	2,500	4,200	8.2	6.7	4,650	4.7
	10,000	5,000	8,400	7.0	6.3	9,000	3.8
6	5,000	2,200	3,700	8.2	6.8	4,050	4.8
	10,000	4,400	7,400	7.0	6.4	7,800	3.8
7	5,000	2,000	3,350	8.2	6.9	3,650	4.8
	10,000	4,000	6,700	7.0	6.5	7,000	3.9
8	5,000	1,800	3,000	8.2	6.9	3,300	4.8
	10,000	3,600	6,050	7.0	6.6	6,300	4.0

Table 16. Allowable peak overpressures and time to maximum response for inner steel lined ($\frac{a}{t} = \frac{1}{64}$) silos responding in axial compression prior to arrival of radial soil stress.

S/t	Concrete Strength f'_c psi	Static Resistance P_s psi	Revised Static Resistance $P'_s = P_s \times 1.4 \times 1.5$ psi	Natural Period T_N ms	Pulse Duration t_d ms	$\mu = 2$ P_{so} psi	$\mu = 2$ t_m ms
2	5,000	4,200	8,800	8.2	6.2	9,950	4.3
	10,000	8,000	16,800	7.0	5.4	19,000	3.8
3	5,000	3,650	7,650	8.2	6.4	8,550	4.5
	10,000	6,850	14,400	7.0	5.6	16,000	3.9
4	5,000	3,200	6,700	8.2	6.5	7,450	4.6
	10,000	6,000	12,600	7.0	5.8	13,900	4.0
5	5,000	2,800	5,900	8.2	6.6	6,550	4.6
	10,000	5,300	11,100	7.0	5.9	12,150	4.1
6	5,000	2,550	5,350	8.2	6.6	5,950	4.6
	10,000	4,700	9,900	7.0	6.2	10,600	3.7
7	5,000	2,300	4,800	8.2	6.7	5,300	4.7
	10,000	4,300	9,000	7.0	6.3	9,550	3.8
8	5,000	2,100	4,400	8.2	6.7	4,850	4.7
	10,000	3,900	8,200	7.0	6.4	8,650	3.8

Table 17. Allowable peak overpressures and time to maximum response for inner and outer steel lined ($\frac{a}{t} = \frac{1}{64}$) silos responding in axial compression prior to arrival of radial soil stress.

S/t	Concrete Strength f'_c psi	Static Resistance P_s psi	Revised Static Resistance $P'_s - P_s \times 1.4 \times 2.0$ psi	Natural Period T_N ms	Pulse Duration t_d ms	$\mu = 2$ P_{so} psi	$\mu = 2$ t_m ms
2	5,000	5,200	14,550	8.2	5.5	17,250	4.4
	10,000	9,000	25,200	7.0	4.5	30,500	3.6
3	5,000	4,400	12,300	8.2	5.7	14,400	4.6
	10,000	7,650	21,400	7.0	5.0	24,750	4.0
4	5,000	3,850	10,800	8.2	5.9	12,500	4.7
	10,000	6,650	18,600	7.0	5.2	21,200	3.6
5	5,000	3,400	9,500	8.2	6.0	10,900	4.2
	10,000	5,850	16,400	7.0	5.5	18,400	3.8
6	5,000	3,000	8,400	8.2	6.2	9,500	4.3
	10,000	5,200	14,550	7.0	5.7	16,100	4.0
7	5,000	2,700	7,550	8.2	6.4	8,500	4.5
	10,000	4,700	13,150	7.0	5.8	14,500	4.0
8	5,000	2,500	7,000	8.2	6.4	7,850	4.5
	10,000	4,300	12,050	7.0	5.9	13,200	4.1

Table 18. Dynamic analysis of unlined silo in hoop compression after arrival of radial soil stress.

S/t	Concrete Strength f'_c psi	Static Resistance P_c psi	Revised Static Resistance $P'_c = P'_c \times 1.4 \times 4$ psi	Natural Period T_N ms	$\mu = 2$ σ_{radial} psi	t_m ms	$\sigma_z = \frac{\sigma_3}{.02}$ psi	$P_{so} = \frac{\sigma_z}{.875}$ psi
2	5,000	2,500	14,000	1.1	10,650	.88	25,350	29,000
	10,000	5,000	28,000	.9	21,250	.72	50,600	57,800
3	5,000	2,000	11,200	1.6	8,500	1.12	20,200	23,100
	10,000	4,000	22,400	1.4	17,000	1.12	40,500	46,250
4	5,000	1,650	9,250	2.2	7,050	1.76	16,800	19,200
	10,000	3,300	18,500	1.8	14,050	1.44	33,450	38,250
5	5,000	1,400	7,850	2.8	6,000	2.24	14,300	16,300
	10,000	2,800	15,700	2.3	11,950	1.84	28,450	32,500
6	5,000	1,250	7,000	3.3	5,350	2.64	12,750	14,550
	10,000	2,500	14,000	2.8	10,650	2.24	25,350	29,000
7	5,000	1,100	6,150	3.9	4,700	3.12	11,200	12,800
	10,000	2,200	12,300	3.1	9,350	2.48	22,250	25,400
8	5,000	1,090	5,600	4.4	4,250	3.52	10,100	11,550
	10,000	2,000	11,200	3.6	8,500	2.88	20,250	23,100

Table 19. Power and stroke requirements for slab- and dome-type closures.

Range ft	P_{so} psi	Ejecta Depth ft	Required Stroke ft	Span ft	Slab Closure S/D	Slab Closure Effective Resistance lb	Slab Closure Indicated hp*	Dome Closure S/D	Dome Closure Effective Resistance lb	Dome Closure Indicated hp*
600	15,000	3.8	5	4	1.9	22,000	0.7	3.5	42,800	1.3
				8	1.8	73,800	2.2	3.2	151,400	4.6
				12	1.7	192,000	5.8	2.8	363,000	11
800	6,600	2.4	3.5	4	2.9	10,100	0.2	7.3	24,000	0.51
				8	2.8	41,300	0.9	6.6	103,100	2.2
				12	2.6	116,200	2.5	6.0	271,200	5.8
1,200	2,000	1.2	2	4	5.5	3,850	0.05	12	13,000	0.16
				8	5.0	19,800	0.22	11	70,400	0.85
				12	4.9	57,400	0.7	10	205,400	2.5
2,000	500	0.3	1	4	8	1,360	0.008	18	7,100	0.04
				8	8	9,100	0.055	16	49,800	0.3
				12	8	28,900	0.18	14	160,000	1

*Travel rate at 1 ft/min assumed.

Table 20. Representative requirements for three different communications terminals.

Communications Terminal	Milstar	DSCS	AHF
Number of Racks*	2	3	2
Terminal Power (kw)**	5.0	9.0	3.0
Cooling (Btu/h)	17,070	30,726	10,242
Weight (lb)	670	1,200	700
Antenna Size	26-in dish	60- to 96-in dish	whip

*Each equipment rack is 2 by 2.5 by 7 ft. Racks may be configured in any mode, e.g. vertical/horizontal that is consistent with the canister design.

**The terminal power estimate provided does not include power required for air circulation/exhaust for cooling equipment or for air circulation for a local power source.

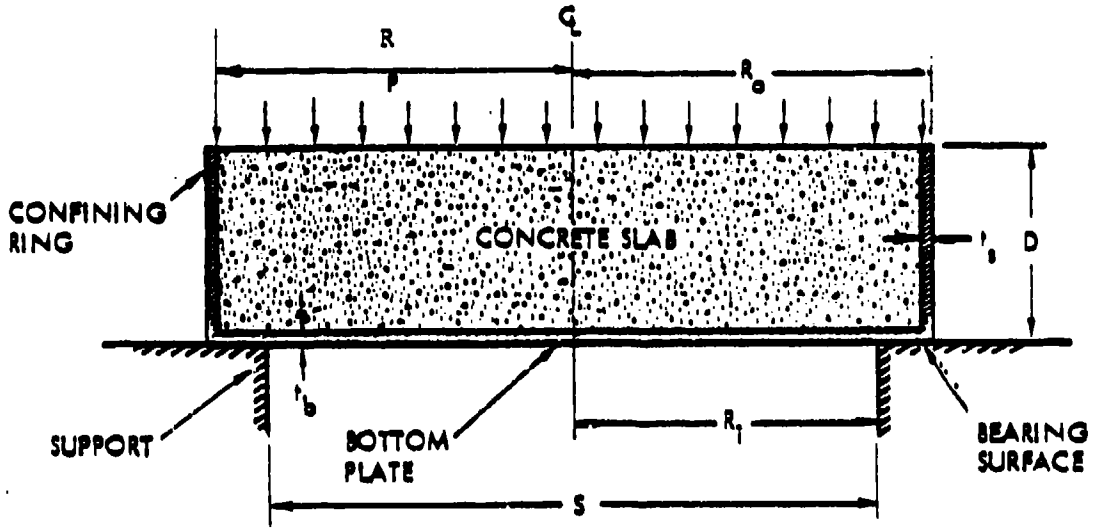

Figure 24. Composite tub-type closure (Refer. 3).

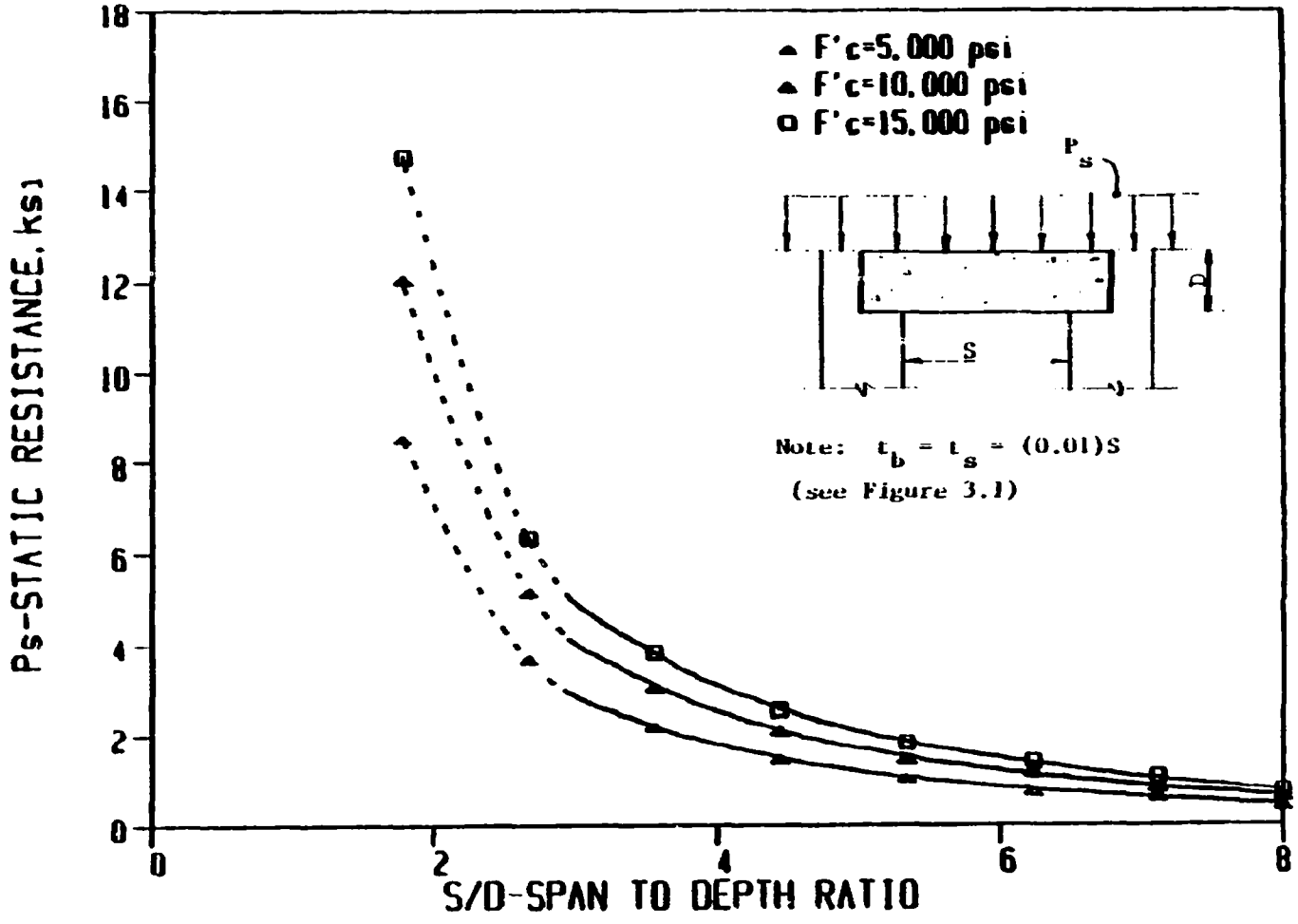

Figure 25. Static resistance of slab-type closures (Equation 3.3).

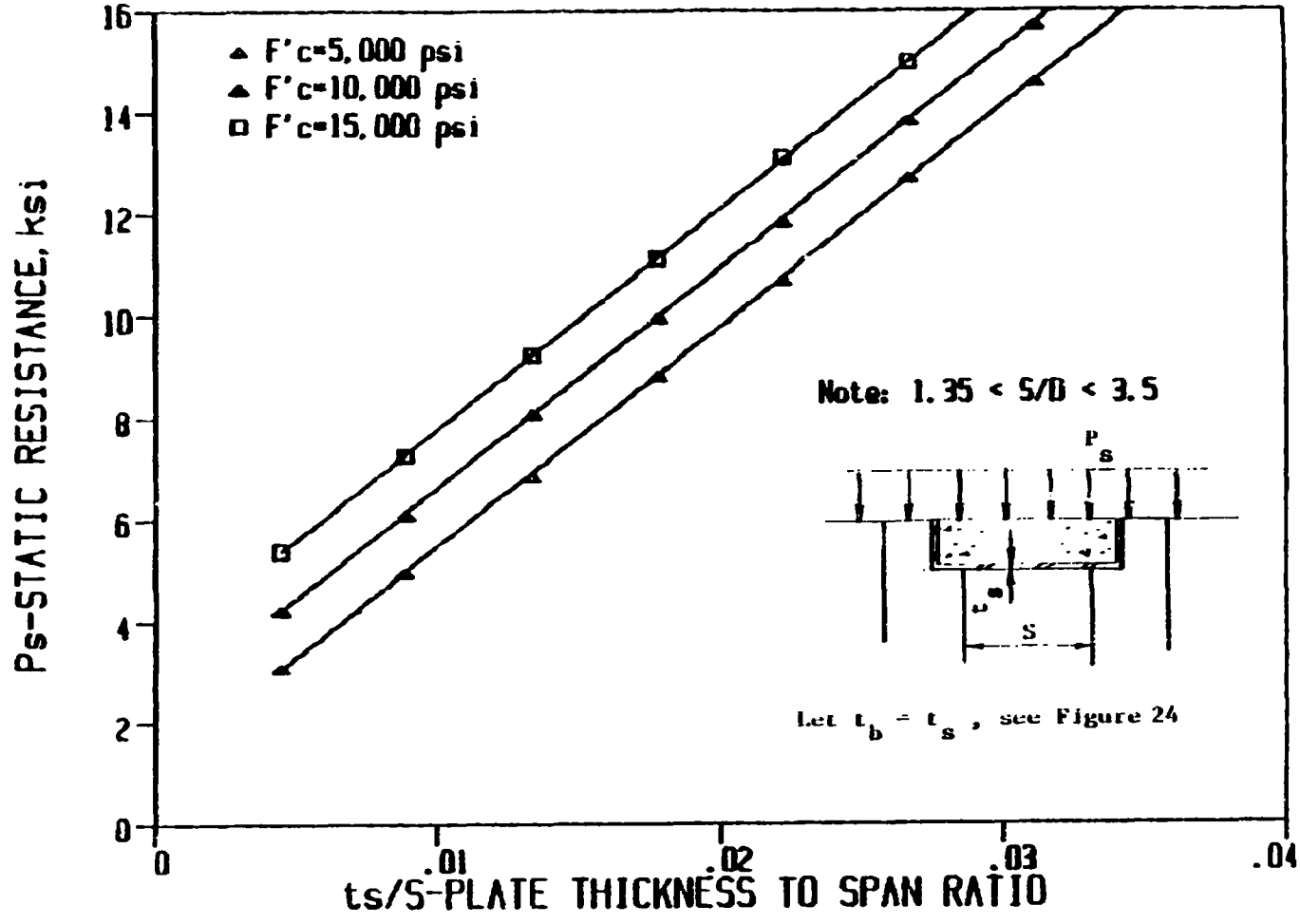

Figure 26. Static resistance of slab-type closures (Equation 3.4).

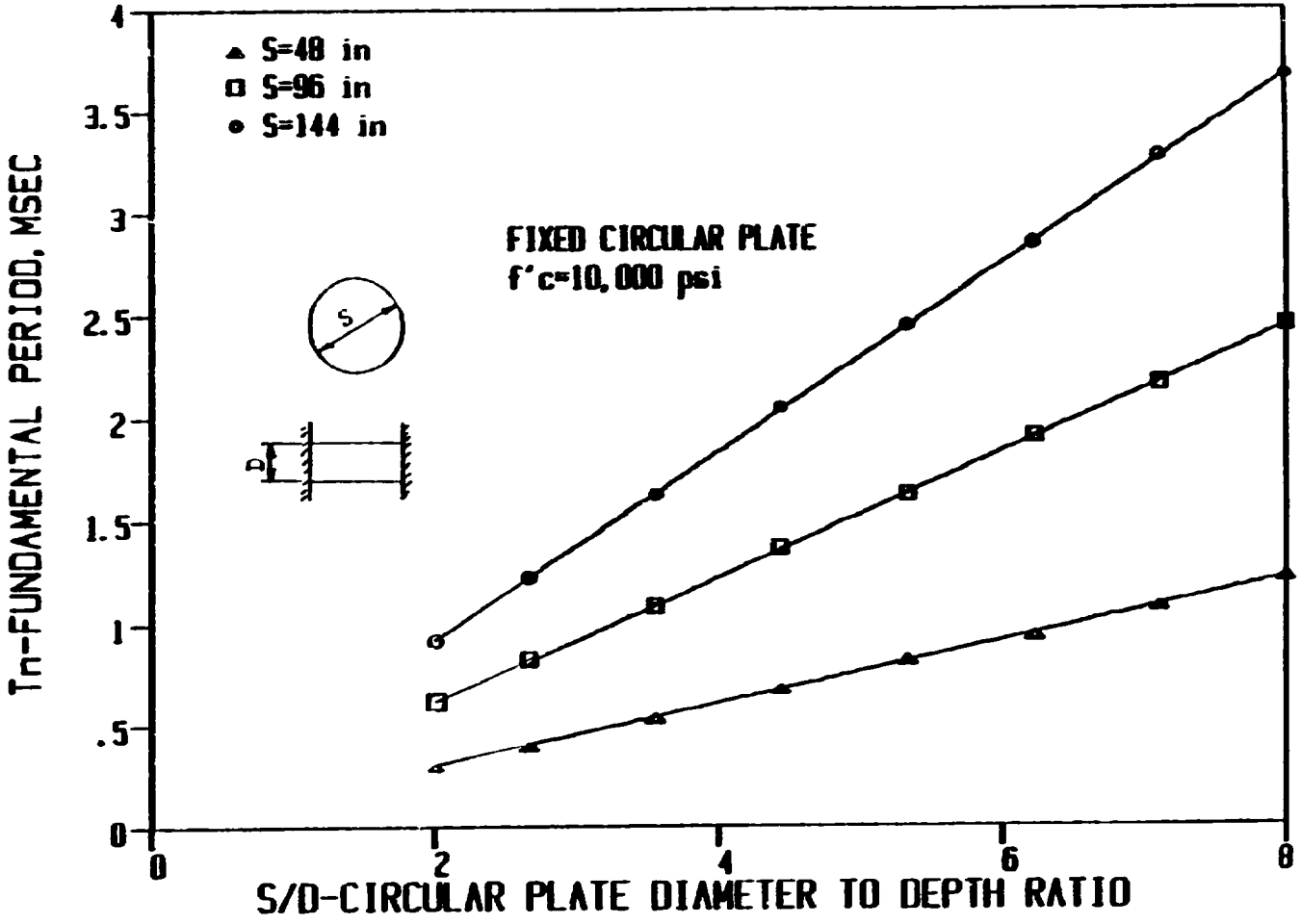

Figure 27. Natural period of circular closure with clamped edges.

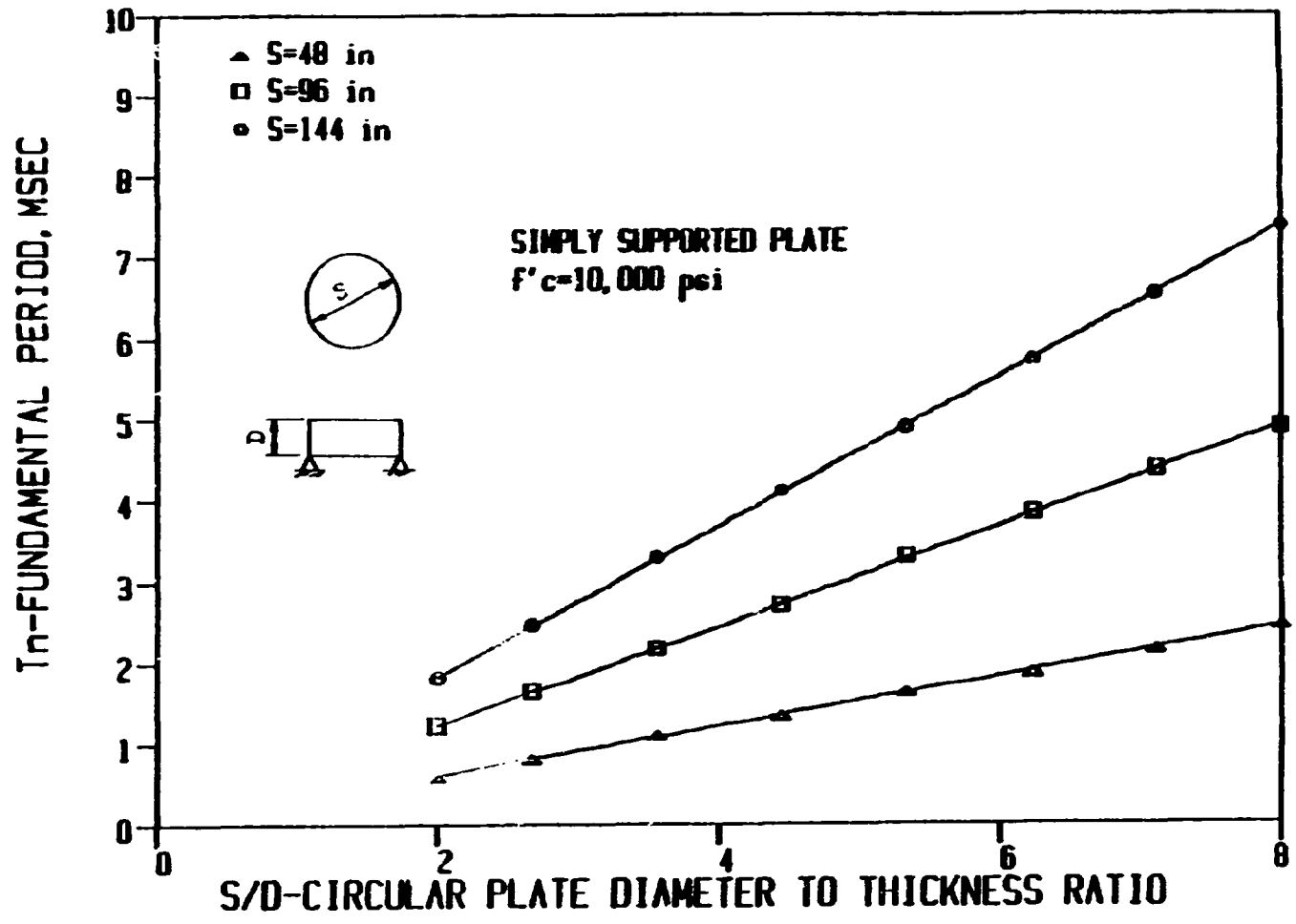

Figure 28. Natural period of circular closure that is simply supported.

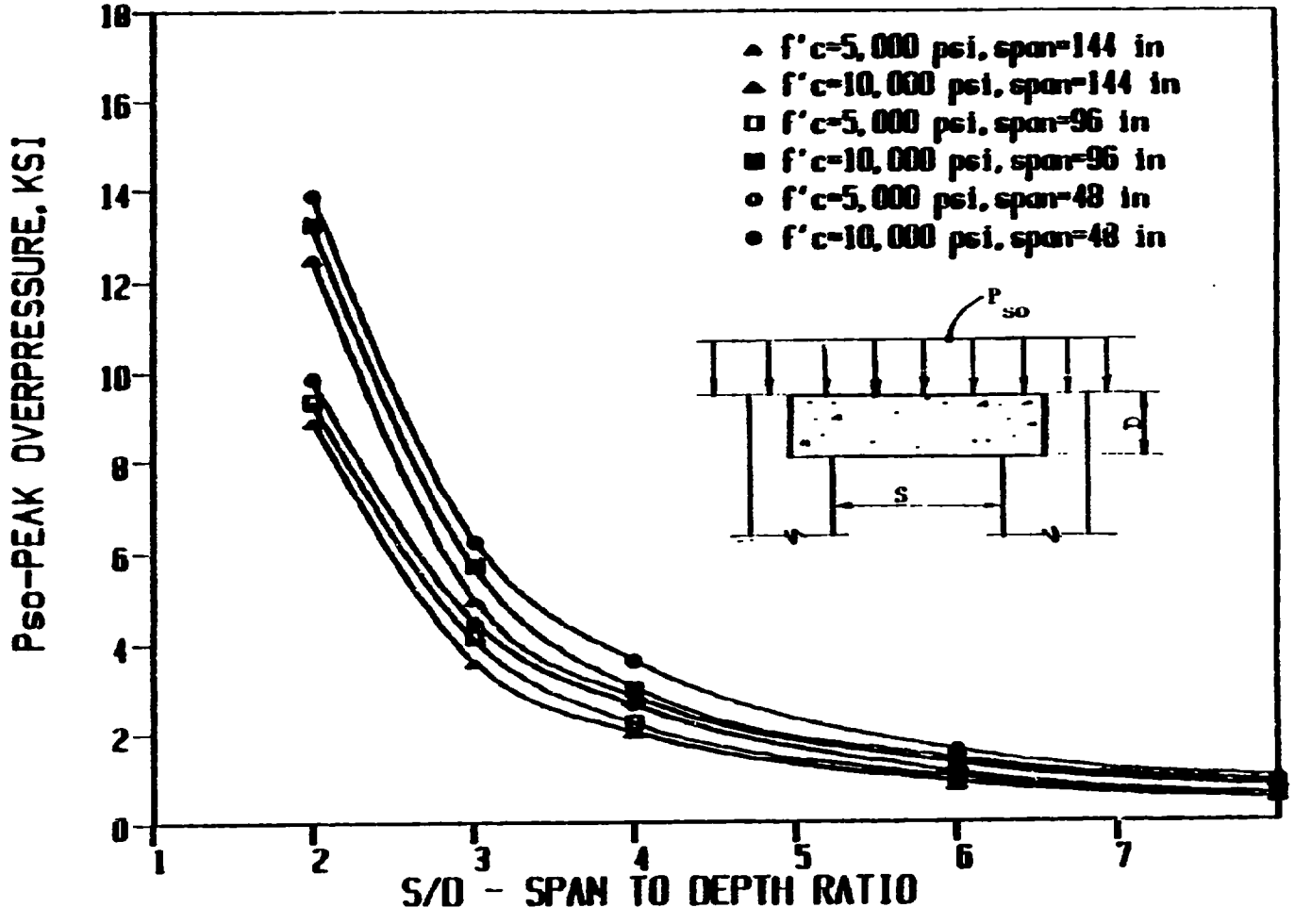

Figure 29. Peak overpressure capacity of slab-type closure, 1-MT weapon, HOB = 0, μ = 2.

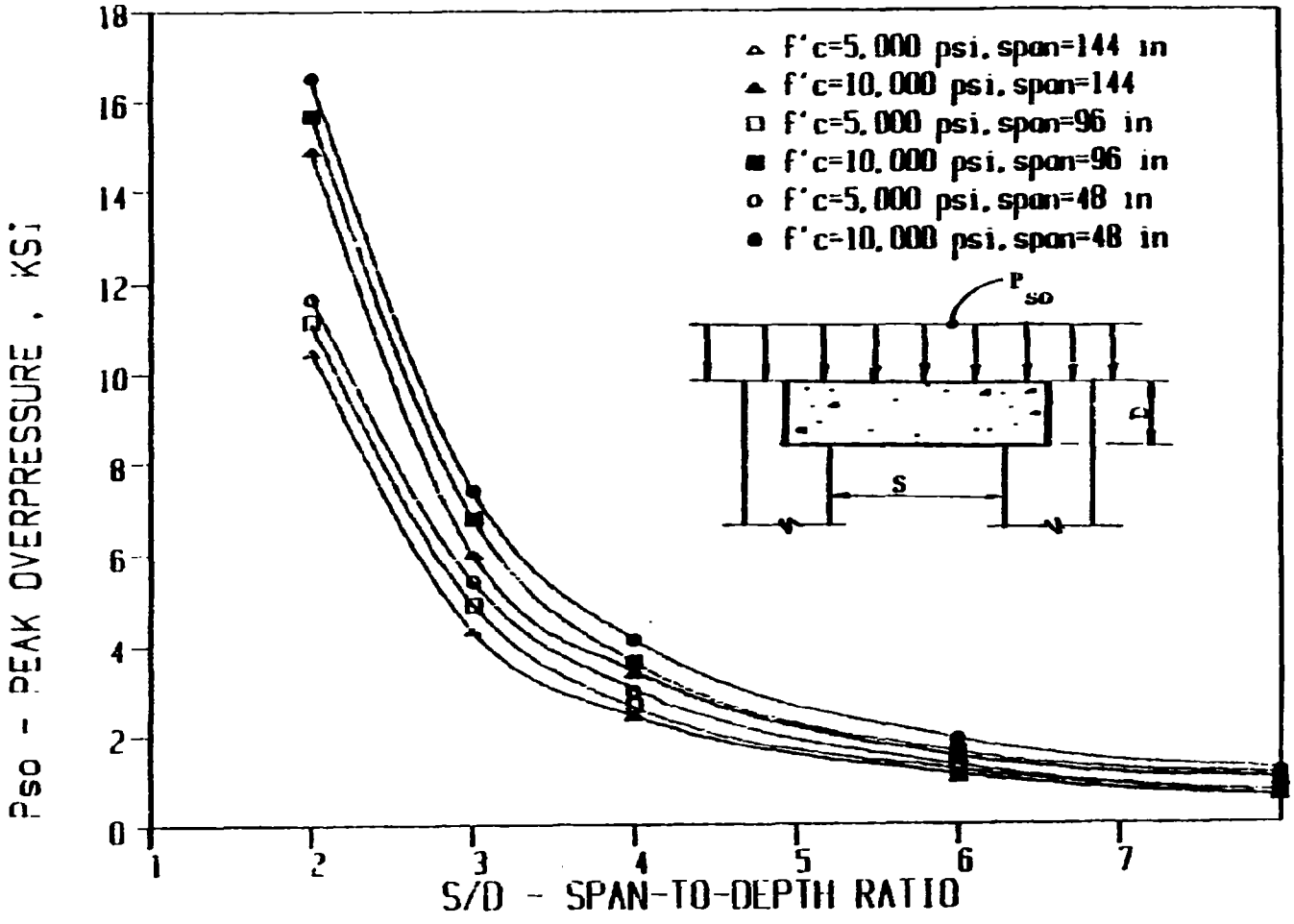

Figure 30. Peak overpressure capacity of slab-type closure, I-HT weapon, HOB = 0, μ = 5.

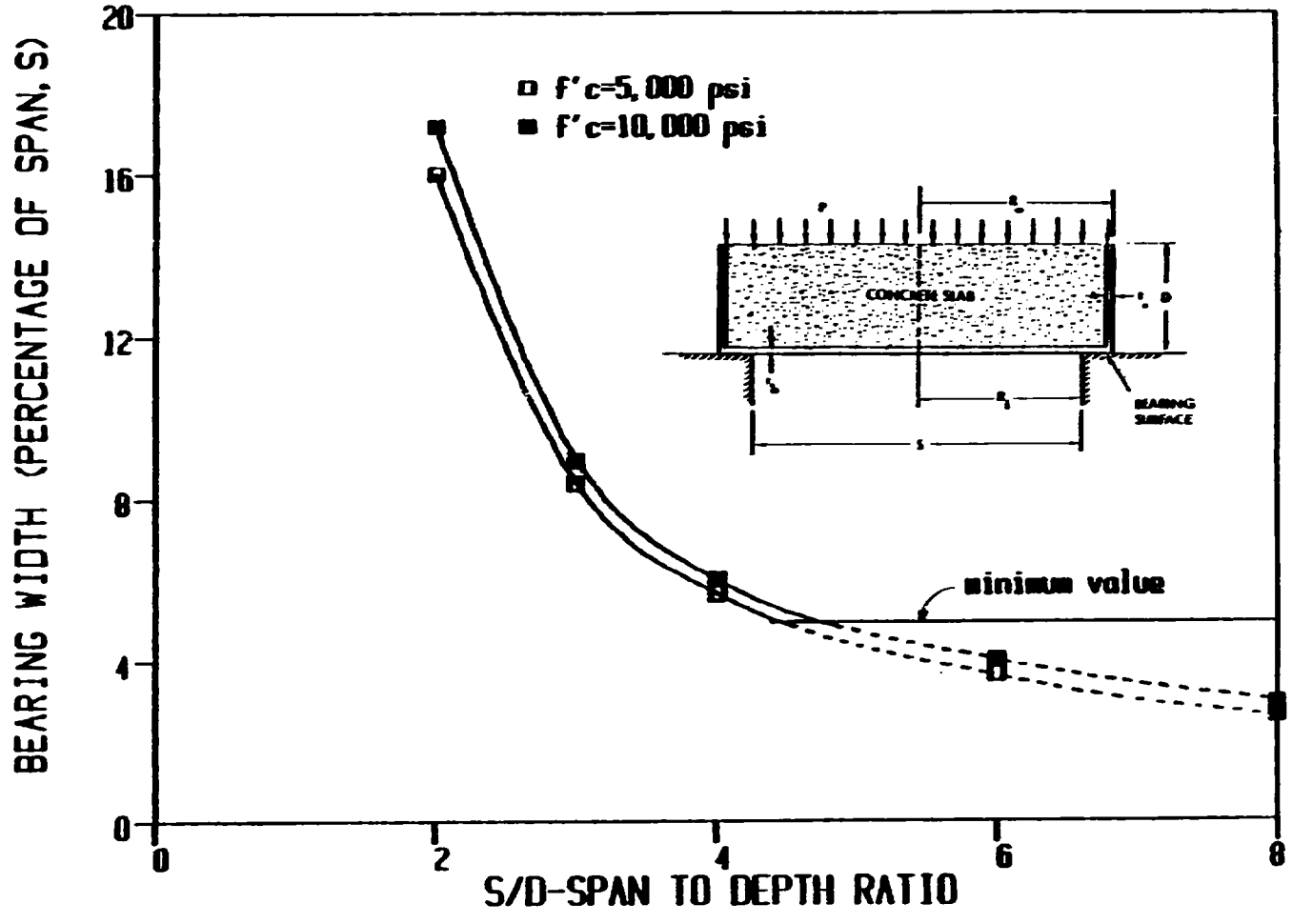

Figure 31. Required bearing width for composite slab closure.

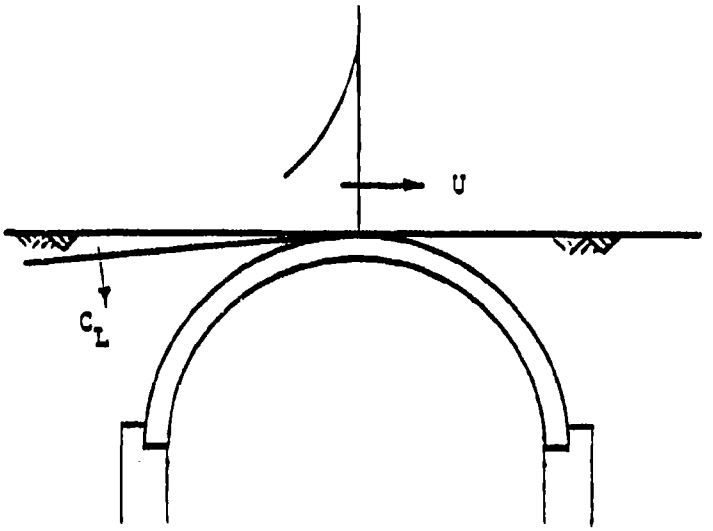

a. Ground surface airblast load

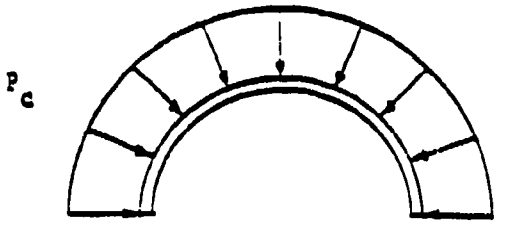

b. Assumed load distribution

Figure 32. Load engulfment and assumed loading for design of dome-type closure.

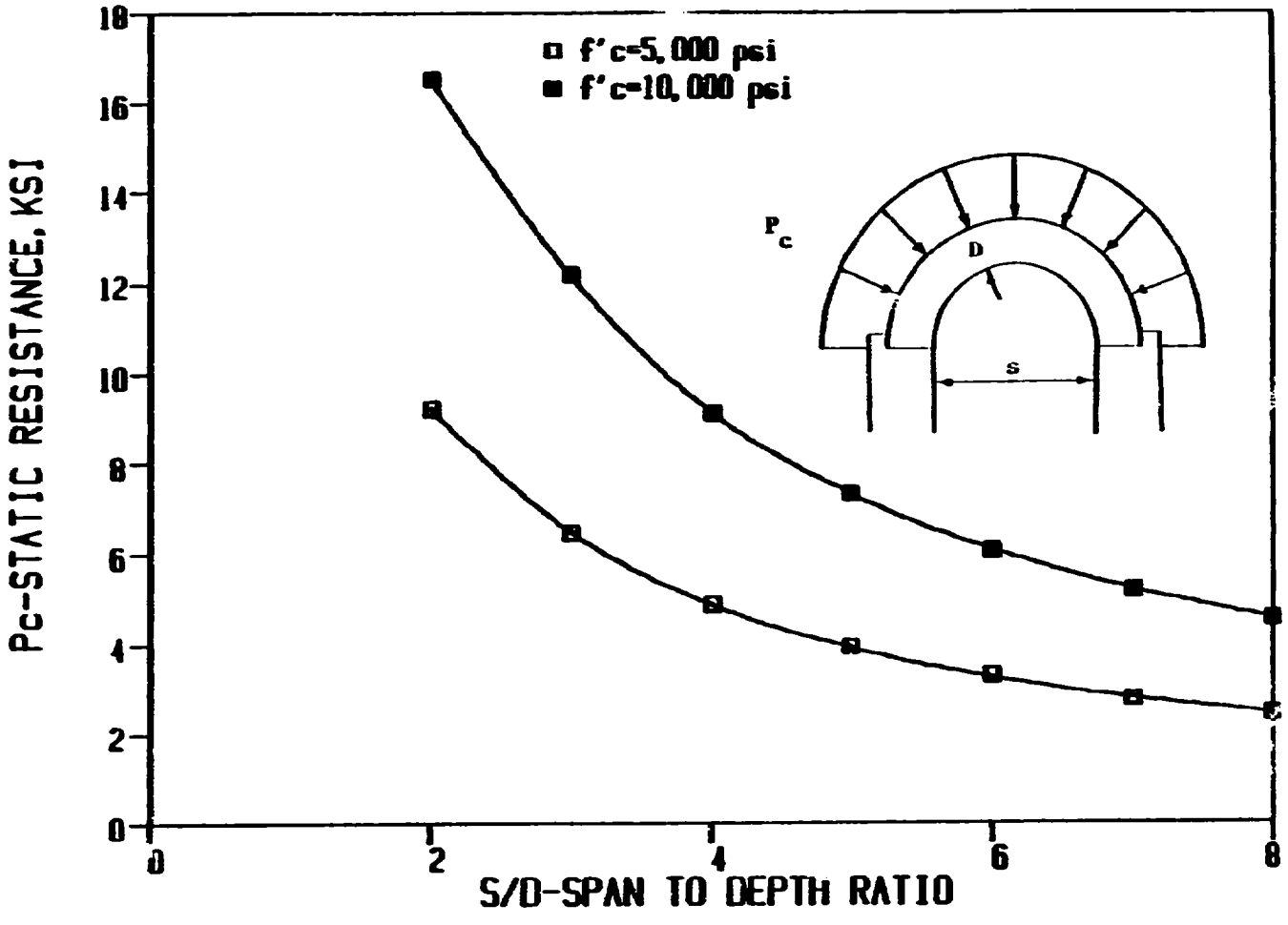

Figure 33. Static resistance of dome-type closure.

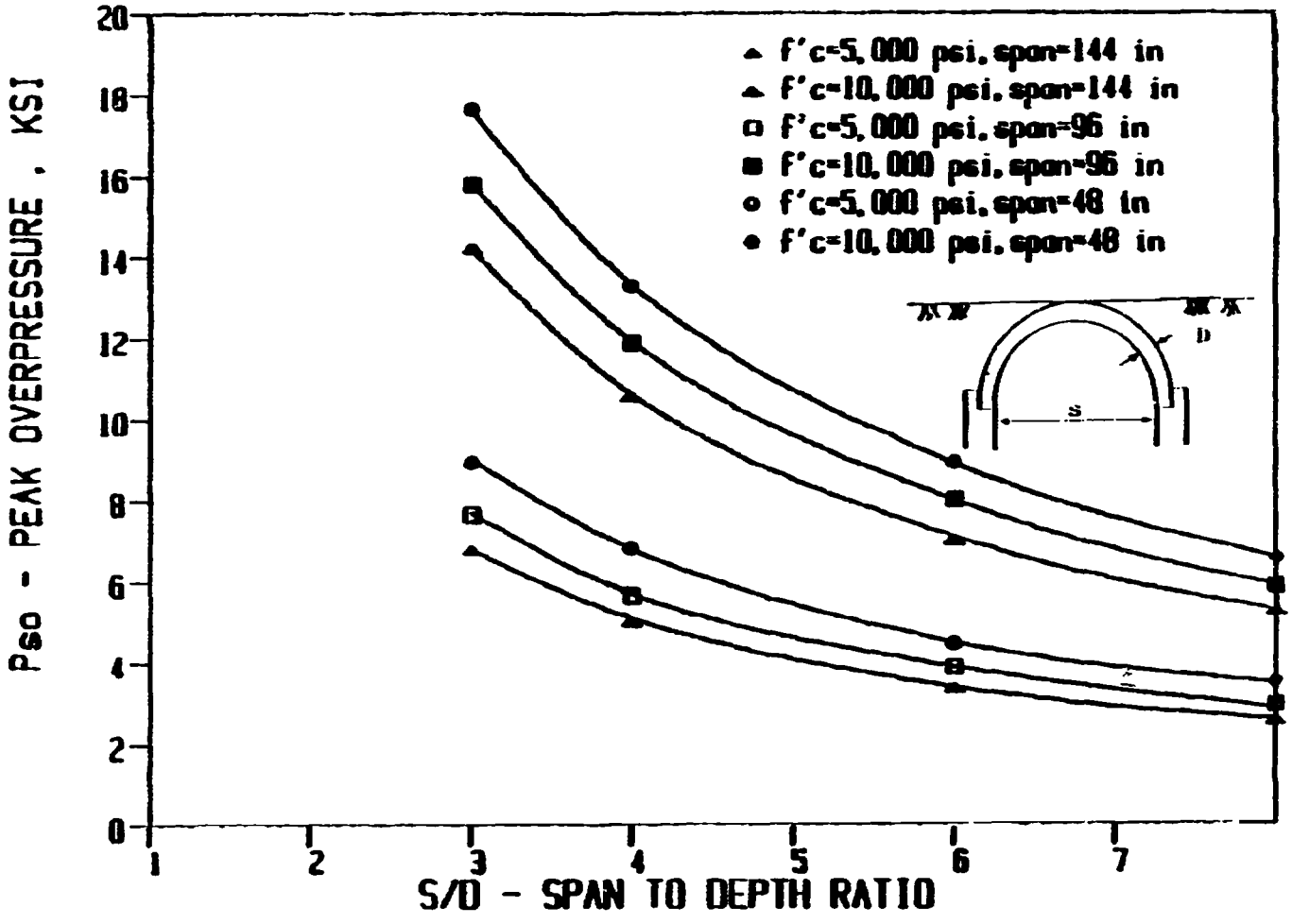

Figure 34. Peak overpressure capacity of dome closure, 1-MT weapon, HOB = 0, $\mu = 2$.

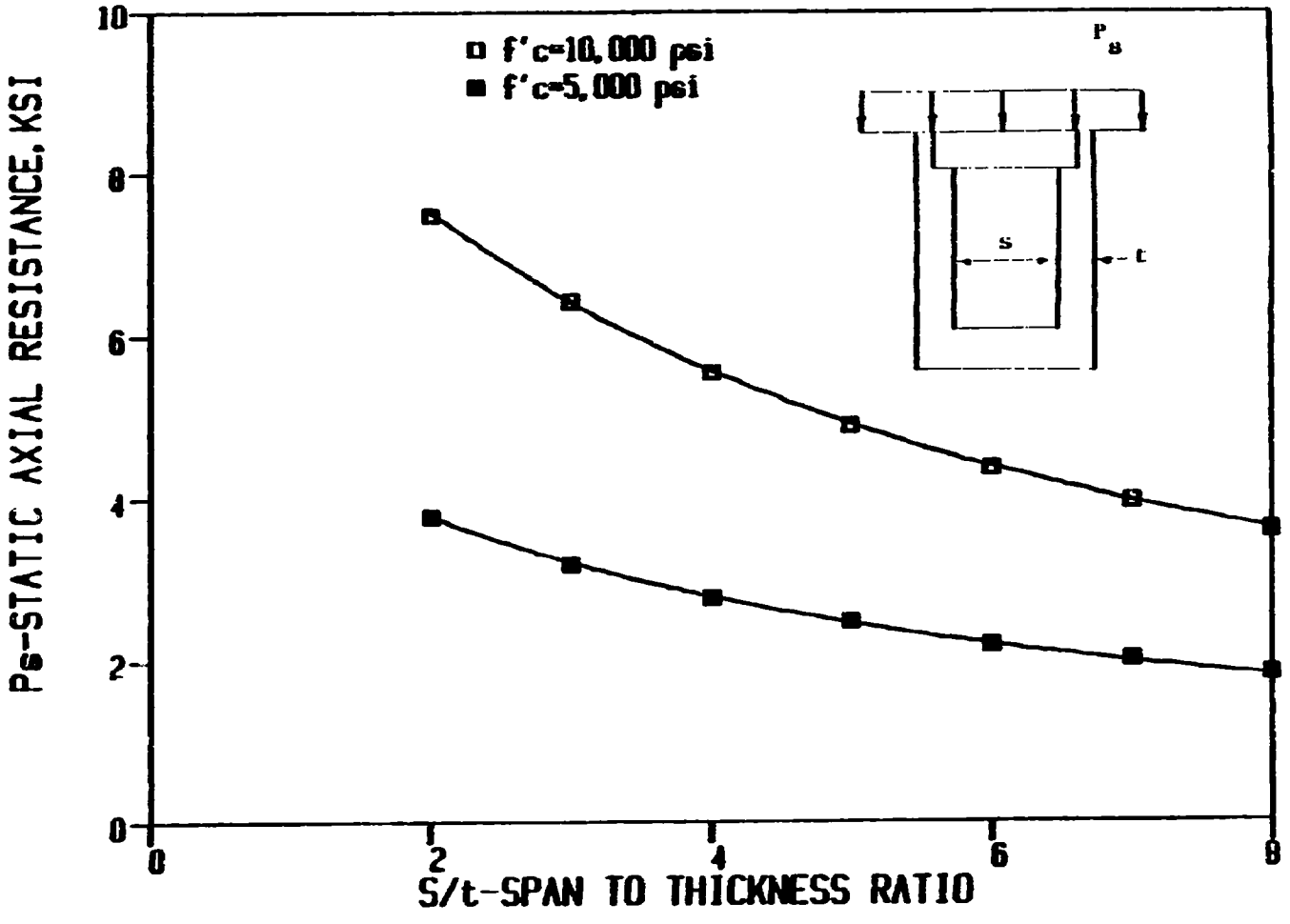

Figure 35. Static axial resistance of silo with no liners.

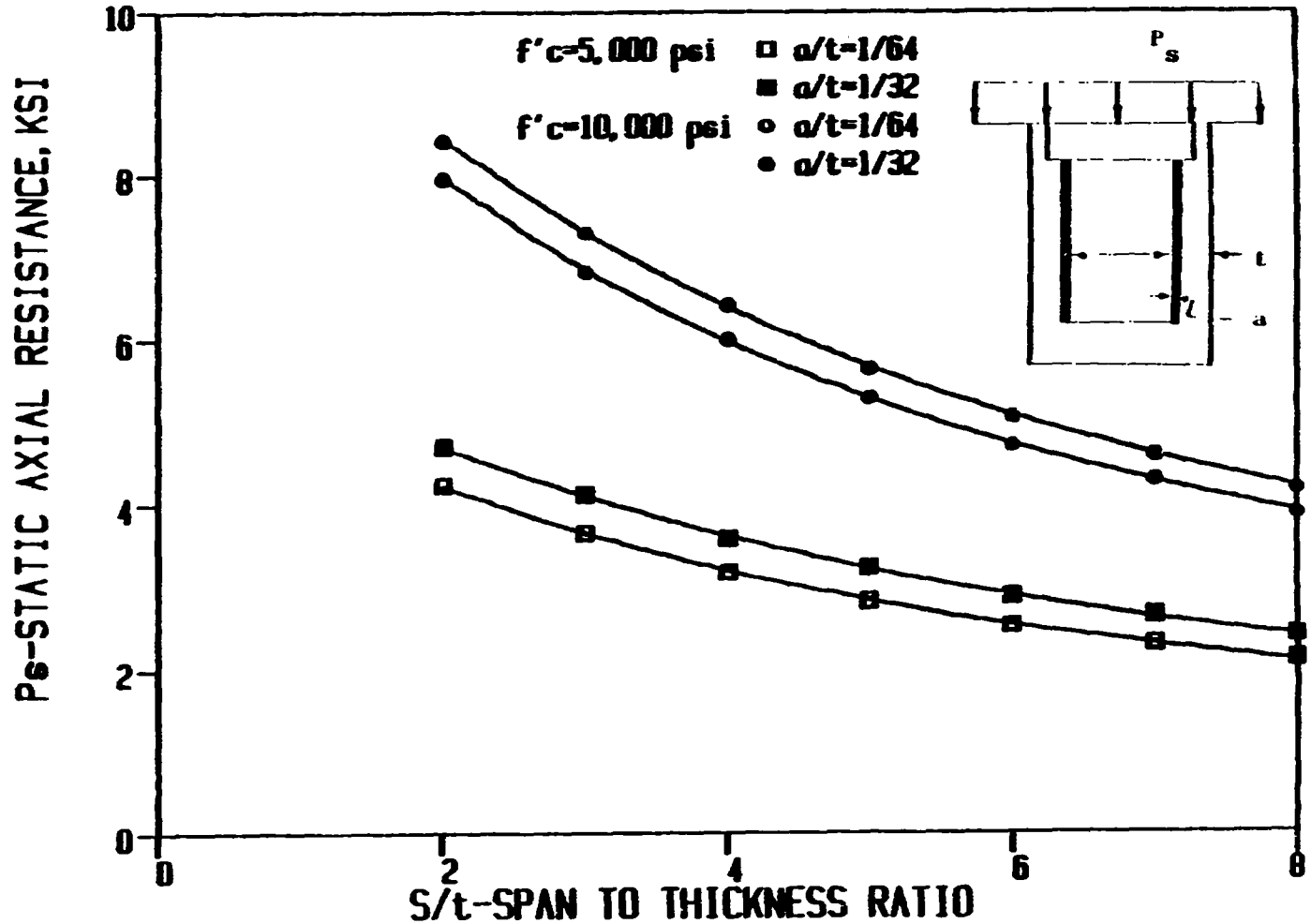

Figure 36. Static axial resistance of silo with internal steel liner only.

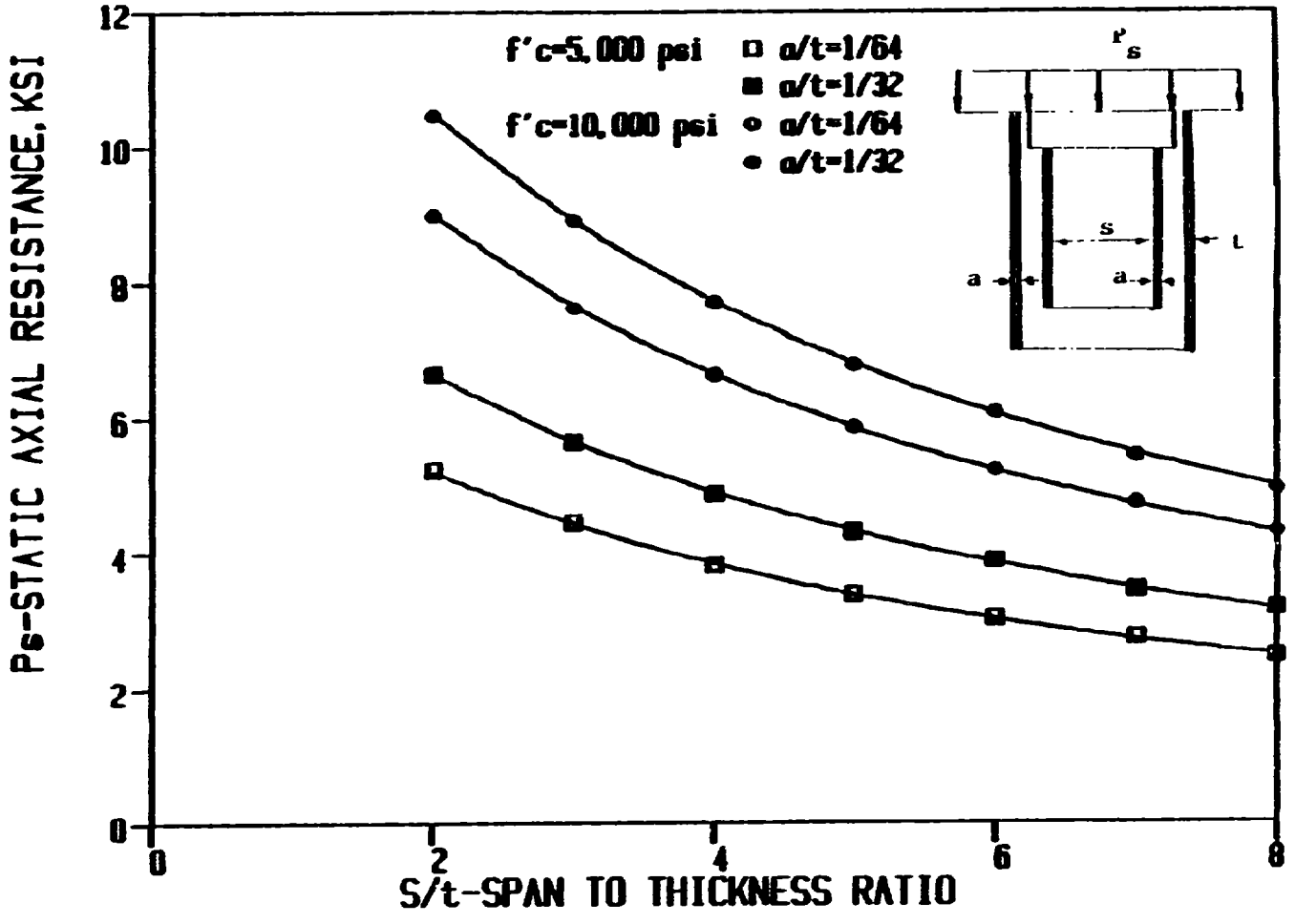

Figure 37. Static axial resistance of silo with internal and external steel liners.

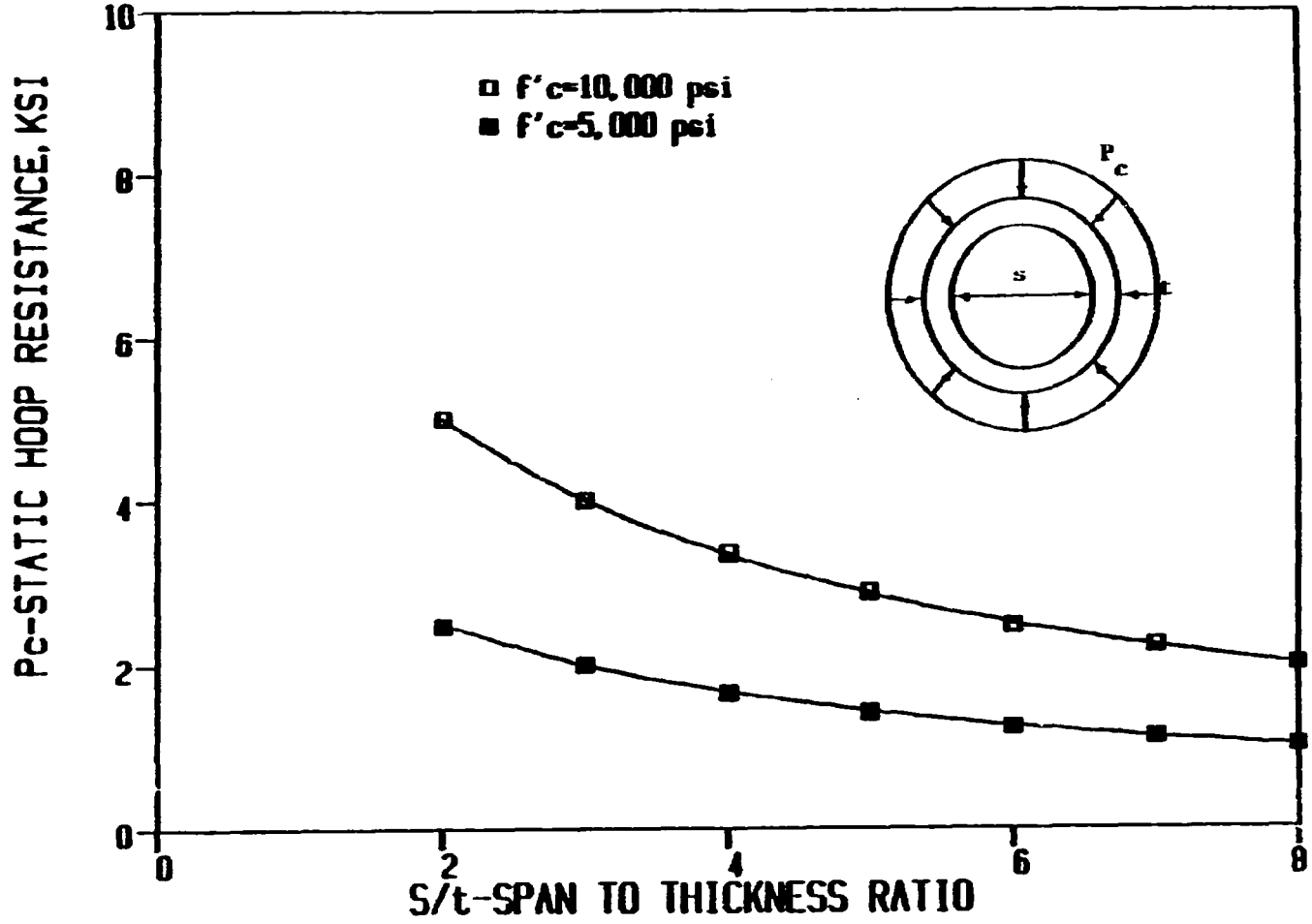

Figure 38. Static hoop (horizontal) resistance of silo with no liners.

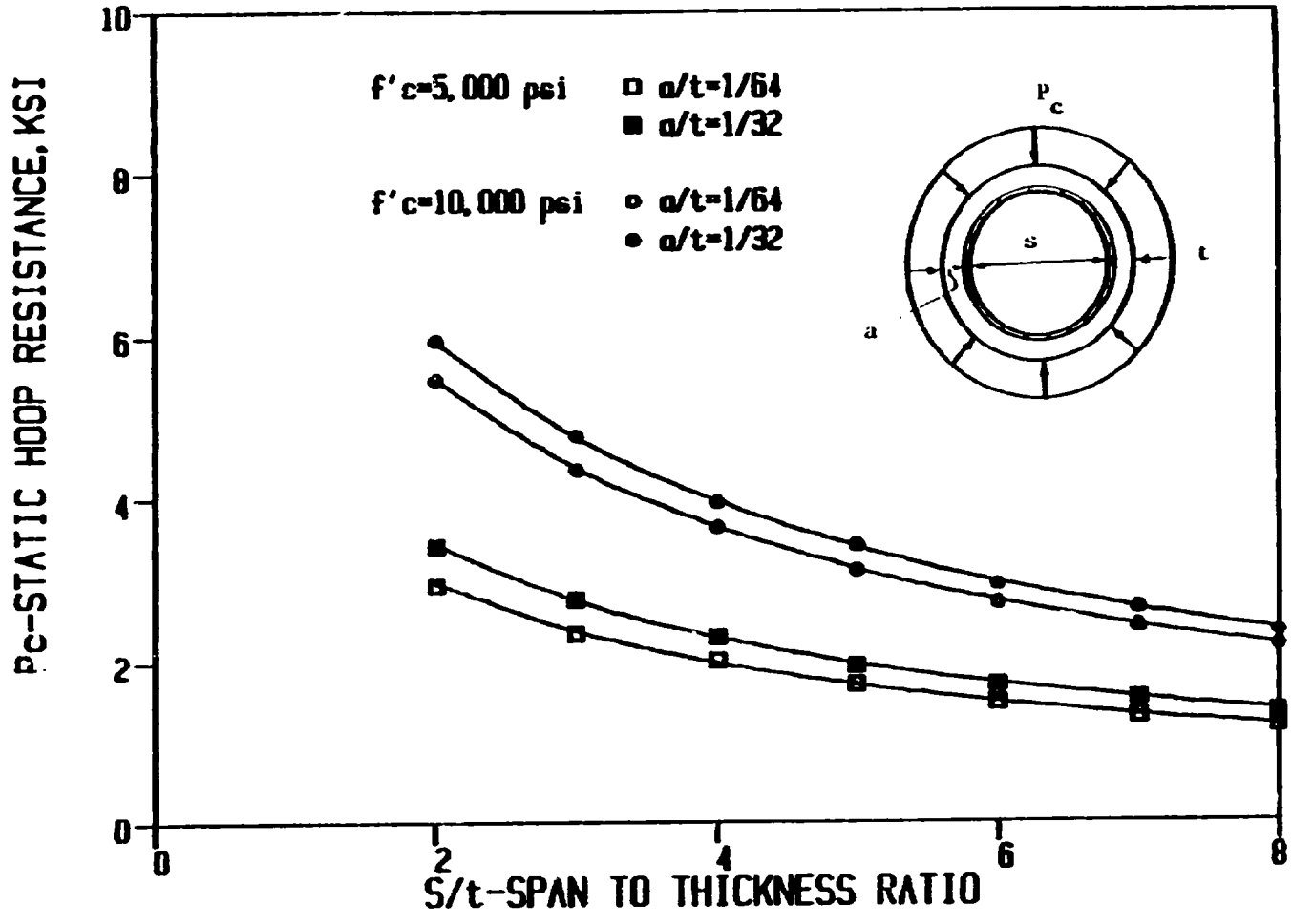

Figure 39. Static hoop (horizontal) resistance of silo with internal steel liner only.

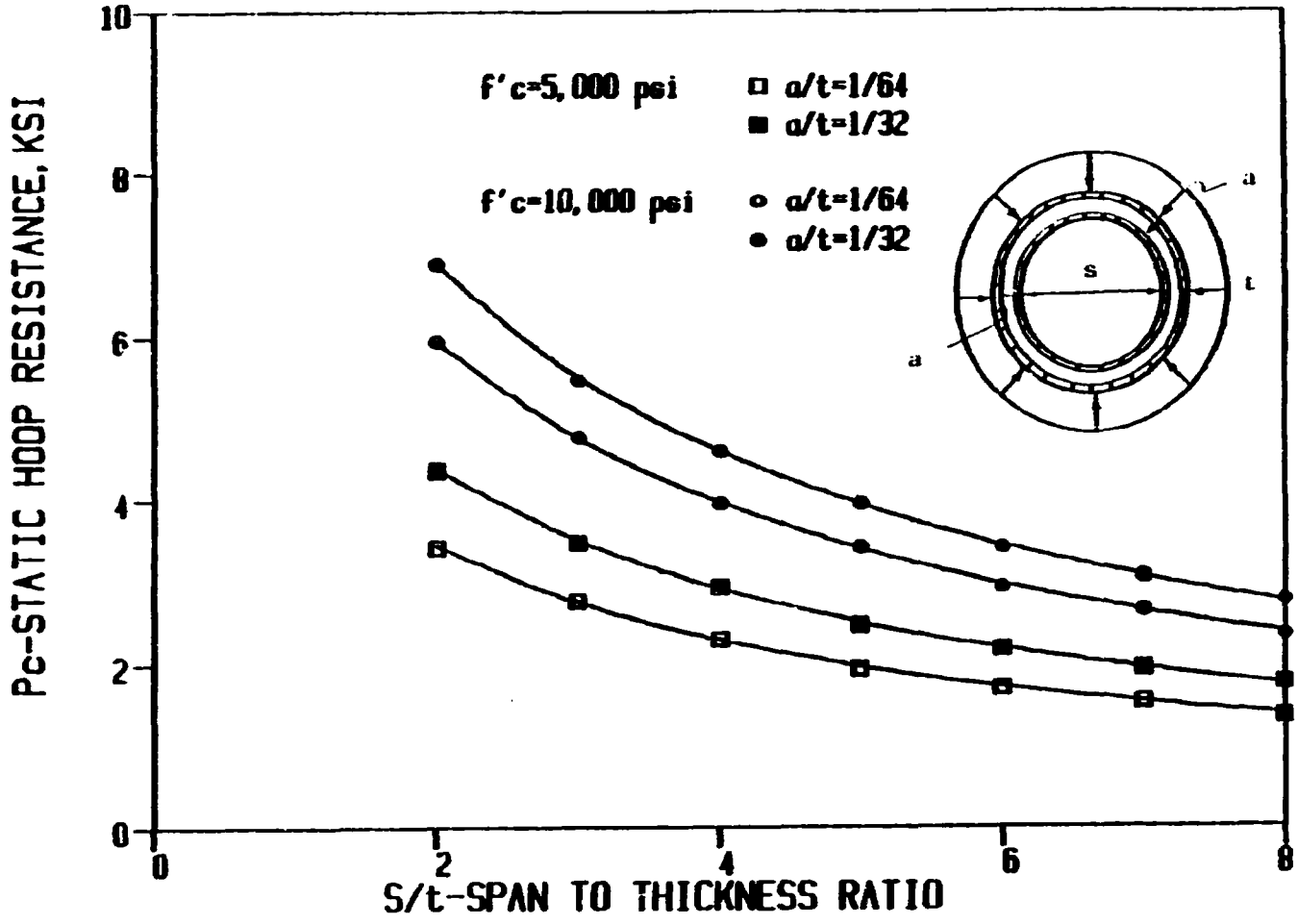

Figure 40. Static hoop (horizontal) resistance of silo with internal and external steel liners.

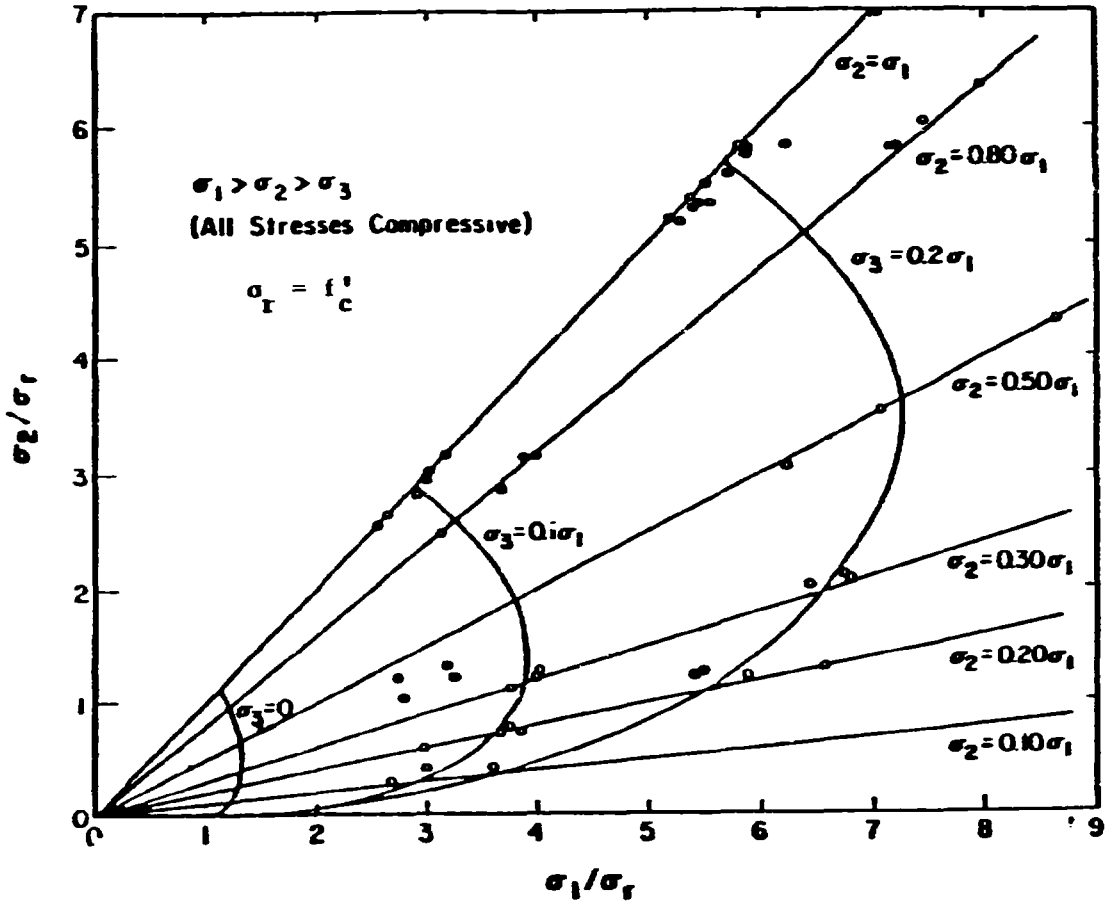

Figure 41. Normalized triaxial compression data (Reference 3).

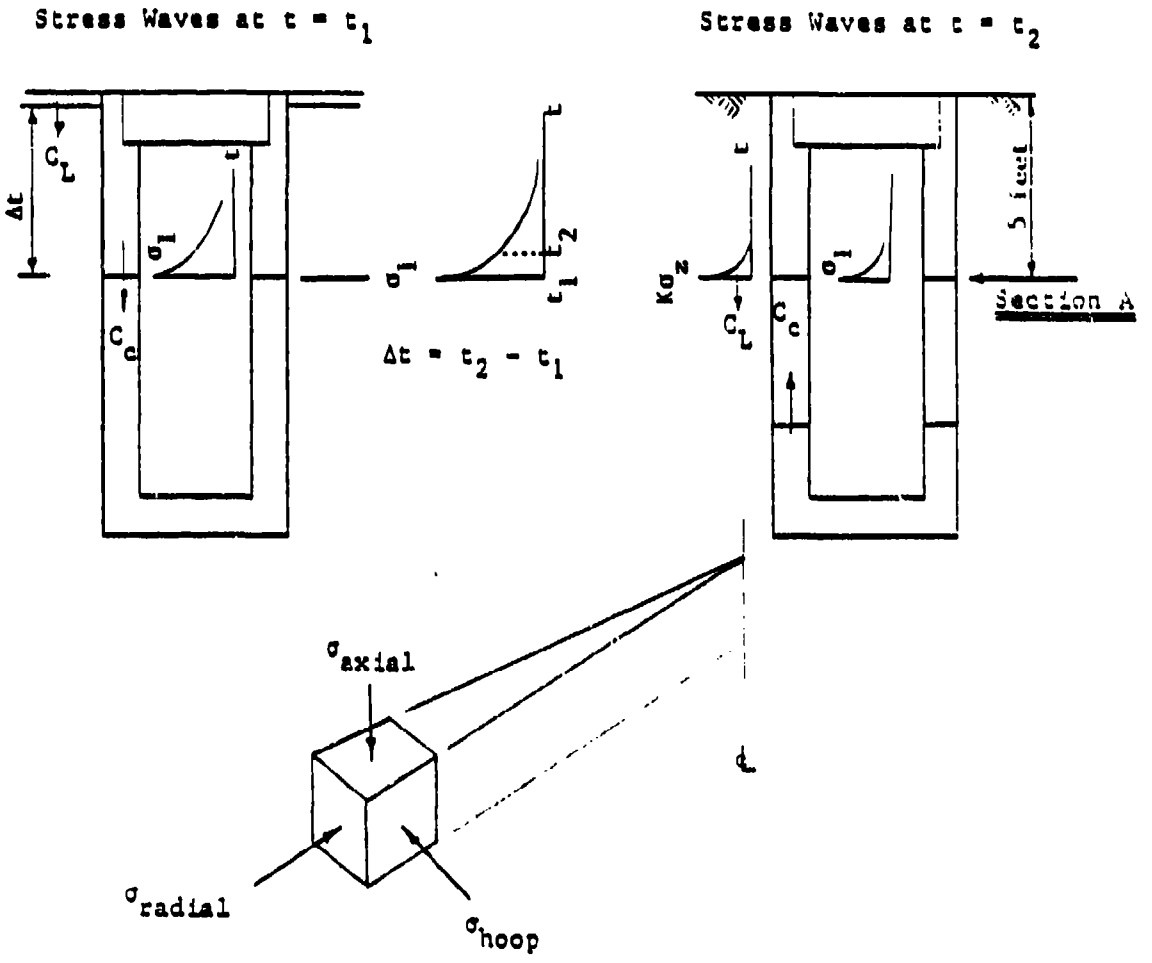

Section A at t = t_1

Prior to Soil Stress Wave Engulfment

Section A at t = t_2

Arrival of Soil Stress Wave

Figure 42. Direct-induced airblast and airblast-induced ground hock engulfment of silo.

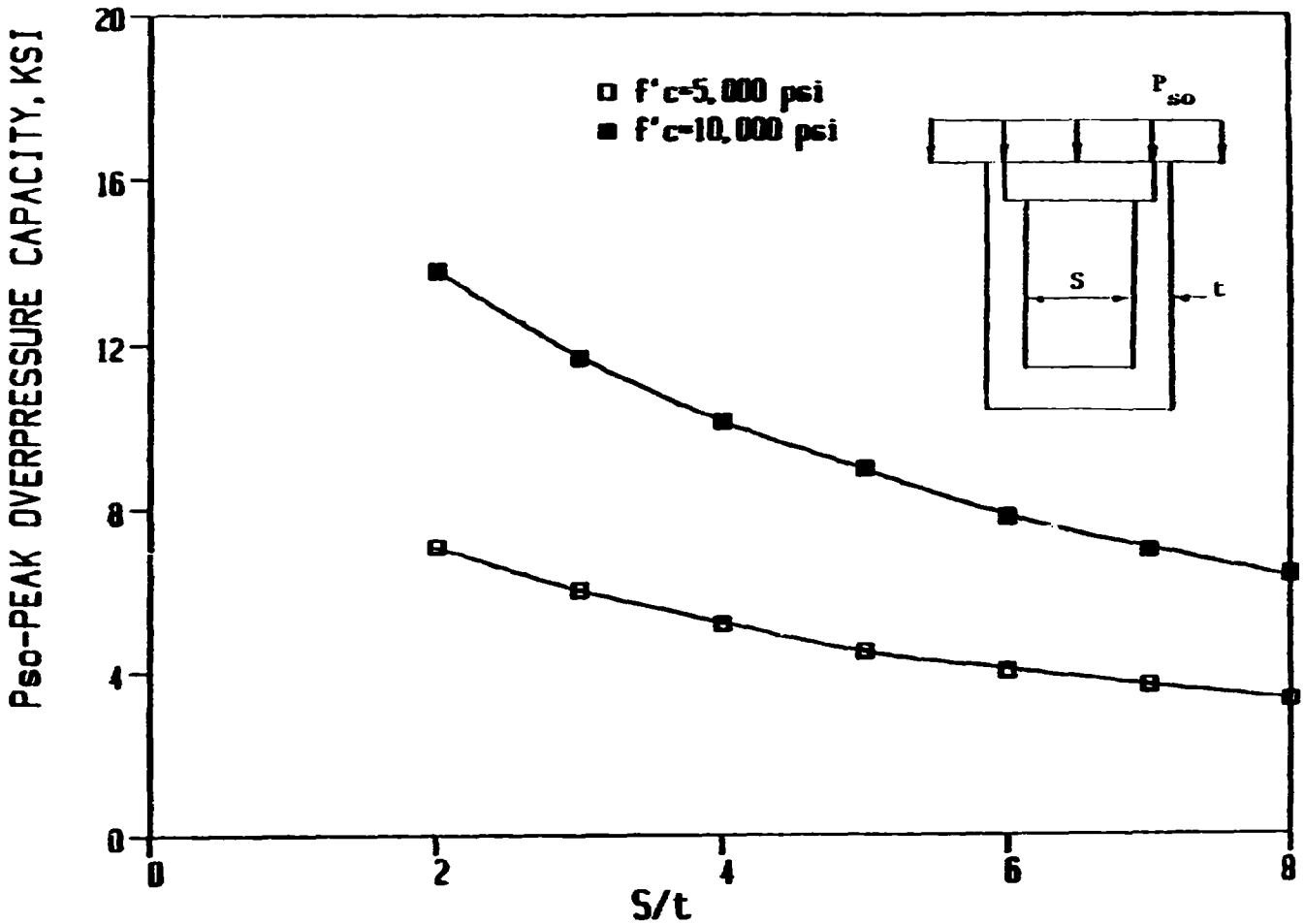

Figure 43. Axial overpressure capacity of unlined silos to a 1-MT weapon prior to arrival of radial soil stress, HOB = 0, μ = 2.

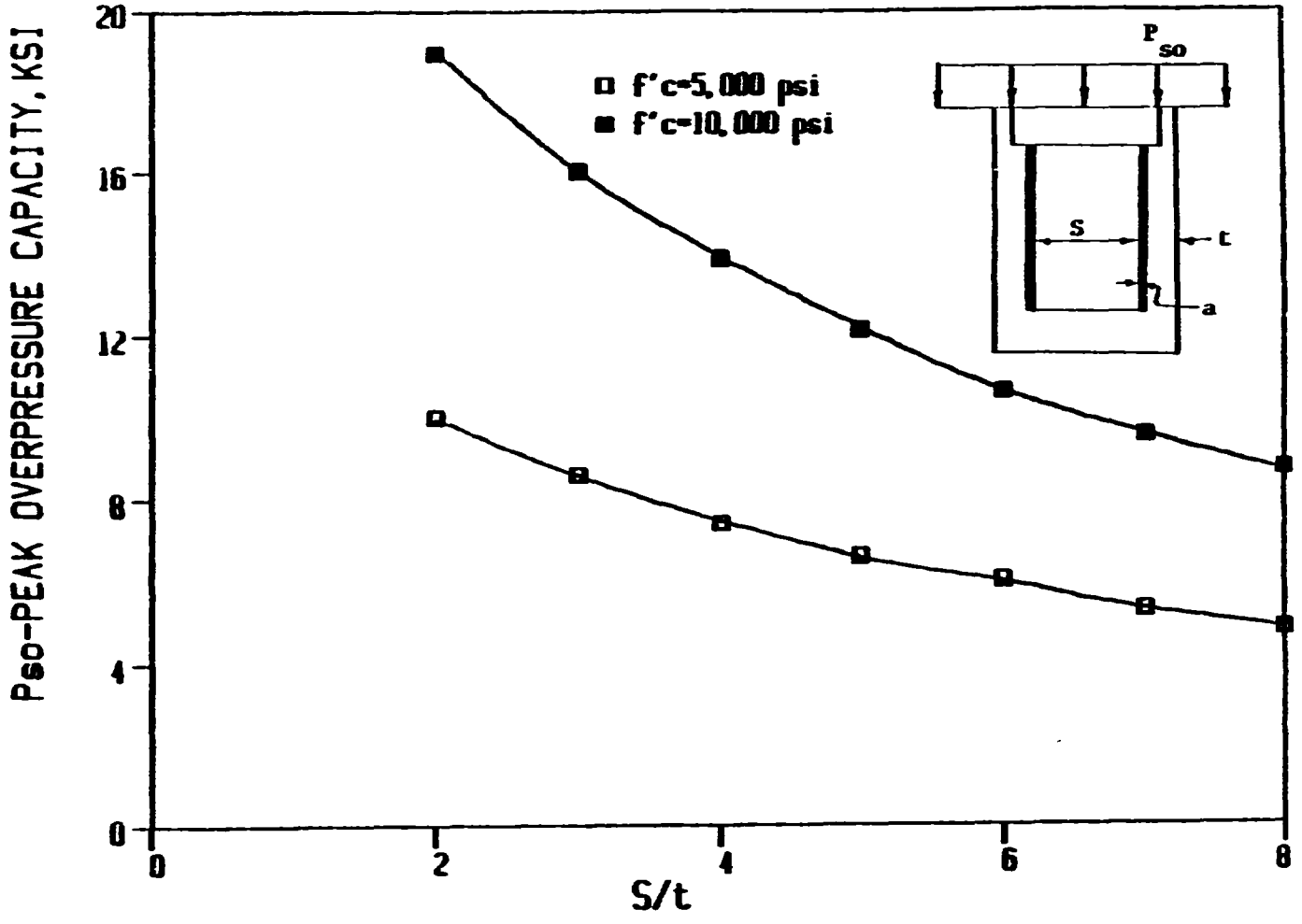

Figure 44. Axial overpressure capacity of interior lined silos, $(\frac{a}{t} - \frac{1}{64})$ to a 1-MT weapon prior to arrival of radial soil stress, HOB = 0, $\mu = 2$.

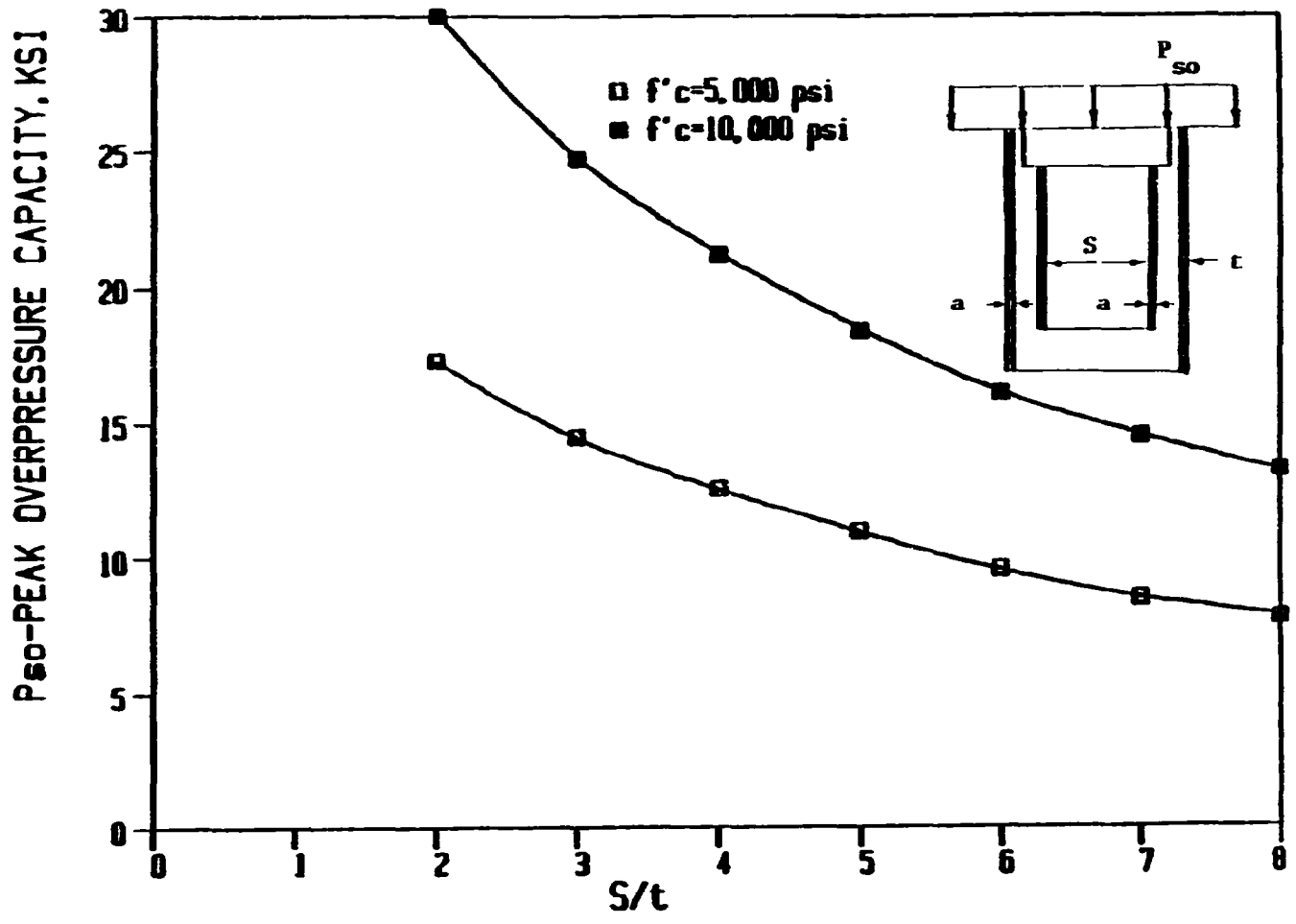

Figure 45. Axial overpressure capacity of inner and outer lined silos ($\frac{a}{t} = \frac{1}{64}$) to a 1-MT weapon prior to arrival of radial soil stress, BOB = 0, $\mu = 2$.

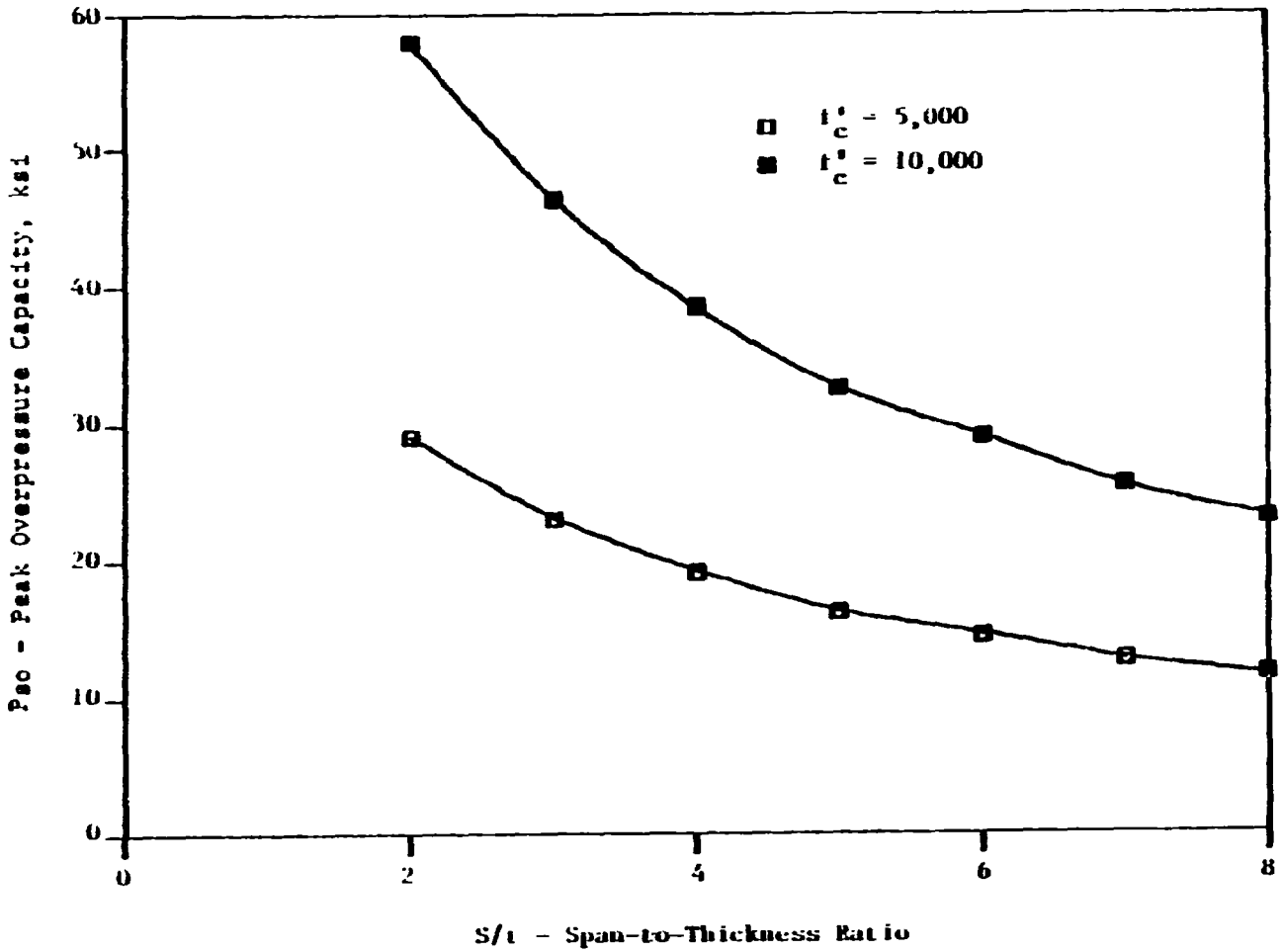

Figure 46. Peak ground surface overpressure capacity (P_{so}) of unlined silo to a 1-MT weapon after arrival of radial soil stress (σ_r), HOB = 0, μ = 2.

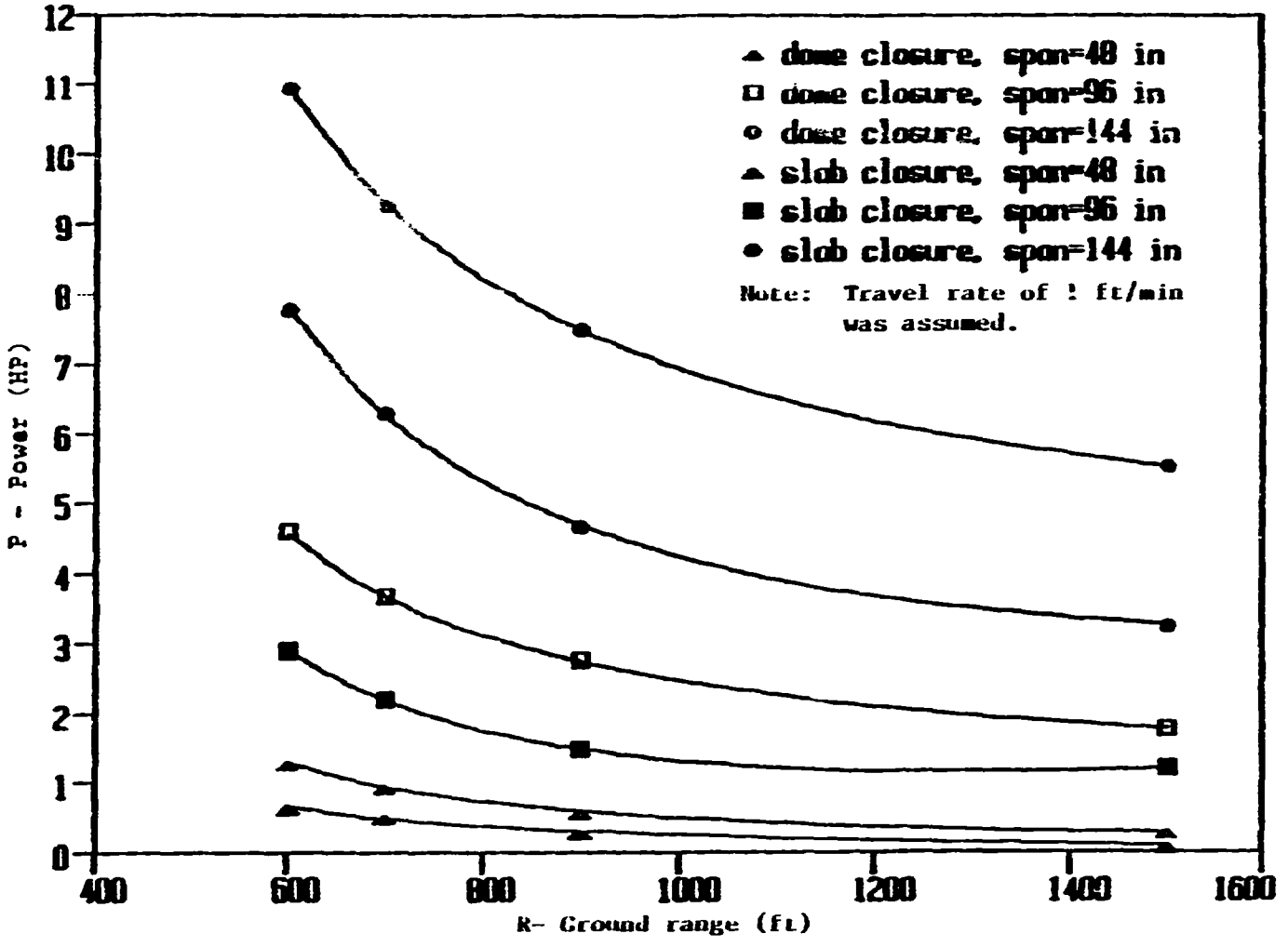

Figure 47. Power required to lift dome- and slab-type closures, 1-MT weapon, HOB = 0 ft.

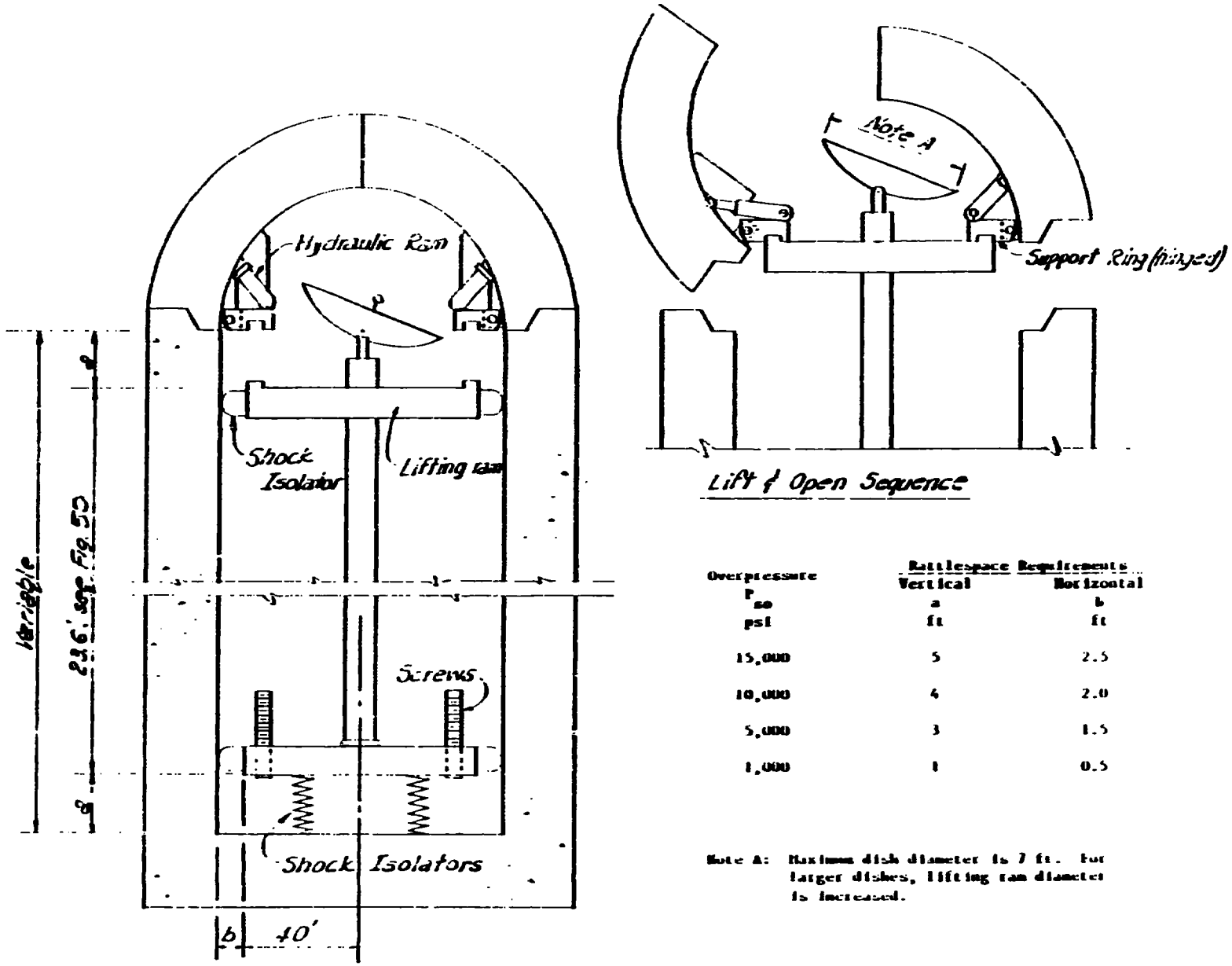

Overpressure P_{so} psi	Battlespace Requirements Vertical a ft	Horizontal b ft
15,000	5	2.5
10,000	4	2.0
5,000	3	1.5
1,000	1	0.5

Note A: Maximum dish diameter is 7 ft. For larger dishes, lifting ram diameter is increased.

Figure 48. Lifting concept for dome closures.

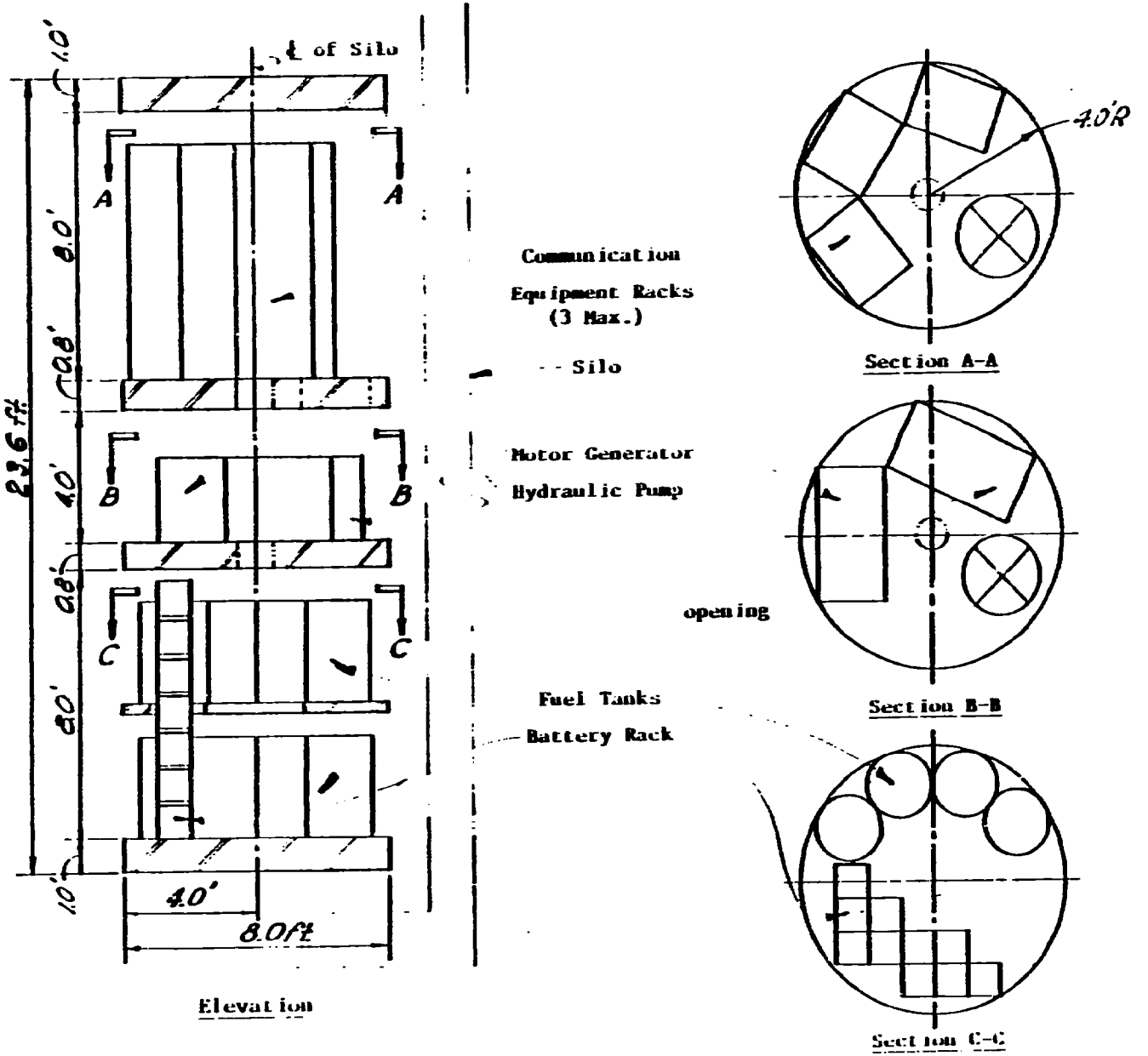

Figure 49. Equipment configuration for a one-week operational period, domed closure.

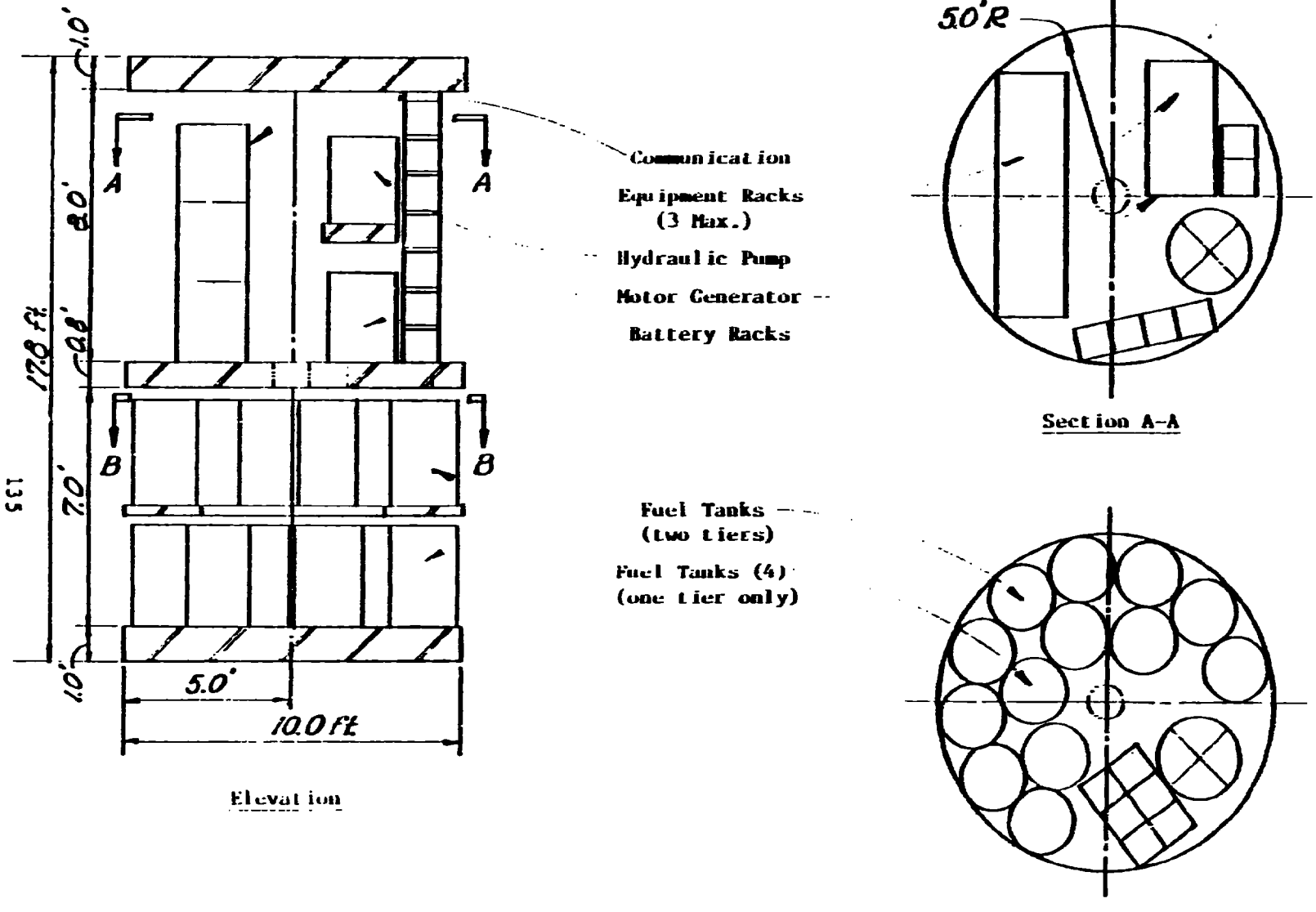

Elevation

Figure 50. Equipment configuration for a one-month operational period, domed closure.

SECTION 4
RELATIVE COSTS AND TRADE-OFFS

Presented in this section are relative costs for the family of silos considered versus range and overpressure for a 1-MT surface burst. The cost are not intended to represent true totals for a complete system but sufficient so that trade-off studies can be made to determine the best selection of combinations of silo structures for minimum cost.

4.1 RELATIVE COST OF SILO ELEMENTS.

The estimates have been determined using construction cost data (Reference 15); however, these are not total costs. The cost of real estate, site preparation, excavation and backfill have not been included. Also, the cost of communication equipment and shock isolation systems have not been included. The cost does include concrete, concrete placement, forms, reinforcing steel, steel plates (rolled, machined and welded as necessary) and the lifting mechanisms to include the power supply. The unit costs of the steel plate based on size configuration complexity, machining, and fabrication were provided by Mr. E.C. Loflin who has had considerable experience in such matters with the Marathon-LeTourneau Company. The power requirements for lifting the closure in most cases also satisfies the power requirement for operating the communication equipment.

4.1.1 Slab Costs.

The cost of in-place concrete (f'_c = 5,000 psi) is estimated at $300/yd^3 and the cost of machined, rolled and welded plate as shown in Table 21. The volume of concrete, weight of steel and cost of slab closures for use at the 15,000-, 10,000-, 5,000- and 500-psi overpressure levels are shown in Table 21. The relative cost of the slab closure versus range is shown in Figure 51.

4.1.2 Dome Costs.

The cost of in-place concrete (f'_c = 5,000 psi) is estimated at $350/yd^3 and the cost of machined, rolled and welded plate as shown in Table 22. The volume of concrete, weight of steel and cost of dome closures for use at the

15,000-, 10,000-, 5,000- and 500-psi overpressure levels are shown in Table 22. The relative cost of the dome closure versus range is shown in Figure 52.

4.1.3 Silo Costs.

Two lengths of silo will be considered, i.e. 10 and 20 feet. The cost of in-place concrete to include any formwork and reinforcing steel for the silos is estimated at $450/yd^3. The cost of the machined steel bearing plate is $1.65/lb. The cost of the rolled and welded inner and outer steel liners is shown in Table 23. The volume of concrete, weight of steel bearing plate and weight of steel liners as appropriate for the various overpressure levels for silo lengths of 10 and 20 feet are shown in Table 23. The relative cost of the 10- and 20-foot-long silos versus range is shown in Figure 53.

4.1.4 Base Slab Costs.

It is assumed that the base slab will have the same general dimensions as the slab closure. It will be assumed that the base will have one cover plate when liners are used with the silo. The cost of in-place concrete is estimated at $350/yd^3. The cost of the steel cover plate is estimated at $1.65/lb. The volume of concrete, weight of steel cover plate and cost of base slab for the 15,000-, 10,000-, 5,000- and 500-psi overpressure levels are shown in Table 24. The relative cost of the base slabs versus range is shown in Figure 54.

4.1.5 Lifting Mechanism Costs.

The size of the hydraulic loading rams, power requirements and costs to lift slab and dome closures are shown respectively in Tables 25 and 26. The stroke and power requirements are based on the thickness of ejecta the closures must punch through. Shown in Figures 55 and 56 are the costs of the lifting mechanism for slab and dome closures, respectively, versus range for 4-, 8- and 12-foot-diameter silos.

4.1.6 Relative Costs of Silo Systems.

Based on the results of the costs of individual components, the relative costs of completed slab- and dome-type structural systems are shown in

Figures 57 and 58, respectively, for silo lengths of 20 feet. Even though the dome closure system provides some additional, usable volume, the silo length of 20 feet was used in determining the total relative costs. It should be noted that the cost of real estate, site preparation, excavation and backfill, communication equipment, and shock isolation systems have not been included.

4.2 THREAT SCENARIO FOR HARDENED COMMUNICATION SYSTEMS.

Depending on the system of interest and a postulated attack scenario, a planner should be able to use the information in this report to make decisions on how hard an antenna structure should be and if there is merit in considering two lesser hardened structures instead of one relatively harder structure.

4.2.1 Redundancy.

The hardened antennae structure may serve one or several facilities depending on the functional nature of the communication system of interest. It is conceivable that for a single communication system, two hardened antennae structures could be considered. Likewise, more than two hardened antennae structures could be considered for a system of communication facilities. The selection of a redundant hardened communication structure will depend on the importance and/or hardness level of the primary communication facility. It is also possible that two structures at a lower rated hardness level have a better chance of survival than a single structure rated at a much higher level.

4.2.2 Hardness Cost Trade-Offs.

Shown in Figures 57 and 58 are the relative construction costs of several silo structures, including the cost of power supplies and lifting mechanisms to open closures and raise antennae.

For example, assume a structure with a dome closure, see Figure 58 for relative costs. Based on practical limitations of space required for equipment and rattlespace, the inside diameter of such structures will most likely exceed 8 feet, see Figures 48, 49, and 50. Observe that the rattlespace requirements at the high overpressures are appreciable.

Therefore, for example purposes based on realistic assumptions, determine the cost of one dome closure structure that is 12 feet in diameter and 20 feet long and located at the 15,000-psi overpressure level. From Figure 58, the relative cost of this structure is about: $530,000.

Compare this with the cost of two 12-foot-diameter structures that are 20 feet long (actually the comparative dimension would be less because the rattlespace is less) and located at the 5,000-psi overpressure level. Again from Figure 58, the relative cost of two structures is about: 2 x $180,000 = $360,000. Consequently, the construction cost of building two structures at the 5,000-psi range (880 feet from GZ) is about $170,000 less than building one structure at the 15,000-psi range (600 feet from GZ). The estimated cost of excavating and backfilling for each structure would be about $15,000. Hence in this case, if the cost of the communication system is less than $150,000, two structures at the lower overpressure level could be built for the price of one structure at the higher overpressure level. The cost of the shock isolation system for the structure at the 15,000-psi level is assumed to be about the same as the cost for the shock isolation systems for the two structures located at the 5,000-psi pressure level.

Based on the information shown in Figures 57 and 58, a planner should not only be able to develop estimates showing the relative costs for hardening antennae structures, but also be able to prepare a realistic cost estimate for the facility.

Table 21. Relative cost of slab-type closure.

Overpressure P_{so} psi	Inside Diameter of Silo S ft	Volume of Concrete yd^3	Cost of Concrete ($300/$yd^3$) $	Weight of Steel lb	Unit Cost of Steel ($/lb)	Cost of Steel $	Total Relative Cost $
15,000 (R = 600 ft)	12	45.1	15,785*	29,700	1.90	56,430	72,215
	8	13.4	4,690*	8,800	1.65	14,520	19,210
	4	1.7	595*	1,100	1.50	1,650	2,245
10,000 (R = 690 ft)	12	45.1	13,530	29,700	1.90	56,430	69,960
	8	13.4	4,020	8,800	1.65	14,520	18,540
	4	1.7	510	1,100	1.50	1,650	2,160
5,000 (R = 880 ft)	12	23.3	8,155*	19,680	1.90	37,400	45,555
	8	7.0	2,450*	5,870	1.65	9,685	12,135
	4	0.9	315*	748	1.65	1,234	1,549
500 (R = 1,975 ft)	12	7.6	2,280	11,680	1.90	22,192	24,472
	8	2.25	675	3,460	1.50	5,190	5,865
	4	0.28	84	433	1.90	823	907

*10,000-psi concrete ($350/$yd^3$).

Table 22. Relative cost of dome-type closure.

Overpressure P_{so} psi	Inside Diameter of Silo S ft	Volume of Concrete yd^3	Cost of Concrete ($350/$yd^3$) $	Weight of Steel lb	Unit Cost of Steel ($/lb)	Cost of Steel $	Total Relative Cost $
15,000 (R = 600 ft)	12	60.8	24,320*	48,640	2.35	114,300	138,600
	8	18.0	7,200*	14,410	1.90	27,400	34,600
	4	2.3	920*	1,800	2.35	4,200	5,100
10,000 (R = 690 ft)	12	39.8	15,920*	38,140	1.90	72,500	88,400
	8	11.8	4,720*	11,300	1.90	21,500	26,200
	4	1.5	600*	1,410	2.35	3,300	3,900
5,000 (R = 880 ft)	12	39.8	13,930	38,140	1.90	72,500	86,400
	8	11.8	4,130	11,300	1.90	21,500	25,600
	4	1.5	525	1,410	2.35	3,300	3,800
500 (R = 1,975 ft)	12	15.9	5,565	24,460	1.90	46,500	52,100
	8	4.7	1,645	7,250	2.35	17,000	18,600
	4	0.6	210	900	2.35	2,100	2,300

*10,000-psi concrete ($400/$yd^3$).

Figure 23. Relative cost of 10- and 20-foot-long silos.

Overpressure P_{so} psi	Inside Diameter of Silo S ft	Volume of Concrete yd^3	Cost of Concrete ($450/$yd^3$) $	Weight of Bearing Plate lb	Cost of Bearing Plate ($1.65/lb) $	Weight of Liners lb	Unit Cost of Liners ($/lb)	Cost of Liners $	Total Relative Cost $
				L = 10 ft					
15,000	12	125.7	56,565	5,758	9,500	51,848	1.80	93,300	159,400
	8	55.9	25,155	1,745	2,880	23,064	1.65	38,000	66,000
	4	14.0	6,300	465	770	5,761	1.50	8,600	15,700
10,000	12	40.2	18,090	5,758	9,500	16,591	1.80	29,900	57,500
	8	17.9	8,055	1,745	2,880	7,374	1.65	12,200	23,100
	4	4.5	2,025	465	770	1,843	1.50	2,800	5,600
5,000	12	27.3	12,285	2,941	4,850	4,925	1.50	7,400	24,500
	8	12.1	5,445	905	1,490	2,189	1.50	3,300	10,200
	4	3.0	1,350	252	420	547	1.50	800	2,600
500	12	23.6	10,620	1,664	2,740	0		0	13,400
	8	10.5	4,725	523	860	0		0	5,600
	4	2.6	1,170	155	250	0		0	1,400

Figure 23. Relative cost of 10- and 20-foot-long silos (continued).

Overpressure P_{so} psi	Inside Diameter of Silo S ft	Volume of Concrete yd^3	Cost of Concrete ($450/$yd^3$) $	Weight of Bearing Plate lb	Cost of Bearing Plate ($1.65/lb) $	Weight of Liners lb	Unit Cost of Liners ($/lb)	Cost of Liners $	Total Relative Cost $
				L = 20 ft					
15,000	12	251.3	113,130	5,758	9,500	103,696	1.80	186,600	309,200
	8	111.8	50,310	1,745	2,880	46,087	1.65	76,000	129,200
	4	28.0	12,600	465	770	11,522	1.50	17,300	30,700
10,000	12	80.4	36,180	5,758	9,500	33,182	1.80	59,700	105,400
	8	35.8	16,110	1,745	2,880	14,748	1.65	24,300	43,300
	4	9.0	4,050	465	770	3,687	1.50	5,500	10,300
5,000	12	54.6	24,570	2,941	4,850	9,850	1.65	16,300	45,700
	8	24.2	10,890	905	1,490	4,378	1.50	6,600	19,000
	4	6.1	2,700	252	420	1,095	1.50	1,600	4,700
500	12	47.1	21,240	1,664	2,740	0		0	24,000
	8	21.0	9,450	523	860	0		0	10,300
	4	5.2	2,340	155	250	0		0	2,600

Table 24. Relative cost of base slab.

Overpressure P_{so} psi	Inside Diameter of Silo S ft	Volume of Concrete yd^3	Cost of Concrete ($400/$yd^3$) $	Weight of Steel lb	Cost of Steel ($1.65/lb)	Total Relative Cost $
15,000 (R = 600 ft)	12	25.1	11,295*	1,152	1,900	13,195
	8	7.5	3,375*	512	845	4,220
	4	0.9	405*	128	211	616
10,000 (R = 690 ft)	12	25.1	10,040	1,152	1,900	11,940
	8	7.5	3,000	512	845	3,845
	4	0.9	360	128	211	571
5,000 (R = 880 ft)	12	16.75	7,538*	1,152	1,900	9,438
	8	5.0	2,250*	512	845	3,095
	4	0.6	270*	128	211	481
500 (R = 1,975 ft)	12	6.3	2,520	1,152	1,900	4,420
	8	1.9	760	512	845	1,605
	4	0.2	80	128	211	291

*10,000-psi concrete ($450/$yd^3$).

Table 25. Cost of hydraulic cylinders and power supply for slab closure systems.

Overpressure P_{so} psi	Span ft	Hydraulic Cylinder						Hydraulic Power Supply			Relative Total Cost
		Diameter in	Stroke in	Pressure psi	Displacement gal	Cost $	Force lb	hp	Flow gal/min	Cost $	
15,000 (R = 600 ft)	12	10	60	3,060	20.4	8,500	235,620	7-1/2	4.1	2,200	10,700
	8	6		3,000	7.4	1,900	84,810	5	1.5	2,000	3,900
	4	3-1/4		3,000	2.2	1,100	24,900	3	0.5	1,800	2,900
6,600 (R = 800 ft)	12	10	42	1,500	14.3	5,400	117,810	5	2.9	2,000	7,400
	8	6		1,500	5.2	1,510	42,405	5	1.1	2,000	3,500
	4	3-1/4		1,500	1.5	1,000	12,450	3	0.3	1,800	2,800
2,000 (R = 1,200 ft)	12	7	24	2,000	4	1,000	6,900	3	0.8	1,800	2,800
	8	4		2,000	1.3	950	25,140	3	0.3	1,800	2,750
	4	2		2,000	0.4	850	6,280	3	0.1	1,800	2,650
500 (R = 2,000 ft)	12	5	12	1,500	1	850	29,460	3	0.2	1,800	2,650
	8	3-1/4		1,500	0.5	850	12,450	3	0.1	1,800	2,650
	4	1-1/2		1,500	0.1	700	2,651	3	0.02	1,800	2,500

Table 26. Cost of hydraulic cylinders and power supply for dome closure systems.

Overpressure P_{oo} psi	Span ft	Hydraulic Cylinder Diameter in	Stroke in	Pressure psi	Displacement gal	Cost $	Force lb	Hydraulic Power Supply hp	Flow gal/min	Cost $	Relative Total Cost
15,000 (R = 600 ft)	12	14	60	3,000	40	19,050	461,820	7-1/2	8	2,200	21,200
	8	10		3,000	20.4	8,425	235,620	5	4.1	2,000	12,500
	4	5		3,000	5.1	1,510	58,920	5	1.1	2,000	3,500
6,600 (R = 800 ft)	12	14	42	2,000	28	16,832	307,880	7-1/2	5.6	2,200	19,000
	8	10		2,000	14.3	8,470	157,080	5	2.9	2,000	10,500
	4	5		2,000	3.6	1,240	39,280	3	0.7	1,800	3,000
2,000 (R = 1,200 ft)	12	12	24	2,000	11.8	8,700	226,200	5	2.4	2,000	10,700
	8	7		2,000	4	7,200	76,980	5	0.8	2,000	9,200
	4	3-1/4		2,000	0.9	1,235	16,600	3	0.2	1,800	3,000
500 (R = 2,000 ft)	12	12	12	1,500	5.9	1,900	169,650	5	1.2	2,000	4,000
	8	7		1,500	2	2,200	57,735	3	0.4	1,800	4,000
	4	2-1/2		1,500	0.3	372	7,365	3	0.06	1,800	2,500

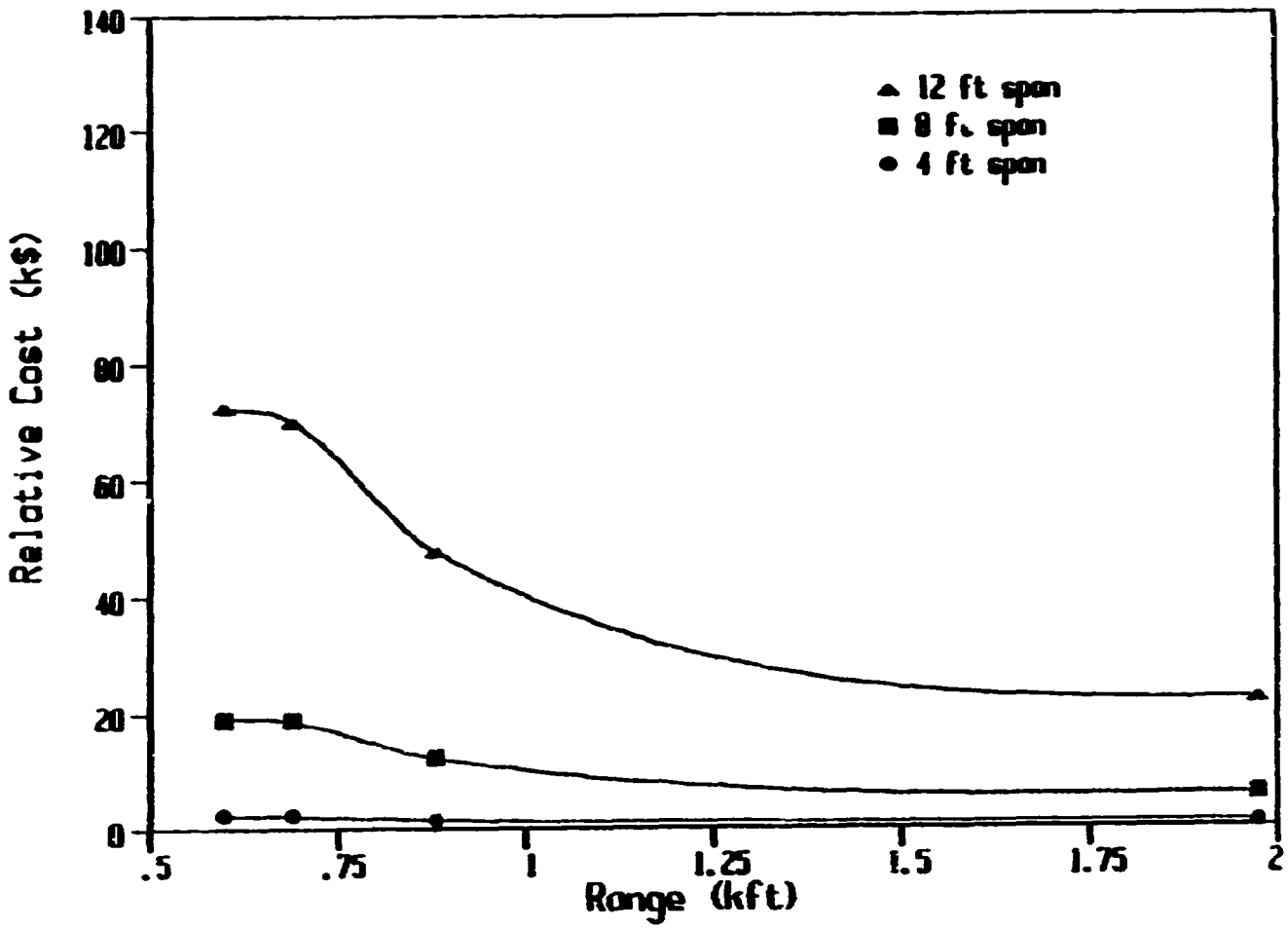

Figure 51. Relative cost of slab-type closure.

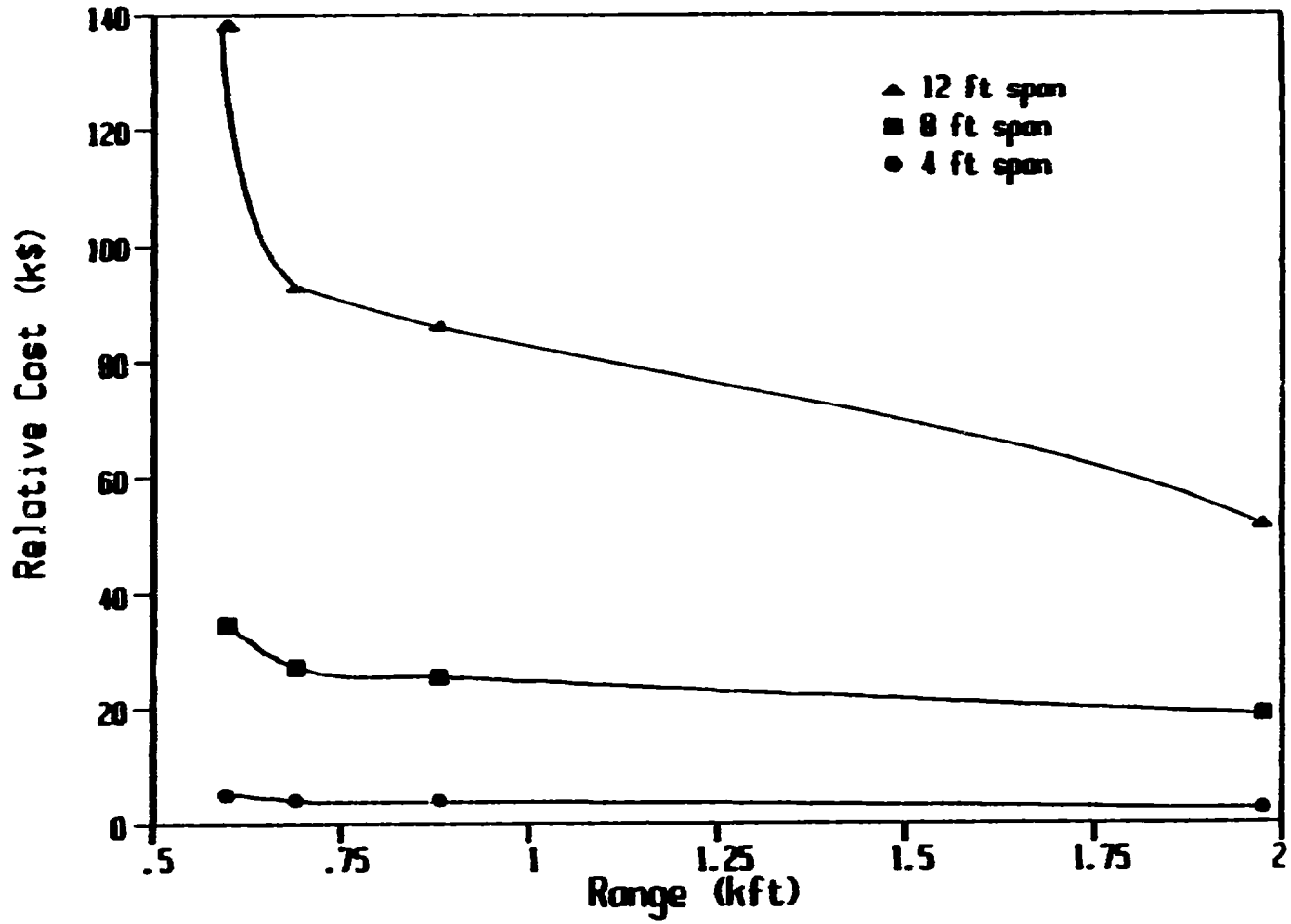

Figure 52. Relative cost of dome-type closure.

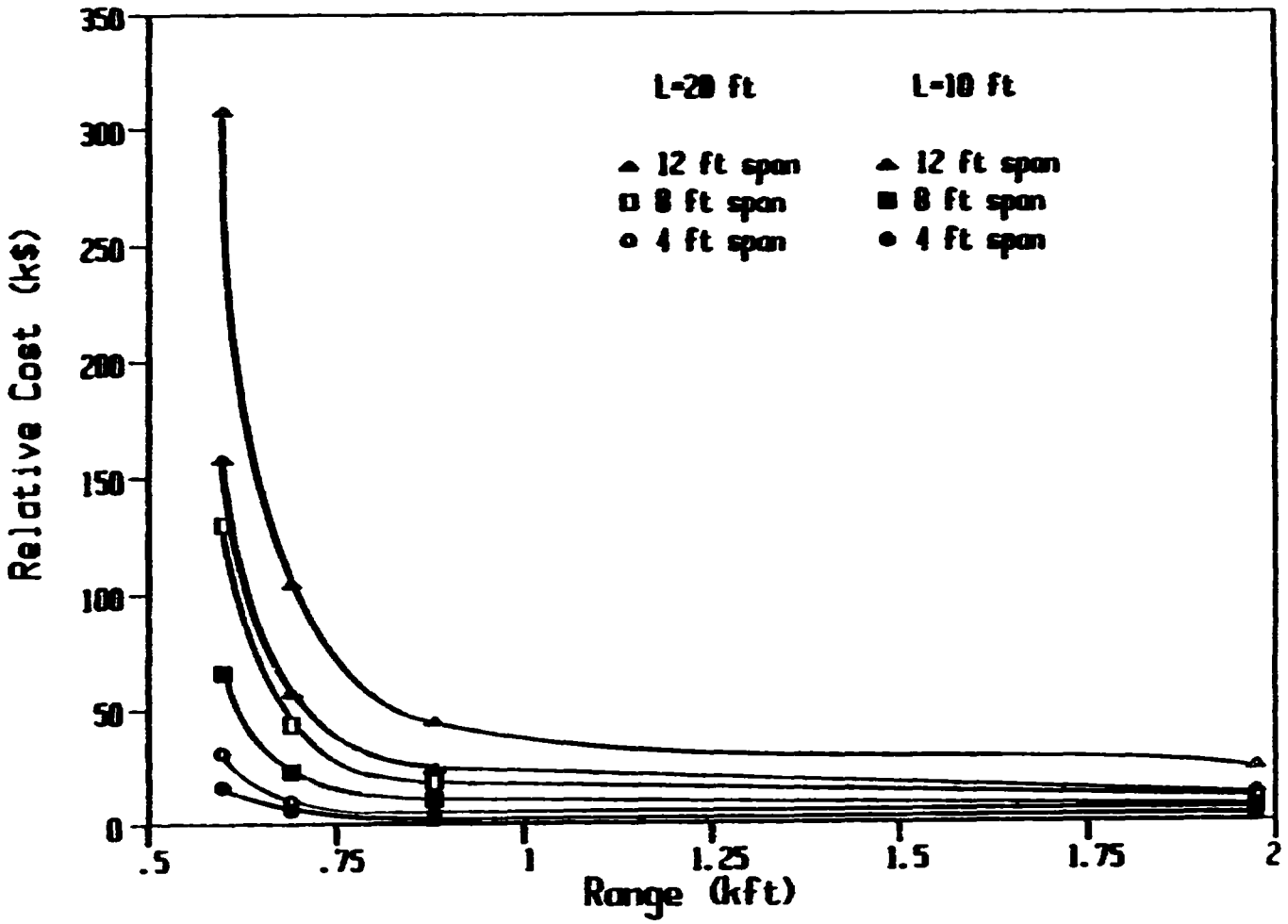

Figure 53. Relative cost of 10- and 20-foot-long silos.

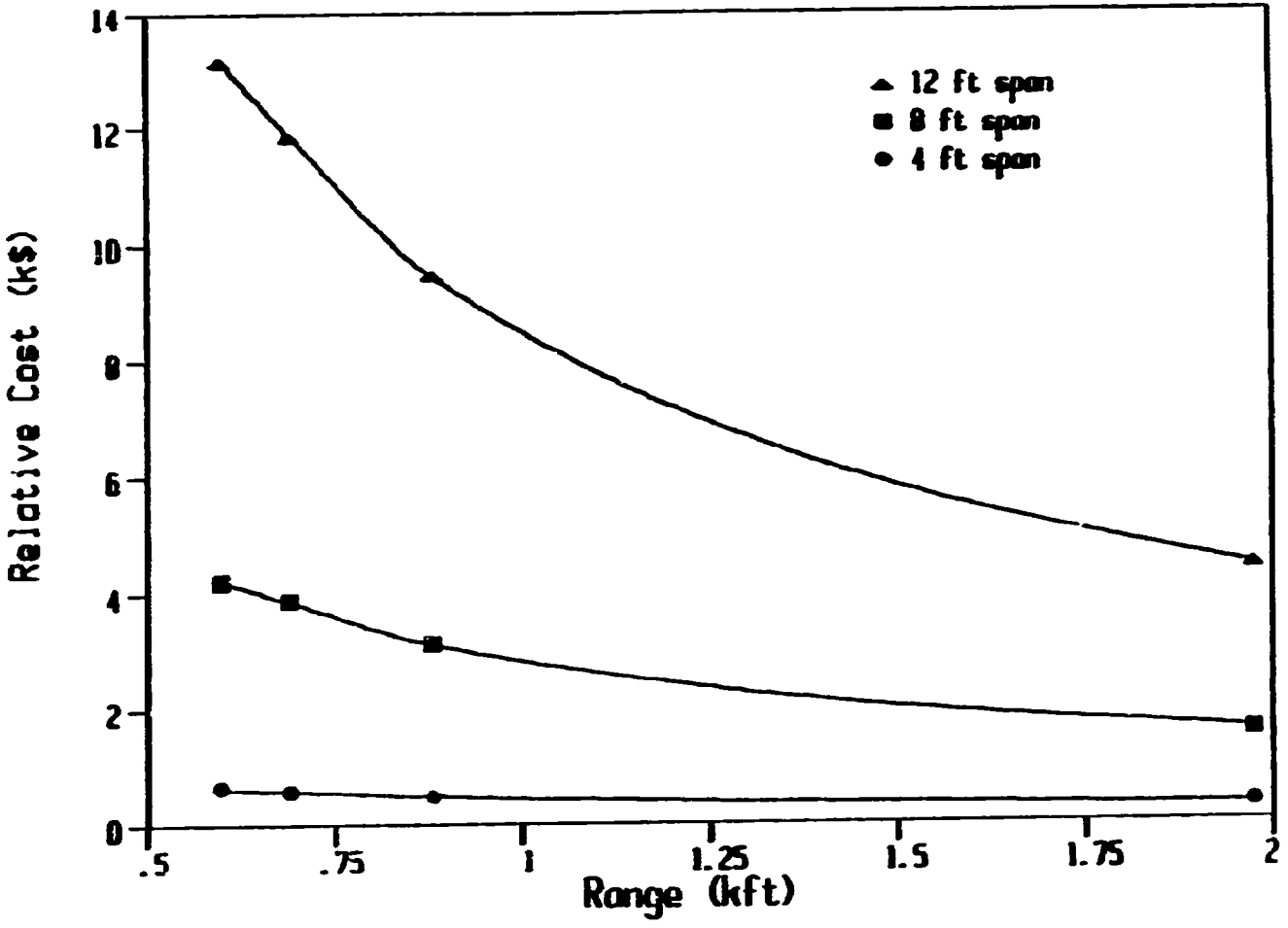

Figure 54. Relative cost of base slab.

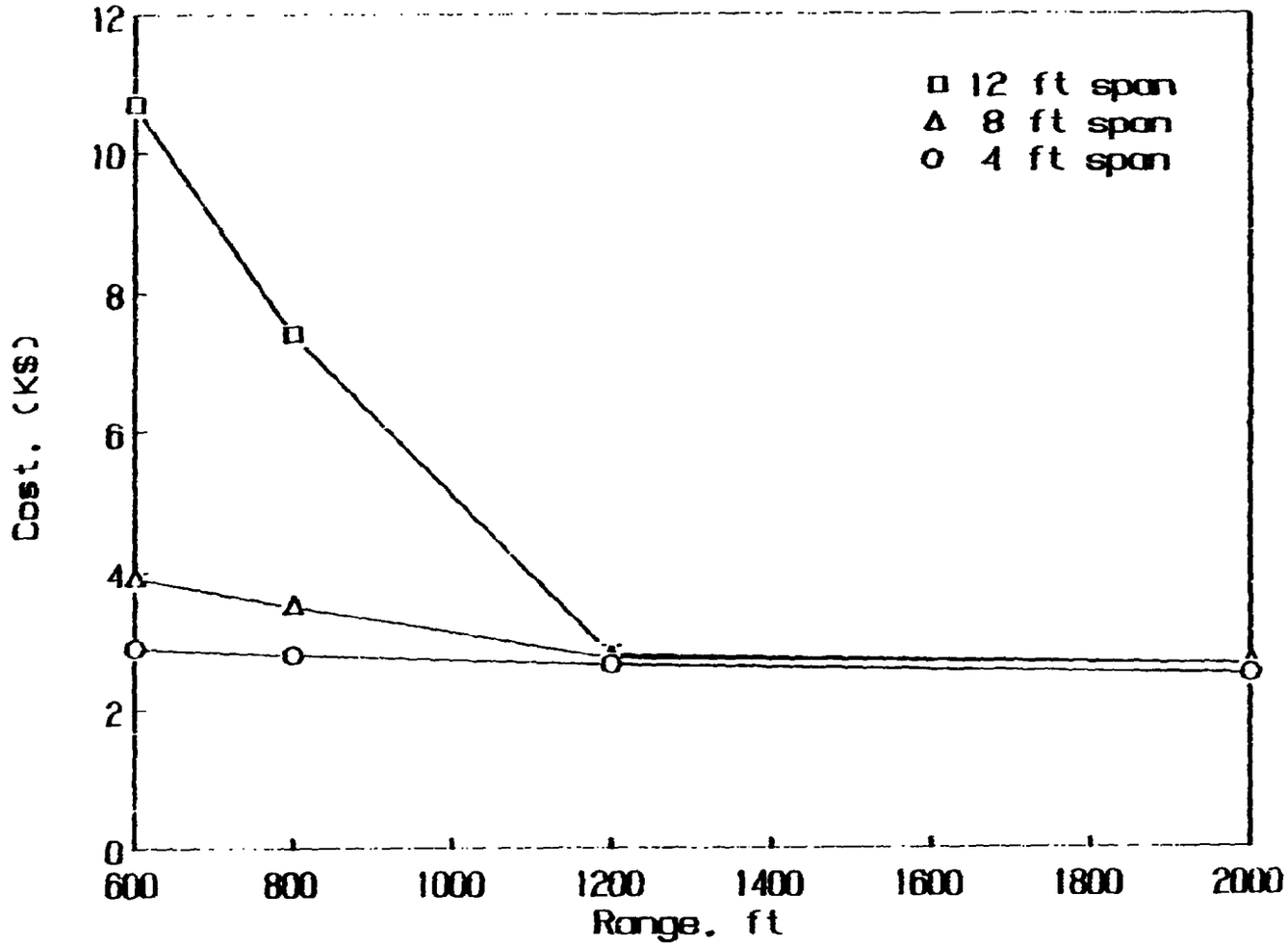

Figure 55. Cost of hydraulic cylinder and power supply for slab closure system.

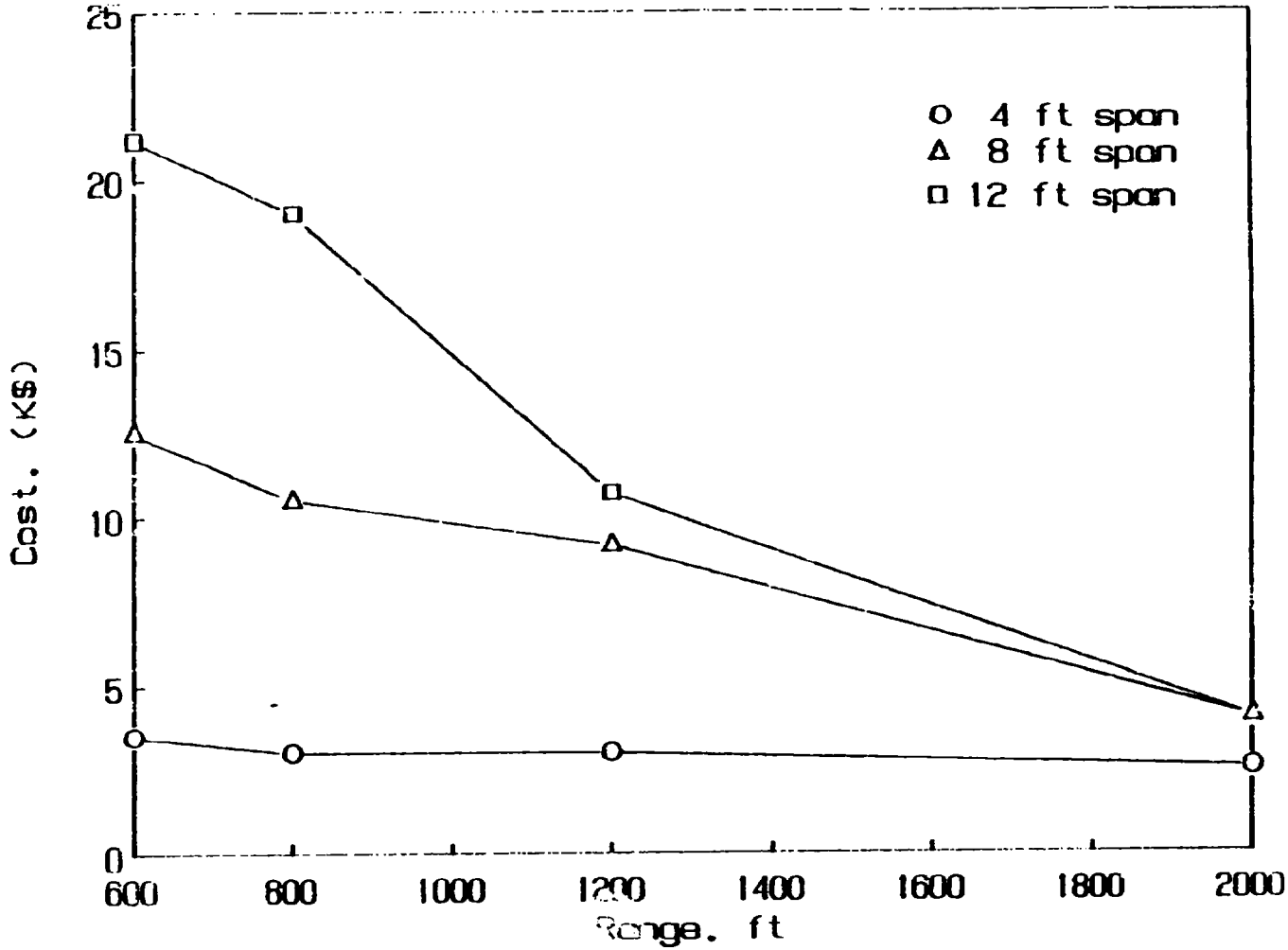

Figure 56. Cost of hydraulic cylinder and power supply for dome closure system.

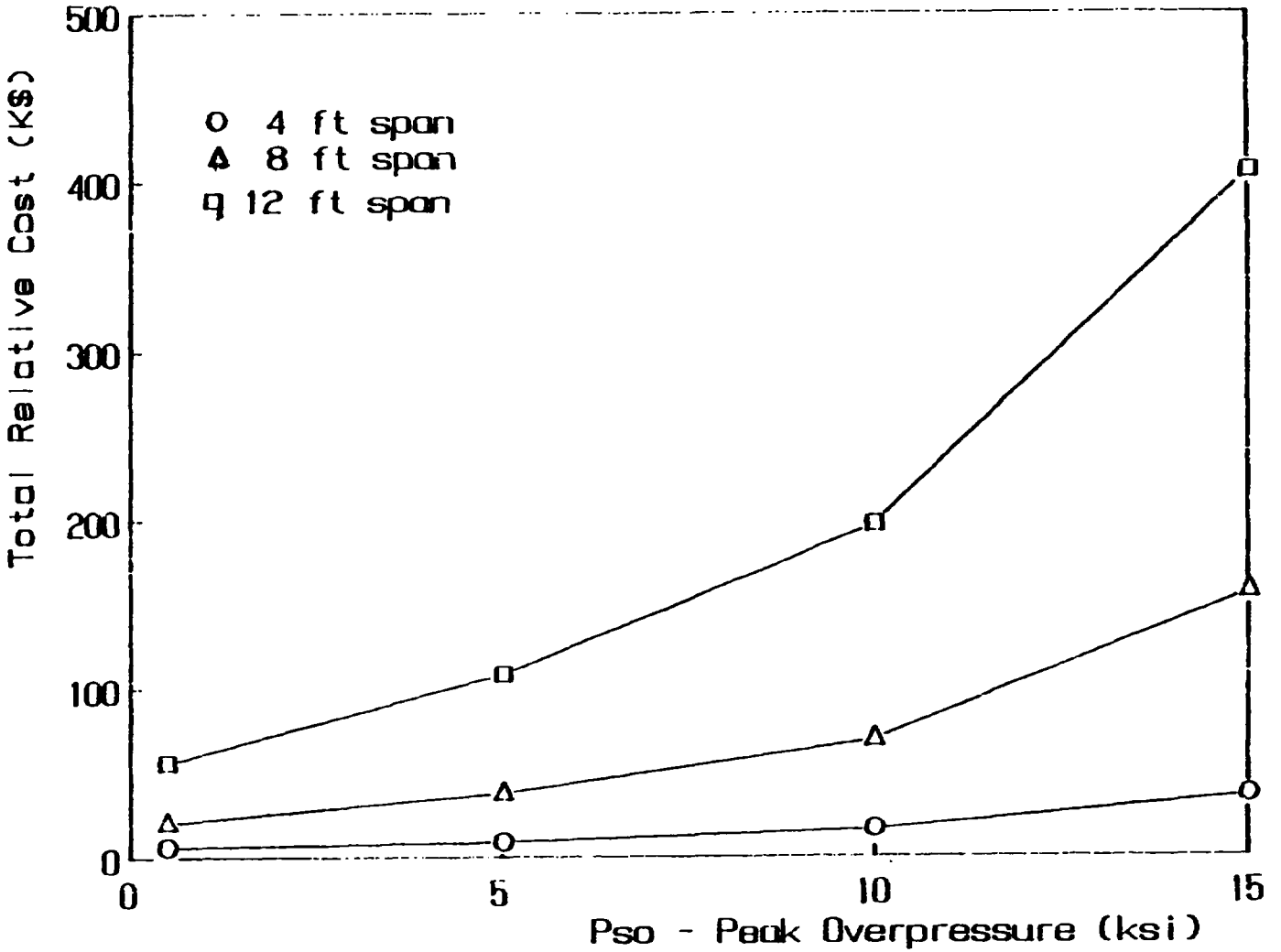

Figure 57. Total relative cost of hardened antennae structure, slab closure, 1-MT surface burst.

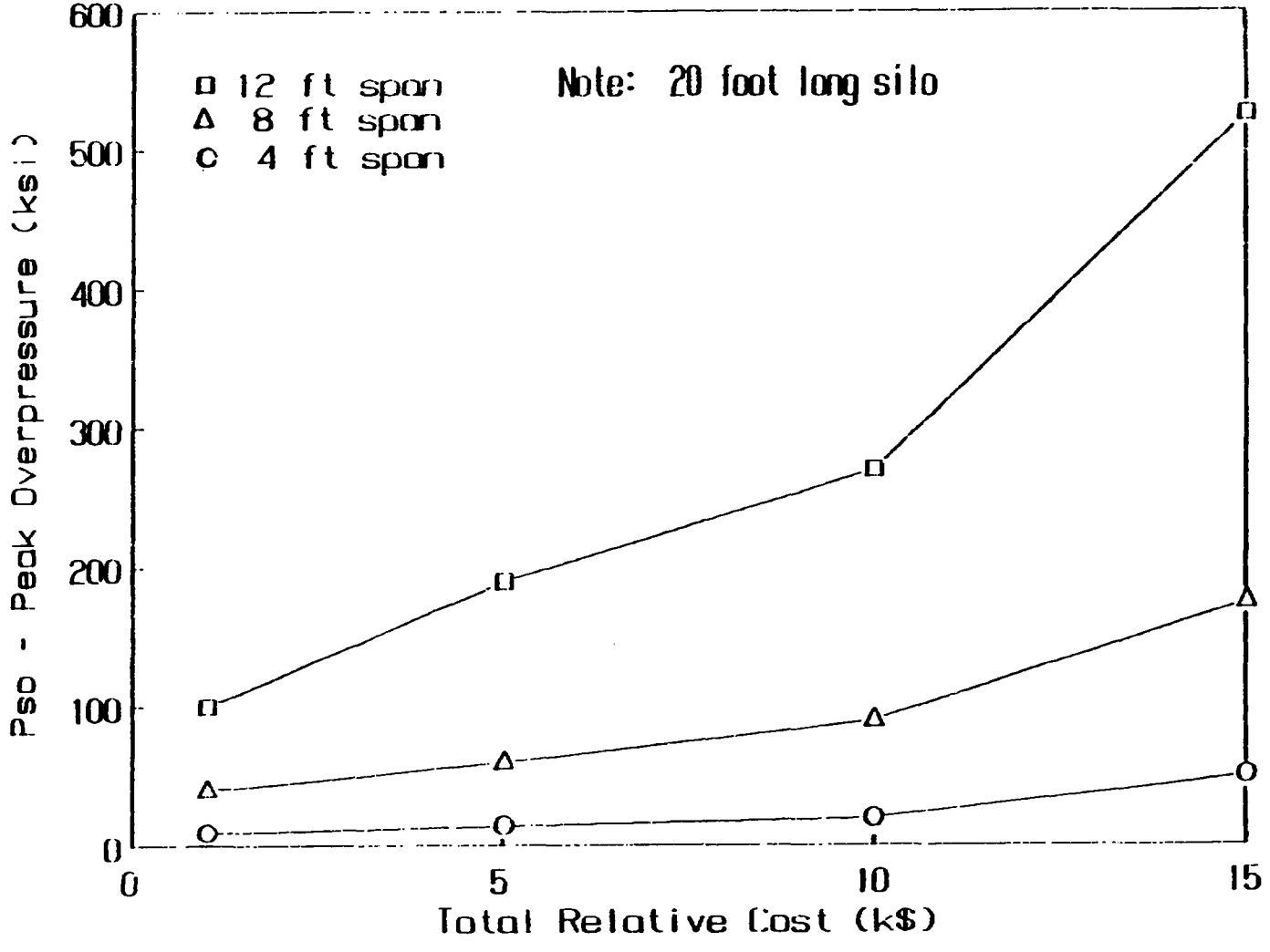

Figure 58. Total relative cost of hardened antennae structure, dome closure, 1-MT surface burst.

SECTION 5

DISCUSSION, CONCLUSIONS AND RECOMMENDATIONS

In this section, the discussion and conclusion remarks have been combined with recommendations presented separately.

5.1 DISCUSSION AND CONCLUSIONS.

In general, the authors believe that work presented in this report represents an excellent source document for the initial design and preparation of cost estimates for hardened communication structures. Based on operational considerations, novel closure designs were examined that show promise for antenna structures. Some of the pertinent features presented in the report are discussed in the following paragraphs.

5.1.1 Response Spectra.

Vertical and horizontal response spectra were developed for a 1-MT surface burst for three ground ranges associated with overpressure levels of 500, 5,000 and 15,000 psi, for airblast-induced shock; direct-induced shock; and late-time, crater-induced motion (primarily horizontal).

The controlling vertical and horizontal response spectra are that produced by airblast-induced shock.

5.1.2 Equipment Fragility Level.

Shown in Figure 23 are "sure safe" vertical and horizontal shock spectra for several different types of equipment. Comparing these values to those shown in Figures 20 and 21 for vertical and horizontal shock spectra for a 1-MT weapon, it is apparent that the equipment (pipes, radio receivers, electrical panel boards, batteries, air-conditioning units, etc.) would require shock isolation in order to survive even at the 500-psi level.

5.1.3 Design of Structural Elements.

Procedures for determining the static resistance and dynamic design were presented for slab-type closures, dome-type closures, silos and base slabs

for silos. In addition, the solutions were presented in graphic form making it possible to design a hardened antenna structure directly to resist the effects of a 1-MT surface detonation over a sandy silty soil. The method should also produce a good first-trial design for other soil conditions.

5.1.4 Lifting Concept for Dome Closure.

The dome closure allows the antenna to occupy space just under the closure which is an efficient utilization of this space from a lifting and operation standpoint, see Figure 48. The engagement distance for the lifting ram to make contact with the closure is governed by the vertical rattlespace requirements. The antenna rides up with the lifting ram and after the dome opens is in position for sending and receiving communications.

5.1.5 Lifting Concept for Slab Closure.

Several sliding slab concepts for both whip and directional antennae are shown in Figures 1 and 2. For the whip antenna, the split closure only needs to open enough to allow the antenna to be raised. For the pop-up and fold-out directional antennae, the split closure needs to open more to allow the antenna to be raised. For the pop-up directional antenna, the entire closure needs to slide out of the way. Assuming that 3 feet of ejecta (soil cover) over a slab represents the maximum depth of ejecta for which the closure can operate (slide horizontally), then based on ejecta depths with range shown in Figure 8, the maximum ground surface overpressure for consideration would be about 5,000 psi (880 feet) for this type of slab closure. For greater overpressure levels, rise- and rotate-type closures would probably be required. At the 5,000 psi range, the peak horizontal displacement would be about 1.5 feet and the permanent horizontal displacement would be about 0.75 feet. These large displacements require special design consideration for large horizontal excursions for a sliding-type closure.

5.1.6 Equipment Space Requirements.

Space requirements were based on the size of receiving and transmitting equipment for communication, alternate power supplies to operate the lifting

mechanisms for both the closure and antenna as well as the communication equipment, air-conditioning systems, air-exhaust systems and a sump pump. A space 8 feet in diameter by 24 feet long is required to house all the equipment necessary for one week of continuous operation. A space 10 feet in diameter by 18 feet long is required to house all the equipment necessary for one month of continuous operation. For a structure with a slab-type closure, the silo would need to be longer than a silo with a dome-type closure to accommodate space for a dished antenna.

5.1.7 Rattlespace Requirements.

The estimated rattlespace requirements have also been included in Figure 48 to provide an appropriate vertical and horizontal shock isolation system to protect the equipment located on the internal support system. These present first-cut estimates and probably would be refined during the final design when better values of coupling and system frequencies are determined.

5.1.8 Hardness-Cost Trade-Offs.

The primary construction costs versus overpressure for antenna structures having 4, 8, and 12 foot inside diameters are shown in Figure 57 for slab closures and Figure 58 for dome closures. By first comparisons, it would appear that the structure with the dome closure costs a great deal more than a comparable structure with a slab closure. It should be noted that the dome closure provides more usable space, and that the slab closure system would require a greater length silo to provide comparable usable space; hence, the cost would increase. It can be observed that costs are greater with increases in the diameter and the pressure the system must resist. It is believed that sufficient information is provided to make hardness-cost trade-off evaluations for communication systems typical to those described in this report.

5.2 RECOMMENDATIONS.

Recommendations are presented for use of this report and a test program supportive of hardened structures to house antennae.

5.2.1 Initial Design of Hardened Antenna Structures.

It is recommended that the information in this report be used for the initial design of hardened structures to house whip and directional antennae. It is also recommended that the cost information presented be used to make relative cost estimates as well as actual cost estimates for the several types of hardened structures discussed.

5.2.2 Test Program.

The concepts of a split slab closure and a dome closure that opens like petals on a flower require testing before such geometries can be used in a real system. It is recommended that a test program be developed for rise and rotate slabs and for domes that open. The test program should include the mechanical designs for operating the closures as well as raising the antennae systems. Both concepts should be evaluated on how effective they are in pushing through various thicknesses of soil cover (ejecta). Finally, the systems should be tested in a HEST-type environment that simulates the blast and shock from a nuclear event. Some model tests would be desirable, but at least a half-scale test would be required to check out the mechanical, hydraulic and communication equipment in such a system to a realistic blast and shock environment.

Another possible system that could be very effective in mitigating vertical motion to the internal equipment would be the use of a "floating base slab." Upon loading, the silo punches into the soil like a cookie cutter, thus sheltering the base slab from the intense vertical shock. In this manner, only the vertical rattlespace (see Figure 48) at the top of the equipment stack should need to be considered, thus minimizing the length of the silo. Special attention would be required for the horizontal shock isolation. For example, the supporting structure attached to the base slab could use rotatable connections.

SECTION 6
REFERENCES

1. Albritton, G. E., "Deep Slabs Subjected to Static and Blast Loading," Proceedings of the Journal of the Structural Division, American Society of Civil Engineers, No.6919, November 1969.

2. American Society of Civil Engineers, Design of Structures to Resist Nuclear Weapons, Manual 42, ASCE, New York, NY, 1985.

3. Army, Department of the, TM 5-865, prepared by US Army Engineer Division, Huntsville.

4. Beavers, J. E. and Albritton, G. E., "Response of Deep Two-Way Reinforced and Unreinforced Concrete Slabs to Static and Dynamic Loading, Report 7, Static Tests of Deep Slabs Having Various Span-to-Thickness Ratios," Technical Report N-69-2, US Army Engineer Waterways Experiment Station, CE, Vicksburg, MS, May 1971.

5. Biggs, J. M., Introduction to Structural Dynamics, McGraw-Hill Book Company, New York, NY, 1964.

6. Boeing Aerospace Company, "Personnel and C-E Equipment Shock Tolerance," Summary Report, prepared by Boeing Aerospace Company, Seattle, WA, for Department of the Army, US Army Communications Command, Headquarters, Fort Huachuca, September 1977.

7. Chen, P. H., et al., "Response of Concrete-Steel Composite Closure to Uniform Static Overpressure," presented at the American Society of Civil Engineers St. Louis Conference, Paper No. 81-520, October 1981.

8. Crawford, R. E., Higgins, C. J. and Bultmann, E. H., "The Air Force Manual for Design and Analysis of Hardened Structures," AFWL-TR-74-102, Air Force Weapons Laboratory, Air Force Systems Command, Kirtland AFB, NM, October 1974.

9. Eagles, P. S. and Albritton, G. E., "Subscale MX Shelter Closure Structural Response Test Program; Report 1: Phases I and II Closure Static Tests," Technical Report SL-82-5, US Army Engineer Waterways Experiment Station, CE, Vicksburg, MS, June 1982.

10. Flathau, W. J. and Mlakar, P. F., "Considerations in Scaling Advanced Silo Hardening Model Test Data," Technical Report DNA-TR-85-265, prepared by JAYCOR, Structures Division, Vicksburg, MS, for Defense Nuclear Agency, Washington, DC, October 1985.

11. Getchell, J. V. and Watt, J. M. Jr., "Static Loading of MX Model Closures," Technical Report SL-79-4, US Army Engineer Waterways Experiment Station, CE, Vicksburg, MS, May 1979.

12. Guice, L. K. and Kiger, S. A., "Elastic-Plastic Response Charts for Nuclear Overpressures," Miscellaneous Paper SL-84-7, US Army Engineer Waterways Experiment Station, CE, Vicksburg, MS, June 1984.

13. Harris, C. M. and Crede, C. E., Shock and Vibration Handbook, 2nd edition, McGraw-Hill Book Company, New York, NY, 1976.

14. Jordan, D. and Welsh, L. M., "Blast Effects Program for the IBM PC and PC/XT," Handbook DNA-EH-84-02-G prepared by Horizons Technology, Inc., San Diego, CA, for the Defense Nuclear Agency, Washington, DC, December 1984.

15. R. S. Means Company, Inc., Building Construction Cost Data 1986, 44th Annual Edition, Kingston, MA, 1985.

16. The Ralph M. Parsons Company, "Closure Analysis and Test Study, Appendix 2, Subscale Static Test Report," Technical Report 4171-1 (Draft), Los Angeles, CA, April 1969.

17. The Ralph M. Parsons Company, "Closure Analysis and Test Study, Volume I," SAMSO TR 69-213 Vol.I, prepared for Department of the Air Force, Space and Missile Systems Organization, Air Force Systems Command, Norton AFB, CA, July 1969.

18. The Ralph M. Parsons Company, "Closure Analysis and Test Study, Volume II," SAMSO TR 69-213 Vol.II, prepared for Department of the Air Force, Space and Missile Systems Organization, Air Force Systems Command, Norton AFB, CA, July 1969.

19. Richart, F. E. Jr., Woods, R. D. and Hall, J. R. Jr., Vibration of Soils and Foundations, Prentice-Hall, Inc., Englewood Cliffs, NJ.

20. Rohani, B., "Theoretical Studies of Stress Wave Propagation in Laterally Confined Soils," Miscellaneous Paper (Draft), US Army Engineer Waterways Experiment Station, CE, Vicksburg, MS, July 1970.

21. Sutherland, H. and Reese, R.C., Introduction to Reinforced Concrete Design, John Wiley & Sons, Inc.

22. Vaughan, D. K., Isenberg, J. and Wong, F. S., "Effects of Scale in the Response of MX Vertical Shelters," Report DNA 53172, prepared by Weidlinger Associates, Menlo Park, CA, for Defense Nuclear Agency, Washington, DC, January 1980.

DISTRIBUTION LIST

DNA-TR-88-109

DEPARTMENT OF DEFENSE

ASSISTANT TO THE SECRETARY OF DEFENSE
ATOMIC ENERGY
ATTN: EXECUTIVE ASSISTANT

DEFENSE INTELLIGENCE AGENCY
ATTN: DB-6E2 D SUNSHINE
ATTN: RTS-2B

DEFENSE NUCLEAR AGENCY
ATTN: SPSD
ATTN: SPWE
ATTN: TDTR
4 CYS ATTN: TITL

DEFENSE NUCLEAR AGENCY
ATTN: TDNM
2 CYS ATTN: TDTT W SUMMA

DEFENSE TECHNICAL INFORMATION CENTER
2 CYS ATTN: DTIC/FDAB

STRATEGIC AND THEATER NUCLEAR FORCES
ATTN: DR E SEVIN

THE JOINT STAFF
ATTN: J-5 NUC & CHEMICAL DIV
ATTN: JAD/SFD
ATTN: JAD/SSD
ATTN: J8 NUC FORCE ANALYSIS DIV

DEPARTMENT OF THE ARMY

DEP CH OF STAFF FOR OPS & PLANS
ATTN: DAMO-NCZ

HARRY DIAMOND LABORATORIES
ATTN: SLCHD-NW-P

U S ARMY BALLISTIC RESEARCH LAB
ATTN: SLCBR-SS-T (TECH LIB)
ATTN. SLCBR-TB-B (G BULMASH)

U S ARMY ENGR WATERWAYS EXPER STATION
ATTN: B BARKER
ATTN: C WELCH
ATTN: D RICKMAN
ATTN: E JACKSON
ATTN: F DALLRIVA
ATTN: J BALSARA

U S ARMY NUCLEAR & CHEMICAL AGENCY
ATTN: MONA-NU

U S ARMY NUCLEAR EFFECTS LABORATORY
ATTN: ATAA-TDC R BENSON

DEPARTMENT OF THE NAVY

NAVAL RESEARCH LABORATORY
ATTN: CODE 2627 (TECH LIB)
ATTN: CODE 4770 G COOPERSTEIN
ATTN: CODE 7920 A WILLIAMS

NAVAL WEAPONS EVALUATION FACILITY
ATTN: CLASSIFIED LIBRARY

OFC OF THE DEPUTY CHIEF OF NAVAL OPS
ATTN: OP 654

DEPARTMENT OF THE AIR FORCE

AERONAUTICAL SYSTEMS DIVISION
ATTN: ASD/ENSSS H GRIFFIS

AIR UNIVERSITY LIBRARY
ATTN: AUL-LSE

BALLISTIC SYSTEMS DIVISION
ATTN: ASMS
ATTN: MYE

FOREIGN TECHNOLOGY DIVISION, AFSC
ATTN: SDMDA/S SPRING

HQ USAF/XOXFS
ATTN: AFXOOTS

WEAPONS LABORATORY
ATTN: HO R DUFFNER
ATTN: NTA A SHARP
ATTN: NTES
ATTN: SUL

WRIGHT RESEARCH & DEVELOPMENT CENTER
ATTN: AFWAL MLBT W ANSPACH

DEPARTMENT OF ENERGY

DEPARTMENT OF ENERGY
ATTN: OMA/DP-225

LAWRENCE LIVERMORE NATIONAL LAB
ATTN: J KNOX
ATTN: J KELLER
ATTN. P CHRZANOWSKI

LOS ALAMOS NATIONAL LABORATORY
ATTN: R S DINGUS
ATTN: J NORMAN
ATTN: R S THURSTON
ATTN: R W SELDEN

SANDIA NATIONAL LABORATORIES
ATTN: A CHABAI DIV 9311

OTHER GOVERNMENT

CENTRAL INTELLIGENCE AGENCY
ATTN: OSWR/NED
ATTN: S WALLENHURST

DEPARTMENT OF DEFENSE CONTRACTORS

ACTA, INC
ATTN: J D COLLINS

ACUREX CORP
ATTN: C NARDO

AEROJET GENERAL CORP
ATTN: A COLLINS

AEROSPACE CORP
ATTN: H BLAES
ATTN: JAMES KAWAMOTO
ATTN: L SELZER

APPLIED RESEARCH ASSOCIATES, INC
ATTN: J KEEFER

APTEK, INC
ATTN: T MEAGHER

BOEING TECHNICAL & MANAGEMENT SVCS, INC
ATTN: E YORK
ATTN: R BURWELL

CALIFORNIA RESEARCH & TECHNOLOGY, INC
ATTN: K KREYENHAGEN

CALIFORNIA RESEARCH & TECHNOLOGY, INC
ATTN: J THOMSEN

CALSPAN CORP
ATTN: M DUNN
ATTN: M HOLDEN

CARPENTER RESEARCH CORP
ATTN: H J CARPENTER

DENVER RESEARCH INSTITUTE
ATTN: JOHN WISOTSKI

G B LABORATORY, INC
ATTN: G BURGHART

GENERAL ATOMICS, INC
ATTN: CHARLES CHARMAN

GENERAL ELECTRIC CO
ATTN: A GARBER
ATTN: B MAGUIRE

H & H CONSULTANTS, INC
ATTN: J HALTIWANGER
ATTN: W HALL

HERCULES, INC
ATTN: P MCALLISTER

INSTITUTE FOR DEFENSE ANALYSES
ATTN: CLASSIFIED LIBRARY

JAYCOR
2 CYS ATTN: W FLATHAU
2 CYS ATTN: W G SMITH

KAMAN SCIENCES CORP
ATTN: L MENTE
ATTN: R RUETENIK

KAMAN SCIENCES CORP
ATTN: F SHELTON
ATTN: J HOFFMAN

KAMAN SCIENCES CORP
ATTN: DASIAC

KAMAN SCIENCES CORPORATION
ATTN: DASIAC

KARAGOZIAN AND CASE
ATTN: J KARAGOZIAN

LACHEL PIEPENBURG AND ASSOCIATES
ATTN: D PIEPENBURG

LOCKHEED MISSILES & SPACE CO, INC
ATTN: T KELIHER

MCDONNELL DOUGLAS CORP
ATTN: M POTTER

MCDONNELL DOUGLAS CORPORATION
ATTN: L COHEN

PACIFIC-SIERRA RESEARCH CORP
ATTN: H BRODE

R & D ASSOCIATES
ATTN: P RAUSCH

R & D ASSOCIATES
ATTN: J WEBSTER

RAND CORP
ATTN: B BENNETT

S-CUBED
ATTN: G GURTMAN

SCIENCE APPLICATIONS INTL CORP
ATTN: W YENGST

SCIENCE APPLICATIONS INTL CORP
ATTN: J COCKAYNE
ATTN: W LAYSON

SCIENCE APPLICATIONS INTL CORP
ATTN: J MANSHIP

SOUTHERN RESEARCH INSTITUTE
ATTN: C PEARS

SRI INTERNATIONAL
ATTN: J COLTON
ATTN: M SANAI

TECH REPS, INC
ATTN: F MCMULLAN

TECHNOLOGY DEVELOPMENT ASSOCIATES
ATTN: N DISPENSIERE

TOYON RESEARCH CORP
ATTN: J CUNNINGHAM

TRW INC
ATTN: A ZIMMERMAN
ATTN: M SEIZEW
ATTN: P BRANDT
ATTN: R BACHARACH

TRW SPACE & DEFENSE, DEFENSE SYSTEMS
ATTN: E ALLEN
ATTN: L BERGER

ATTN: N GUILES
ATTN: V BLANKINSHIP

UNIVERSITY OF COLORADO
ATTN: THOMAS GEERS

WEIDLINGER ASSOC, INC
ATTN DARREN TENNANT
ATTN: H LEVINE

WEIDLINGER ASSOCIATES, INC
ATTN: M BARON